



HAL
open science

Retrieving global sources of aerosols from MODIS observations by inverting GOCART model

O. Dubovik, T. Lapyonok, Y. J. Kaufman, M. Chin, P. Ginoux, A. Sinyuk

► To cite this version:

O. Dubovik, T. Lapyonok, Y. J. Kaufman, M. Chin, P. Ginoux, et al.. Retrieving global sources of aerosols from MODIS observations by inverting GOCART model. *Atmospheric Chemistry and Physics Discussions*, 2007, 7 (2), pp.3629-3718. hal-00328053

HAL Id: hal-00328053

<https://hal.science/hal-00328053>

Submitted on 18 Jun 2008

HAL is a multi-disciplinary open access archive for the deposit and dissemination of scientific research documents, whether they are published or not. The documents may come from teaching and research institutions in France or abroad, or from public or private research centers.

L'archive ouverte pluridisciplinaire **HAL**, est destinée au dépôt et à la diffusion de documents scientifiques de niveau recherche, publiés ou non, émanant des établissements d'enseignement et de recherche français ou étrangers, des laboratoires publics ou privés.

Retrieving global sources of aerosols from MODIS observations by inverting GOCART model

O. Dubovik^{1,2}, T. Lapyonok^{3,4}, Y. J. Kaufman⁵, M. Chin⁵, P. Ginoux⁶, and A. Sinyuk^{3,4}

¹Laboratoire de Optique Atmosphérique, Université de Lille 1/CNRS, Villeneuve d'Ascq, France

²Major part of this study was done while worked at: Laboratory for Terrestrial Physics, NASA Goddard Space Flight Center, Greenbelt, MD, USA

³Laboratory for Terrestrial Physics, NASA Goddard Space Flight Center, Greenbelt, MD, USA

⁴Science Systems and Applications, Inc., Lanham, MD, USA

⁵Laboratory for Atmospheres, NASA Goddard Space Flight Center, Greenbelt, MD, USA

⁶Geophysical Fluid Dynamics Laboratory, NOAA, Princeton, NJ, USA

Received: 22 November 2006 – Accepted: 16 February 2007 – Published: 12 March 2007

Correspondence to: O. Dubovik (dubovik@loa.univ-lille1.fr)

Retrieving global sources of aerosols from MODIS observations

O. Dubovik et al.

Title Page

Abstract

Introduction

Conclusions

References

Tables

Figures

⏪

⏩

◀

▶

Back

Close

Full Screen / Esc

Printer-friendly Version

Interactive Discussion

Abstract

Knowledge of the global distribution of tropospheric aerosols is important for studying the effects of aerosols on global climate. Chemical transport models rely on archived meteorological fields, accounting for aerosol sources, transport and removal processes can simulate the global distribution of atmospheric aerosols. However, the accuracy of global aerosol modeling is limited. Uncertainty in location and strength of aerosol emission sources is a major factor in limiting modeling accuracy. This paper describes an effort to develop an algorithm for retrieving global sources of aerosol from satellite observations by inverting the GOCART aerosol transport model.

To optimize inversion algorithm performance, the inversion was formulated as a generalized multi-term least-squares-type fitting. This concept uses the principles of statistical optimization and unites diverse retrieval techniques into a single flexible inversion procedure. It is particularly useful for choosing and refining a priori constraints in the retrieval algorithm. For example, it is demonstrated that a priori limitations on the partial derivatives of retrieved characteristics, which are widely used in atmospheric remote sensing, can also be useful in inverse modeling for constraining time and space variability of the retrieved global aerosol emissions. The similarities and differences with the standard “Kalman filter” inverse modeling approach and the “Phillips-Tikhonov-Twomey” constrained inversion widely used in remote sensing are discussed. In order to retain the originally high space and time resolution of the global model in the inversion of a long record of observations, the algorithm was expressed using adjoint operators in a form convenient for practical development of the inversion from codes implementing forward model simulations.

The inversion algorithm was implemented using the GOCART aerosol transport model. The numerical tests we conducted showed successful retrievals of global aerosol emissions with a $2^\circ \times 2.5^\circ$ resolution by inverting the GOCART output. For achieving satisfactory retrieval from satellite sensors such as MODIS, the emissions were assumed constant within the 24 h diurnal cycle and aerosol differences in chem-

Retrieving global sources of aerosols from MODIS observations

O. Dubovik et al.

Title Page

Abstract

Introduction

Conclusions

References

Tables

Figures

⏪

⏩

◀

▶

Back

Close

Full Screen / Esc

Printer-friendly Version

Interactive Discussion

ical composition were neglected. Such additional assumptions were needed to constrain the inversion due to limitations of satellite temporal coverage and sensitivity to aerosol parameters. As a result, the algorithm was defined for the retrieval of emission sources of fine and coarse mode aerosols from the MODIS fine and coarse mode aerosol optical thickness data respectively. Numerical tests showed that such assumptions are justifiable, taking into account the accuracy of the model and observations and that it provides valuable retrievals of the location and the strength of the aerosol emissions. The algorithm was applied to MODIS observations during two weeks in August 2000. The global placement of fine mode aerosol sources retrieved from inverting MODIS observations was coherent with available independent knowledge. This was particularly encouraging since the inverse method did not use any a priori information about the sources and it was initialized under a “zero aerosol emission” assumption. The retrieval reproduced the instantaneous global MODIS observations with a standard deviation in fitting of aerosol optical thickness of ~ 0.04 . The optical thickness during high aerosol loading events was reproduced with a standard deviation of $\sim 48\%$. Applications of the algorithm for the retrieval of coarse mode aerosol emissions were less successful, mainly due to the currently existing lack of MODIS data over high reflectance desert dust sources.

Possibilities for enhancing the global satellite data inversion by using diverse a priori constraints on the retrieval are demonstrated. The potential and limitations of applying our approach for the retrieval of global aerosol sources from aerosol remote sensing are discussed.

1 Introduction

Knowledge of the global distribution of tropospheric aerosols is important for studying the effects of aerosols on global climate. Satellite remote sensing is the most promising approach to collect information about global distributions of aerosol (King et al., 1999; Kaufman et al., 2002). However, in spite of recent advances in space technology, the

Retrieving global sources of aerosols from MODIS observations

O. Dubovik et al.

Title Page

Abstract

Introduction

Conclusions

References

Tables

Figures

⏪

⏩

◀

▶

Back

Close

Full Screen / Esc

Printer-friendly Version

Interactive Discussion

satellite data do not yet provide the required accuracy and details of time and space variability of aerosol properties. Tropospheric aerosol may have strong local variations and any single satellite needs at least several days of observations to provide global nearly cloudless images. Also, satellite characterization of aerosol is limited to day-time clear-sky conditions. Comprehensive global simulations of atmospheric aerosols with adequate time and space resolution can be obtained using global models that rely on estimated emissions and account for aerosol transport and removal processes. At present, there are a number of well-established Global Circulation Models (GCMs) – that generate their own meteorology (e.g. models by Roechner et al., 1996; Tegen et al., 1997, 2000; Koch et al., 1999; Koch, 2001; Ghan et al., 2001a, b; Reddy and Boucher, 2004) and Chemical Transport Models (CTMs) – that adopt the meteorological data (e.g. models by Balkanski et al., 1993; Chin et al., 2000, 2002; Ginoux et al., 2001; Takamura et al., 2000, 2002). However, the accuracy of global aerosol models is limited by uncertainties in estimates of aerosol emission sources, knowledge of atmospheric processes and the meteorological field data utilized. As a result, even the most recent models are mainly expected to capture only the principal global features of aerosol transport, while the quantitative estimates of average regional properties of aerosol may disagree between different models by magnitudes exceeding the uncertainty of remote sensing aerosol observations (e.g. see Kinne et al., 2003, 2006; Sato et al., 2003). Therefore, there are diverse continuing efforts focused on harmonizing and improving global aerosol modeling by refining all modeling components including meteorology, atmospheric processes and emissions. The availability of aerosol remote sensing products, especially global aerosol fields provided by satellite observations, is of critical importance for verifying and constraining aerosol modeling. For example, the direct comparisons of model outputs with observed aerosol properties are used for evaluating model accuracy and for identification of possible modeling problems (e.g. Takamura et al., 2000; Chin et al., 2002, 2003, 2004; Kinne et al., 2003, 2006). The observations can also be used as input for elaborate mathematical procedures that constrain and adjust tracer transport models by optimizing the agreement between

Retrieving global sources of aerosols from MODIS observations

O. Dubovik et al.

Title Page

Abstract

Introduction

Conclusions

References

Tables

Figures

⏪

⏩

◀

▶

Back

Close

Full Screen / Esc

Printer-friendly Version

Interactive Discussion

model predictions and the observations. For example, model predictions can be adjusted and enhanced by assimilating observations into the model. Collins et al. (2000, 2001) improved regional aerosol model predictions by assimilating the available satellite retrievals of aerosol optical thickness. Weaver et al. (2006) suggested a procedure for assimilating atmospheric radiances measured from satellite into the aerosol field produced by the GOCART global transport model. Another way of improving global aerosol modeling is retrieving (or adjusting) aerosol emissions from available observations by inverting a global model. Such an approach is particularly promising because the knowledge of aerosol emission sources is widely recognized as a major factor in limiting the accuracy of global aerosol modeling. Inversion techniques have been shown to be rather effective for refining the fidelity of the trace gas chemical modeling (e.g. Kaminski et al., 1999b; Khattatov et al., 2000; Kasibhatla et al., 2000; Elbern et al., 1997; Para et al., 2003). However, implementing the same techniques for inverting aerosol models appears to be more challenging. Indeed, a description of the aerosol field generally requires a larger number of parameters compared to a description of atmospheric gases, partly because of relatively high temporal and spatial variability (see discussion in Sect. 2.5). Additionally, direct implementation of basic inversion methods (that use the Jacobi matrices of first derivatives) is computationally demanding and, therefore, hardly applicable in aerosol global modeling. In these regards, designing an inversion on the basis of adjoint operators is rather promising. The adjoint operators (Marchuk, 1977, 1986; Cacuci, 1981; Tarantolla, 1987) allow direct calculation (without explicit usage of Jacobi matrices) of gradients of the quadratic form with respect to model input parameters. Such calculations have similar computational requirements to those of forward modeling. Correspondingly, the model inversion can be successfully implemented via adjoint operators provided the speed of the gradient method convergence is acceptable. The adjoint techniques are widely used in meteorology and oceanography for data assimilation (Le Dimet and Talagrand, 1986; Talagrand and Courtier, 1987; Courtier and Talagrand, 1987; Navon, 1997; etc.) and have been successfully applied for atmospheric gases inverse modeling applications (Kaminski et al.,

Retrieving global sources of aerosols from MODIS observations

O. Dubovik et al.

Title Page

Abstract

Introduction

Conclusions

References

Tables

Figures

⏪

⏩

◀

▶

Back

Close

Full Screen / Esc

Printer-friendly Version

Interactive Discussion

1999a; Elbern et al., 2000; Menut et al., 2000, Vukicevic and Hess, 2000; Vautard et al., 2000; Elbern and Schmidt, 2001; Schmidt and Martin, 2003; Menut, 2003). Hakami et al. (2005) used an adjoint approach for the retrieval of regional sources of black carbon from aircraft, shipboard and surface measured black carbon data collected during the ACE-Asia field campaign. Our paper explores the possibility of deriving the global distribution and strength of aerosol emission sources from satellite observations. We are employing the adjoint approach for implementing an inversion of an aerosol transport model. Figure 1 illustrates the general retrieval concept. In addition we analyze possible parallels and analogies between inverse modeling and retrieval approaches widely used in atmospheric remote sensing. Such analyses may be helpful for adopting some efficient methods developed in remote sensing applications into inverse modeling. For example, numerous remote sensing applications utilize the *Phillips-Tikhonov-Twomey* inversion technique developed in early sixties by Phillips (1962), Tikhonov (1963) and Twomey (1963). The technique suggests constraining ill-posed problems by using a priori limitations on the derivatives of the retrieved function. Here, we discuss the possibility to constrain temporal and/or spatial aerosol variability by applying a priori limitations of the derivatives of aerosol mass with respect to time and space coordinates. Also, we are formulating the inversion problem as a multi-term least squares approach. This approach is convenient for utilizing multiple a priori constraints in the same retrieval (Dubovik, 2004).

Our approach resulted in an algorithm that retrieves global aerosol sources by inverting the Goddard Chemistry Aerosol Radiation and Transport (GOCART) model. The performance of the algorithm is illustrated by numerical tests, as well as by applications of the algorithm to actual satellite observations. We demonstrate the possibility of deriving global aerosol emissions from MODIS aerosol observations. The algorithm potentials and limitations are discussed.

Retrieving global sources of aerosols from MODIS observations

O. Dubovik et al.

[Title Page](#)[Abstract](#)[Introduction](#)[Conclusions](#)[References](#)[Tables](#)[Figures](#)[⏪](#)[⏩](#)[◀](#)[▶](#)[Back](#)[Close](#)[Full Screen / Esc](#)[Printer-friendly Version](#)[Interactive Discussion](#)

2 Methodology of inverse modeling

The spatial and temporal behavior of atmospheric constituents is simulated in chemistry models by solving the continuity equation (Brasseur et al., 1999; Jacob, 1999):

$$\frac{\partial m}{\partial t} = -\mathbf{v} \cdot \nabla m + \left(\frac{\partial m}{\partial t} \right)_{\text{diff}} + \left(\frac{\partial m}{\partial t} \right)_{\text{conv}} + S - R, \quad (1)$$

5 where \mathbf{v} is the transport velocity vector, m is mass (suffixes “diff” and “conv” denote turbulent diffusivity and convection, respectively). S and R denote source and loss terms respectively. The characteristics m , \mathbf{v} , S and R in Eq. (1) are explicit functions of time t and spatial coordinates $\mathbf{x}=(x, y, z)$. The continuity equation does not yield a general analytical solution and is usually solved numerically by using discrete analogues. The
10 different component processes in the numerical equivalent of Eq. (1) are isolated and treated sequentially for each time step Δt (e.g. see Jacob, 1999):

$$m(t + \Delta t, \mathbf{x}) = T(t, \mathbf{x}) (m(t, \mathbf{x}) + s(t, \mathbf{x})) \Delta t, \quad (2)$$

where $s(t, \mathbf{x})$ – mass emission, $T(t, \mathbf{x})$ – transport operator that can be approximated as:

$$15 \quad T(t, \mathbf{x}) = T_n T_{n-1} \dots T_3 T_2 T_1, \quad (3)$$

and T_i ($i=1, \dots, n$) are operators of isolated transport processes such as advection, diffusion, convection, wet scavenging, etc. Thus, the calculation of mass at any given time can be reduced to numerical integration of known transport and source functions:

$$m(t, \mathbf{x}) = \int_{t_0}^t T(t', \mathbf{x}) (m(t', \mathbf{x}) + s(t', \mathbf{x})) dt'. \quad (4)$$

20 If the transport operator $T(t, \mathbf{x})$ is linear, Eq. (4) can be equivalently written via matrix equation:

$$\mathbf{M} = \mathbf{T} (\mathbf{M}_0 + \mathbf{S}), \quad (5)$$

Retrieving global sources of aerosols from MODIS observations

O. Dubovik et al.

Title Page

Abstract

Introduction

Conclusions

References

Tables

Figures

⏪

⏩

◀

▶

Back

Close

Full Screen / Esc

Printer-friendly Version

Interactive Discussion

Retrieving global sources of aerosols from MODIS observations

O. Dubovik et al.

Title Page

Abstract

Introduction

Conclusions

References

Tables

Figures

⏪

⏩

◀

▶

Back

Close

Full Screen / Esc

Printer-friendly Version

Interactive Discussion

where \mathbf{M}_0 is a vector of mass values in all locations at time t_0 ; \mathbf{M} and \mathbf{S} are correspondingly the vectors of mass and emission values at all locations and considered times $t_0, t_1, \dots, t_{n-1}, t_n$; \mathbf{T} is the coefficient matrix defining the transport of mass to each location \mathbf{x} and time step t_k from all locations \mathbf{x} and previous time steps $t_{i < n}$.

Thus, the source vector can be retrieved by solving the matrix equation if the mass measurements $\mathbf{M}^{\text{meas}} = \mathbf{M} + \mathbf{\Delta}_M$ are available.

2.1 Statistical optimization of linear inversion

If the statistical behavior of the errors $\mathbf{\Delta}_M$ is known one can use this knowledge to optimize the solution of Eq. (5). In that way, the solution $\hat{\mathbf{S}}$ should not only closely reproduce observations \mathbf{M}^{meas} but also the remaining deviations $\hat{\mathbf{\Delta}}_M = \mathbf{M}^{\text{meas}} - \mathbf{M}(\hat{\mathbf{S}})$ should have a distribution close to the expected error properties described by the Probability Density Distribution (PDF) of errors $P(\mathbf{\Delta}_M)$. According to the well-known Method of Maximum Likelihood (MML) the optimum solution $\hat{\mathbf{S}}$ corresponds to a maximum of the PDF as follows (e.g. Edie et al., 1971):

$$P(\mathbf{\Delta}_M) = P(\mathbf{M}^{\text{meas}} - \mathbf{M}(\mathbf{S})) = P(\mathbf{M}(\mathbf{S}) | \mathbf{M}^{\text{meas}}) = \max. \quad (6)$$

Where PDF $P(\mathbf{M}(\mathbf{S}) | \mathbf{M}^{\text{meas}})$ written as a function of retrieval parameters \mathbf{S} for given set of available observations \mathbf{M}^{meas} is known as a Likelihood Function. The MML is a fundamental principle of statistical estimation that provides a statistically optimum solution in many senses. For example, the asymptotical error distribution (infinite number of Δ_M realizations) of MML estimates has the smallest possible variances. Most statistical properties of the MML solution remain optimal for a limited number of observations (e.g. see Edie et al., 1971). The normal (or Gaussian) distribution is widely considered as the best model for describing actual error distribution (Tarantola, 1987; Edie et al., 1971; etc.):

$$P(\mathbf{M}(\mathbf{S}) | \mathbf{M}^{\text{meas}}) = ((2\pi)^m \det(\mathbf{C}_M))^{-1/2} \exp\left(-\frac{1}{2} (\mathbf{M}(\mathbf{S}) - \mathbf{M}^{\text{meas}})^T \mathbf{C}_M^{-1} (\mathbf{M}(\mathbf{S}) - \mathbf{M}^{\text{meas}})\right), \quad (7)$$

where $(\dots)^T$ denotes matrix transposition, \mathbf{C}_M is the covariance matrix of Δ_M , $\det(\mathbf{C})$ denotes the determinant of \mathbf{C}_M , and m is the dimension of the vectors $\mathbf{M}(\mathbf{S})$ and \mathbf{M}^{meas} . The maximum of the PDF exponential term in Eq. (7) corresponds to the minimum of the quadratic form in the exponent. Therefore, the MML solution is a vector $\hat{\mathbf{S}}$ corresponding to the minimum of the following quadratic form:

$$\Psi(\mathbf{S}) = \frac{1}{2} (\mathbf{M}(\mathbf{S}) - \mathbf{M}^{\text{meas}})^T \mathbf{C}_M^{-1} (\mathbf{M}(\mathbf{S}) - \mathbf{M}^{\text{meas}}) = \min. \quad (8)$$

Thus, with the assumption of normal noise, the MML principle requires searching for a minimum in the product of the squared terms of $(\mathbf{M}^{\text{meas}} - \mathbf{M}(\mathbf{S}))$ in Eq. (7). This is the basis for the widely known Least Square Method (LSM).

For linear $\mathbf{M}(\mathbf{S})$ (as in Eq. 5) the LSM solution can be written as (e.g. Rao, 1965):

$$\hat{\mathbf{S}} = (\mathbf{T}^T \mathbf{C}_m^{-1} \mathbf{T})^{-1} \mathbf{T}^T \mathbf{C}_m^{-1} \mathbf{M}^* \quad (9)$$

Here, \mathbf{M}^* – vector of measurements corrected by the effect of the aerosol mass \mathbf{M}_0 presented in the atmosphere prior observations i.e. $\mathbf{M}^* = \mathbf{M}^{\text{meas}} - \mathbf{T}\mathbf{M}_0$.

2.2 Inversion constrained by a priori estimates of unknowns

If the problem is ill-posed and Eq. (5) does not have a unique solution, then some a priori constraints need to be applied. The expected distribution of sources is commonly used as an a priori constraint in inverse modeling. In that case the inversion can be considered as a joint solution of Eq. (5) and constraining a priori the system:

$$\begin{cases} \mathbf{M}^{\text{meas}} = \mathbf{M}(\mathbf{S}) + \Delta_M \\ \mathbf{S}^* = \mathbf{S} + \Delta_S \end{cases}, \quad (10)$$

where $\mathbf{S}^* = \mathbf{S} + \Delta_S$ is a vector of a priori estimates of the sources and Δ_S is vector of the errors that usually considered statistically independent of Δ_M and normally distributed

Retrieving global sources of aerosols from MODIS observations

O. Dubovik et al.

Title Page

Abstract

Introduction

Conclusions

References

Tables

Figures

◀

▶

◀

▶

Back

Close

Full Screen / Esc

Printer-friendly Version

Interactive Discussion

with zero means and covariance matrix \mathbf{C}_S . For solving Eq. (10), MML should be applied to the joint PDF of the measurements and a priori estimates:

$$P(\mathbf{M}(\mathbf{S})|\mathbf{M}^{\text{meas}}, \mathbf{S}^*) = P(\mathbf{M}(\mathbf{S})|\mathbf{M}^{\text{meas}})P(\mathbf{S}|\mathbf{S}^*) = \max, \quad (11a)$$

i.e.

$$P(\mathbf{M}(\mathbf{S})|\mathbf{M}^{\text{meas}}, \mathbf{S}^*) \sim \exp\left(-\frac{1}{2}\left(\Delta\mathbf{M}^T\mathbf{C}_m^{-1}\Delta\mathbf{M}\right)\right)\exp\left(-\frac{1}{2}\left(\Delta\mathbf{S}^T\mathbf{C}_S^{-1}\Delta\mathbf{S}\right)\right) = \max, \quad (11b)$$

where $\Delta\mathbf{M}=\mathbf{M}(\mathbf{S})-\mathbf{M}^*$ and $\Delta\mathbf{S}=\mathbf{S}-\mathbf{S}^*$.

Accordingly, the MML solution of joint Eq. (11) corresponds to a minimum of the following quadratic form:

$$2\Psi(\mathbf{S}) = 2(\Psi_m + \Psi_S) = \Delta\mathbf{M}^T\mathbf{C}_m^{-1}\Delta\mathbf{M} + \Delta\mathbf{S}^T\mathbf{C}_S^{-1}\Delta\mathbf{S}. \quad (12)$$

Thus, in difference Eq. (8), utilizing a priori constraints requires simultaneous minimization both measurement term $2\Psi_m$ and a priori term $2\Psi_S$.

The solution providing a minimum of Eq. (12) can be found using the following equations:

$$\hat{\mathbf{S}} = \left(\mathbf{T}^T\mathbf{C}_m^{-1}\mathbf{T} + \mathbf{C}_S^{-1}\right)^{-1}\left(\mathbf{T}^T\mathbf{C}_m^{-1}\mathbf{M}^* + \mathbf{C}_S^{-1}\mathbf{S}^*\right), \quad (13a)$$

OR

$$\hat{\mathbf{S}} = \mathbf{S}^* - \mathbf{C}_S\mathbf{T}^T\left(\mathbf{C}_m + \mathbf{T}\mathbf{C}_S^{-1}\mathbf{T}^T\right)^{-1}\left(\mathbf{T}\mathbf{S}^* - \mathbf{M}^*\right). \quad (13b)$$

The covariance matrix of estimates $\hat{\mathbf{S}}$ also can be obtained by using two formally equivalent formulations:

$$\mathbf{C}_{\hat{\mathbf{S}}} = \left(\mathbf{T}^T\mathbf{C}_m^{-1}\mathbf{T} + \mathbf{C}_S^{-1}\right)^{-1}, \quad (14a)$$

OR

$$\mathbf{C}_{\hat{\mathbf{S}}} = \mathbf{C}_S - \mathbf{C}_S\mathbf{T}^T\left(\mathbf{C}_m + \mathbf{T}\mathbf{C}_S^{-1}\mathbf{T}^T\right)^{-1}\mathbf{T}\mathbf{C}_S \quad (14b)$$

Retrieving global sources of aerosols from MODIS observations

O. Dubovik et al.

Title Page

Abstract

Introduction

Conclusions

References

Tables

Figures

⏪

⏩

◀

▶

Back

Close

Full Screen / Esc

Printer-friendly Version

Interactive Discussion

Most of efforts in deriving emission sources and in general assimilation of geophysical parameters rely on these basic equations (e.g. Hartley and Prinn, 1993; Elbern et al., 1997; Dee and Da Silva, 1998; Khattatov et al., 2000; Kasibhatla et al., 2000; Para et al., 2003).

Equations (13a) and (13b), as well as Eqs. (14a) and (14b) are considered as generally equivalent (e.g. see Tarantola, 1987). One of the important differences is that the matrix $(\mathbf{T}^T \mathbf{C}_m^{-1} \mathbf{T} + \mathbf{C}_S^{-1})$ inverted in Eqs. (13a) and (14a) has dimension N_S (number of retrieved parameters) while $(\mathbf{C}_m + \mathbf{T} \mathbf{C}_S \mathbf{T}^T)$ inverted in Eqs. (13b) and (14b) has the dimension N_m (number of measurements). In these regards, the pairs of Eqs. (13) and (14) are fully equivalent for the situation when $N_m = N_S$. Equations (13a) and (14a) are preferable for inverting redundant measurements ($N_m > N_S$), whereas Eqs. (13b) and (14b) are preferable for an inverting underdetermined measurement set ($N_m < N_S$). Indeed, Eq. (13a) directly relates to LSM Eq. (9), the estimate $\hat{\mathbf{S}}$ is mostly determined by the measurement term $\mathbf{T}^T \mathbf{C}_m^{-1} \mathbf{M}^*$ and a generally minor a priori term is mainly expected to provide uniqueness and stability of the solution. In contrast, in Eq. (13b) the solution $\hat{\mathbf{S}}$ is expressed in the form of an a priori estimate \mathbf{S}^* corrected or “filtered” by measurements, which is the situation when the small number measurements N_m ($N_m < N_S$) cannot fully determine the set of unknowns a, but can improve the a priori assumed values \mathbf{S}^* . Also, it should be noted that in our consideration, the problem of source retrieval as it is formulated by Eq. (5) assumes the simultaneous retrieval of the entire vector \mathbf{S} that includes global emission sources for the entire time period considered. However, often the problem of emission retrievals (e.g. Hartley and Prinn, 1993) and data assimilation in general (Dee and Da Silva, 1998; Khattatov et al., 2000) is formulated as a time sequential correction of the known parameter field by observations where the optimal estimation Eq. (13b) is used to optimize the forecast of $\mathbf{S}(t_j)$, i.e. emission at time t_j , on the basis of the known values for the emission at previous time t_{j-1} :

$$\mathbf{S}_t = \mathbf{S}_{t-1} - \mathbf{C}_{S_{t-1}} \mathbf{T}_t^T (\mathbf{C}_{m_{t+1}} + \mathbf{T}_t \mathbf{C}_{S_{t-1}}^{-1} \mathbf{T}_t^T)^{-1} (\mathbf{T}_t \mathbf{S}_t - \mathbf{M}_{t+1}^*), \quad (15a)$$

3639

Retrieving global sources of aerosols from MODIS observations

O. Dubovik et al.

Title Page

Abstract

Introduction

Conclusions

References

Tables

Figures

⏪

⏩

◀

▶

Back

Close

Full Screen / Esc

Printer-friendly Version

Interactive Discussion

and the covariance matrix \mathbf{C}_{S_t} is the following:

$$\mathbf{C}_{S_t} = \mathbf{C}_{S_{t-1}} - \mathbf{C}_{S_{t-1}} \mathbf{T}_t^T \left(\mathbf{C}_{M_{t+1}} + \mathbf{T}_t \mathbf{C}_{S_{t-1}}^{-1} \mathbf{T}_t^T \right)^{-1} \mathbf{T}_t \mathbf{C}_{S_{t-1}}. \quad (15b)$$

where the index “ t ” indicates that the vectors are associated with time step t . Correspondingly the Eqs. (15) do not solve Eq. (5) directly but it searches the solution by solving the sequence of the following equations formulated for a single time step:

$$\mathbf{M}_{t+1}^* = \mathbf{M}_{t+1}^{\text{meas}} - \mathbf{T}_t \mathbf{M}_t = \mathbf{T}_t \mathbf{S}_t, \quad (16)$$

where $\mathbf{M}_{t+1}^* = \mathbf{M}_{t+1}^{\text{meas}} - \mathbf{T}_t \mathbf{M}_t$ – vector of mass measured at time step $t+1$ corrected by the effect of the aerosol mass \mathbf{M}_t presented in the atmospheres at the previous time step t ; \mathbf{S}_t – vector of emission source at time step t , \mathbf{T}_t – matrix describing the transport of aerosol mass from time step t to time step $t+1$. The vectors \mathbf{S}_t and \mathbf{M}_t relate to vectors \mathbf{S} and \mathbf{M} used in Eq. (5) as follows:

$$\mathbf{S}^T = (\mathbf{S}_{t+n}, \dots, \mathbf{S}_{t+1}, \mathbf{S}_t)^T \text{ and } \mathbf{M}^T = (\mathbf{M}_{t+n}, \dots, \mathbf{M}_{t+1}, \mathbf{M}_t)^T. \quad (17)$$

The relationship between matrix \mathbf{T}_t and \mathbf{T} can be seen in the Appendix from Eq. (B5).

Correspondingly, instead of the joint system given by Eq. (10), Eqs. (15) solve the following joint system:

$$\begin{cases} \mathbf{M}_{t+1}^{\text{meas}} = \mathbf{M}_t (\mathbf{S}_t) + \mathbf{\Delta}_M \\ \mathbf{S}_t^* = \mathbf{S}_{t-1} + \mathbf{\Delta}_S \end{cases}, \quad (18)$$

where the second line describes an a priori assumption of continuity between emissions at time steps t and $t-1$. (Note that in Eq. (10) the a priori estimates \mathbf{S}^* do not directly assume such continuity). The solution given by Eqs. (15) corresponds to a minimum of the following quadratic form:

$$2 \Psi_{t+1}(\mathbf{S}_t) = \Delta \mathbf{M}_{t+1}^T \mathbf{C}_{M_{t+1}}^{-1} \Delta \mathbf{M}_{t+1} + \Delta \mathbf{S}_t^T \mathbf{C}_{S_{t-1}}^{-1} \Delta \mathbf{S}_t, \quad (19)$$

where $\Delta \mathbf{M}_{t+1} = \mathbf{T}_t \mathbf{S}_t - \mathbf{M}_{t+1}^*$ and $\Delta \mathbf{S}_t = \mathbf{S}_t - \mathbf{S}_{t-1}$.

Retrieving global sources of aerosols from MODIS observations

O. Dubovik et al.

Title Page

Abstract

Introduction

Conclusions

References

Tables

Figures

⏪

⏩

◀

▶

Back

Close

Full Screen / Esc

Printer-friendly Version

Interactive Discussion

This sequential correction (filtering) given by Eqs. (15) are widely known as a “Kalman filter” named after the author (Kalman, 1960) who originated the technique for engineering purposes.

The constrained inversion techniques are also widely used in remote sensing for retrieving vertical profiles of atmospheric properties (pressure, temperature, gaseous concentrations, etc.), where Eqs. (13–14) are associated with the studies by Strand and Westwater (1968) and Rodgers (1976). It should be noted that in remote sensing Eq. (13b) is not related to a sequential time retrieval (as considered by Kalman, 1960), but instead it is formulated Rodgers (1976) for retrieval of the entire vector \mathbf{S} of unknowns as given by Eq. (17). The important difference between Eqs. (13b), (14b) and the Kalman filter Eq. (15) is that the solution \mathbf{S}_t by Eq. (15) is influenced only by the observations performed at one time step $t+1$, while in Eqs. (13b), (14b) (as well as in Eqs. 13a, 14a) the component $\hat{\mathbf{S}}_t$ of the entire solution $\hat{\mathbf{S}}$ can be influenced by the observations of aerosol performed at later time steps.

2.3 Inversion constrained by a priori smoothness constraints (limiting derivatives of the solution)

Equations (13–14) show only one group of methods for the constrained inversion. For example, numerous atmospheric remote sensing retrievals are based on the constrained inversion approach originated in the studies by Phillips (1962), Tikhonov (1963) and Twomey (1963). If one formally applies the Phillips-Tikhonov-Twomey approach for solving Eq. (5), the solution would be the following:

$$\hat{\mathbf{S}} = (\mathbf{T}^T \mathbf{T} + \gamma \Omega)^{-1} \mathbf{T}^T \mathbf{M}^*, \quad (20)$$

Retrieving global sources of aerosols from MODIS observations

O. Dubovik et al.

Title Page

Abstract

Introduction

Conclusions

References

Tables

Figures

⏪

⏩

◀

▶

Back

Close

Full Screen / Esc

Printer-friendly Version

Interactive Discussion

where \mathbf{D}_n is the matrix of n -th differences:

$$\begin{aligned}\Delta^1 &= S_{i+1} - S_i, & (n = 1), \\ \Delta^2 &= S_{i+2} - 2S_{i+1} + S_i, & (n = 2), \\ \Delta^3 &= S_{i+3} - 3S_{i+2} + 3S_{i+1} - S_i, & (n = 3).\end{aligned}\tag{25}$$

For example, matrix \mathbf{D}_2 of the second differences is the following:

$$\mathbf{D}_2 = \begin{pmatrix} 1 & -2 & 1 & 0 & \dots & & \\ 0 & 1 & -2 & 1 & 0 & \dots & \\ 0 & 0 & 1 & -2 & 1 & 0 & \dots \\ & & & \dots & & & \\ & & & & \dots & 0 & 1 & -2 & 1 \end{pmatrix}.\tag{26}$$

5 The correspondent smoothness matrix $\Omega_2 = \mathbf{D}_2^T \mathbf{D}_2$ is given by Eq. (21).

Thus, in many remote sensing applications where one parameter functions $S(x_i)$ are retrieved using smoothness constrained as shown in Eq. (20) is fruitful and popular. For example, such constraints are widely utilized in the retrieval of aerosol concentration size distributions (e.g. Twomey, 1977; King et al., 1978; Nakajima et al., 1996; Dubovik and King, 2000, etc.).

10

Using a priori limitations on the derivatives (shown above) does not seem to be popular and well accepted in geophysical parameters data assimilation and inversion of tracer modeling. (Although, such constraint is certainly included in general formulations of assimilation techniques (e.g. Navon, 1997).) One of the many reason is probably the fact that tracer modeling deals with generally 4-dimensional characteristics. For example, unknown vector \mathbf{S} in Eq. (5) represent global aerosol sources. Correspondingly, instead of one parametric function shown by Eq. (23), we should consider vector \mathbf{S} as discrete equivalent of 4-parametric function:

15

$$S_i = S(t_i, x_j, y_k, z_m),\tag{27}$$

Retrieving global sources of aerosols from MODIS observations

O. Dubovik et al.

Title Page

Abstract

Introduction

Conclusions

References

Tables

Figures

⏪

⏩

◀

▶

Back

Close

Full Screen / Esc

Printer-friendly Version

Interactive Discussion

Retrieving global sources of aerosols from MODIS observations

O. Dubovik et al.

Title Page

Abstract

Introduction

Conclusions

References

Tables

Figures

⏪

⏩

◀

▶

Back

Close

Full Screen / Esc

Printer-friendly Version

Interactive Discussion

i.e. vector \mathbf{S} has $N_t \times N_x \times N_y \times N_z$ total number of elements, where N_t, N_x, N_y and N_z are the total numbers of discrete points for correspondent coordinates t, x, y and z . Obviously, the variability of emission $S(t, x, y, z)$ with time t , vertically with z and horizontally with y and x does not have to be the same. This is why, using single smoothness term in Eq. (22) with single smoothness matrix Ω as the one given in Eq. (21) is not appropriate for constraining the retrieval of four dimensional characteristic $S(t, x, y, z)$. At the same time, some temporal and spatial horizontal and vertical continuity of aerosol emission (the same is applicable for most of geophysical parameters) can naturally be expected. Therefore, applying smoothness constraints on variability of $S(t, x, y, z)$ with each single coordinate instead of using single variability constraint can be useful. However, that would require using several constraints simultaneously. The possible approach for using multiple constraints is discussed in studies by Dubovik and King (2000) and Dubovik (2004).

2.4 Constrained inversion within multi-term LSM

Dubovik and King (2000) and Dubovik (2004) demonstrated that Eqs. (13a) and (20) can be naturally derived and generalized by considering inversions with a priori constraints as a version of multi-term LSM. Formally, both measured and a priori data can be written as

$$\mathbf{f}_k^* = \mathbf{f}_k(\mathbf{a}) + \Delta \mathbf{f}_k, \quad (k = 1, 2, \dots, K), \quad (28)$$

where index k denotes different data sets. This assumes that the data from the same data set have similar error structure independent of errors in the data from other sets. Assuming that $\Delta \mathbf{f}_k$ normally distributed with covariance matrices \mathbf{C}_k , then the MML optimum solution of Eq. (28) corresponds to the minimum of the following quadratic form:

$$2\Psi(\mathbf{a}) = \sum_{k=1}^K (\Delta \mathbf{f}_k)^T (\mathbf{C}_k)^{-1} (\Delta \mathbf{f}_k) = \min \sum_{k=1}^K \gamma_k (\Delta \mathbf{f}_k)^T (\mathbf{W}_k)^{-1} (\Delta \mathbf{f}_k) = 2 \sum_{k=1}^K \gamma_k \Psi_k(\mathbf{a}) = \min \quad , \quad (29)$$

Retrieving global sources of aerosols from MODIS observations

O. Dubovik et al.

Title Page

Abstract

Introduction

Conclusions

References

Tables

Figures

◀

▶

◀

▶

Back

Close

Full Screen / Esc

Printer-friendly Version

Interactive Discussion

where $\Delta \mathbf{f}_k = \mathbf{f}_k(\mathbf{a}) - \mathbf{f}_k^*$

$$\mathbf{W}_k = \frac{1}{\varepsilon_k^2} \mathbf{C}_k \text{ and } \gamma_k = \frac{\varepsilon_1^2}{\varepsilon_k^2}. \quad (30)$$

Here ε_k^2 is the first diagonal element of \mathbf{C}_k , i.e. $\varepsilon_k^2 = \{\mathbf{C}_k\}_{11}$. Using weighting matrix \mathbf{W}_k is, in principle, equivalent to using covariance matrices \mathbf{C}_k , although sometimes it is more convenient because it shows that since the absolute value of the minimum in Eq. (29) is not prescribed, the minimization depends only on relative contribution of each term Ψ_k into total Ψ . The Lagrange parameters γ_k are weighting the contribution of each source relative to the contribution of first data source (obviously, $\gamma_1=1$). The minimum of the multi-term quadratic form given by Eq. (29) can be found by the multi-term equivalent of Eq. (9):

$$\hat{\mathbf{a}} = \left(\sum_{k=1}^K \gamma_k (\mathbf{K}_k)^T (\mathbf{W}_k)^{-1} (\mathbf{K}_k) \right)^{-1} \left(\sum_{k=1}^K \gamma_k (\mathbf{K}_k)^T (\mathbf{W}_k)^{-1} \mathbf{f}_k^* \right). \quad (31)$$

Correspondent covariance matrix can be estimated the following:

$$\mathbf{C}_{\hat{\mathbf{a}}} \approx \left(\sum_{k=1}^K \gamma_k (\mathbf{K}_k)^T (\mathbf{W}_k)^{-1} (\mathbf{K}_k) \right)^{-1} \hat{\varepsilon}^2, \quad (32)$$

where $\hat{\varepsilon}^2$ is estimated from obtained minimum of Ψ as: $\hat{\varepsilon}^2 = \Psi / (N_f - N_a)$, N_f – total number of elements $\{\mathbf{f}_k\}_j$ (in all sets \mathbf{f}_k), N_a – total number of unknown parameters a_j .

Using the above multi-term equations, one can formulate an inversion with smoothness constraints on variability of $S(t, x, y, z)$ with each single coordinate. Specifically, using such multiple smoothness constraints can be considered as solution of the fol-

lowing joint system:

$$\begin{cases} \mathbf{M}^{\text{meas}} = \mathbf{M}(\mathbf{S}) + \Delta_M \\ \mathbf{0}_t^* = \Delta_t^n(t, \mathbf{x}) + \Delta_t \\ \mathbf{0}_x^* = \Delta_x^n(t, \mathbf{x}) + \Delta_x \\ \mathbf{0}_y^* = \Delta_y^n(t, \mathbf{x}) + \Delta_y \\ \mathbf{0}_z^* = \Delta_z^n(t, \mathbf{x}) + \Delta_z \end{cases}, \quad (33)$$

where $\Delta^n(\dots)$ denotes n -th differences of aerosol sources regarding time or coordinates x , y or z . For example, for time coordinate t , second differences (Eq. 25) can be written as:

$$\{\Delta_t^2(t, \mathbf{x})\}_l = \Delta_t^2(t_i, x_j, y_k, z_m) = S(t_{i+1}, x_j, y_k, z_m) - 2S(t_i, x_j, y_k, z_m) + S(t_{i-1}, x_j, y_k, z_m). \quad (34a)$$

where the index l can be calculated, for example, as follows

$$l = (i - 1)N_x N_y N_z + (j - 1)N_y N_z + (k - 1)N_z + (m - 1). \quad (34b)$$

The second line in Eq. (33) states that differences $\Delta^n(t_i)$ are equal to zero with errors Δ_{t_i} . Accordingly, for $n=2$ the vectors $\mathbf{0}_t^*$, $\mathbf{\Delta}^2(t)$ and Δ_t consist of $(N_t - 2) \times N_x \times N_y \times N_z$ zeros, $\Delta_t^2(t_i, x_j, y_k, z_m)$ and Δ_{t_i} correspondingly. The 3rd, 4th and 5th lines in Eq. (33) are defined by the same way for coordinates x , y or z correspondingly. Assuming that Δ_t , Δ_x , Δ_y and Δ_z are normally distributed with zero means and diagonal covariance matrices $\mathbf{C}_t = \varepsilon_t^2 \mathbf{I}_t$, $\mathbf{C}_x = \varepsilon_x^2 \mathbf{I}_x$, $\mathbf{C}_y = \varepsilon_y^2 \mathbf{I}_y$ and $\mathbf{C}_z = \varepsilon_z^2 \mathbf{I}_z$, the multi-term LSM solution of Eq. (33) can be the following:

$$\hat{\mathbf{S}} = \left(\mathbf{T}^T \mathbf{W}_m^{-1} \mathbf{T} + \gamma_t \Omega_t + \gamma_x \Omega_x + \gamma_y \Omega_y + \gamma_z \Omega_z \right)^{-1} \mathbf{T}^T \mathbf{W}_m^{-1} \mathbf{M}^*, \quad (35)$$

where

$$\mathbf{W}_m = \frac{1}{\varepsilon_m^2} \mathbf{C}_m, \quad \gamma_t = \frac{\varepsilon_t^2}{\varepsilon_m^2}, \quad \gamma_x = \frac{\varepsilon_x^2}{\varepsilon_m^2}, \quad \gamma_y = \frac{\varepsilon_y^2}{\varepsilon_m^2}, \quad \gamma_z = \frac{\varepsilon_z^2}{\varepsilon_m^2},$$

3646

Retrieving global sources of aerosols from MODIS observations

O. Dubovik et al.

Title Page

Abstract

Introduction

Conclusions

References

Tables

Figures

◀

▶

◀

▶

Back

Close

Full Screen / Esc

Printer-friendly Version

Interactive Discussion

and $\varepsilon_m^2 = \{\mathbf{C}_m\}_{11}$, $\varepsilon_t^2 = \{\mathbf{C}_t\}_{11}$, $\varepsilon_x^2 = \{\mathbf{C}_x\}_{11}$, $\varepsilon_y^2 = \{\mathbf{C}_y\}_{11}$ and $\varepsilon_z^2 = \{\mathbf{C}_z\}_{11}$. The matrices Ω are determined via correspondent matrices of n -th differences $\Omega = \mathbf{D}_n^T \mathbf{D}_n$. Equation (35) provides minimum of the following quadratic form:

$$2\Psi(\mathbf{S}) = 2\Psi_m(\mathbf{S}) + 2 \sum_{(q=t,x,y,z)} \gamma_q \Psi_q(\mathbf{S}) = 2(\Delta\mathbf{M})^T \mathbf{W}_m^{-1} \Delta\mathbf{M} + 2 \sum_{(q=t,x,y,z)} \gamma_q \mathbf{S}^T \Omega_q \mathbf{S}. \quad (36)$$

- 5 Each of the smoothness terms in this equation can be considered as discrete equivalent of norm of the n -th partial derivatives. For example, for the second term corresponding to time coordinate t one can write:

$$\Psi_t(\mathbf{S}) = \sum_{(i,j,k,m)} \left(\frac{\Delta_t^n(t_i, x_j, y_k, z_m)}{(\Delta t)^n} \right)^2 \Delta t \approx \Psi'_t(\mathbf{S}) = \int_{t_{\min}}^{t_{\max}} \left(\frac{\partial^n S(t, \mathbf{x})}{\partial t^n} \right)^2 dt \quad (37a)$$

and

$$10 \Psi_t(\mathbf{S}) = (\Delta t)^{1-n} (\mathbf{D}_{(n,t)} \mathbf{S})^T \mathbf{D}_{(n,t)} \mathbf{S} = (\Delta t)^{1-n} \mathbf{S}^T (\mathbf{D}_{(n,t)}^T \mathbf{D}_{(n,t)}) \mathbf{S} = (\Delta t)^{1-n} \mathbf{S}^T \Omega_t \mathbf{S}, \quad (37b)$$

where matrix $\mathbf{D}_{(n,t)}$ is the matrix of differences corresponding to n -th partial derivatives regarding time. For example, $\mathbf{D}_{(2,t)} \mathbf{S}$ would produce a vector with the elements equal to second differences as shown in Eq. (34).

- Thus, it was shown above that using multi-term LSM approach, one can use multiple
 15 smoothness constraints in the retrieval of emission sources. Therefore, it is possible utilize knowledge about typical time, horizontal and vertical variability of the emission as a priori constraints in the emission retrieval. As shown in Eqs. (33–37), such smoothness constraints are included as restrictions on n -th partial derivatives of $S(t, x, y, z)$ assuming zero values for correspondent differences in Eq. (33) and the values of Lagrange
 20 parameters determine variations from the zeros. The order of differences employed relates with character of expected variability, for example for one parameter function

$S(t)$ there are following relationships:

$$\begin{aligned}\Delta^1(t) \rightarrow S(t) &= \text{const} && \text{– constant,} \\ \Delta^2(t) \rightarrow S(t) &= A + Bt && \text{– straight line,} \\ \Delta^2(t) \rightarrow S(t) &= A + Bt + Ct^2 && \text{– parabola.}\end{aligned}\tag{38}$$

It can be noted that the constraints employed in Kalman filter Eq. (15) are equivalent to restricting first differences (see Eq. 18), i.e. a priori assuming linear continuity of source variability. In a contrast, using multiple constraints as in Eqs. (35–36) allows to use non-linear continuity as constraint that can be applied not only to time but also to space and vertical variability of emissions.

2.5 Inversion using adjoint equations

The methods analogous to Eq. (13) are used for retrieving sources of CO_2 from surface based and satellite observations (e.g. see Enting et al., 1995; Patra et al., 2003). However, direct implementation of Eqs. (9, 13) for retrieval of aerosol emission sources is not feasible due to very large dimensions of matrix \mathbf{T} and vectors \mathbf{S} and \mathbf{M} . For example, CO_2 emission sources can be assumed monthly or yearly constant for large geographic areas (e.g., Patra et al., 2003, used 22 and 53 global regions). The time and spatial variability of tropospheric aerosol and its emission is much higher. For aerosol, GOCART model (see below) has $2^\circ \times 2.5^\circ$ horizontal resolution (144 longitudes, 91 latitudes) and 30 vertical layers with possibility to have variable source in the each layer. Correspondingly, inversion of a few weeks of observations by Eqs. (9) or (13) requires one to deal with the vector \mathbf{S} having dimensions N_S far exceeding 200 000, even under conservative assumptions of near-surface daily independent sources. Performing direct operations of Eqs. (9, 13) with vectors and matrices of such high dimensionality is problematic. One possibility to avoid dealing with such large vectors and matrices is to perform inversion using sequential retrieval as the one given by Kalman filter formulation Eq. (15), where the retrieval uses generally smaller matrices and vectors containing values of parameters only at single time step t_i . However, in Kalman filter

Retrieving global sources of aerosols from MODIS observations

O. Dubovik et al.

Title Page

Abstract

Introduction

Conclusions

References

Tables

Figures

⏪

⏩

◀

▶

Back

Close

Full Screen / Esc

Printer-friendly Version

Interactive Discussion

Retrieving global sources of aerosols from MODIS observations

O. Dubovik et al.

Title Page

Abstract

Introduction

Conclusions

References

Tables

Figures

⏪

⏩

◀

▶

Back

Close

Full Screen / Esc

Printer-friendly Version

Interactive Discussion

procedure (as it is given in Eq. 15) the retrieval relies only on the observation at single time step and assumption of linear continuity of emission strength. At the same time, the emitted aerosol is transported for a period of time and, therefore, observations during that entire period of time (\sim one or two weeks) can be useful for the retrieval.

In these regards, using Eqs. (9, 13) seems preferable provided Eqs. (9, 13) can be implemented with the computational requirements close to those of forward modeling. This can be achieved if inversion routine adopts the strategies of forward simulations utilized in global modeling. As shown by Eq. (5) transport modeling can be formulated as matrix operator, however, in practice, the transport models are implemented by numerical time integration (Eq. 4) via sequential computing of chemical transport during each time step Δt (Eq. 2) and with separate treatment of isolated processes (Eq. 3). Similar approach can be employed in inverse modeling by means of developing so-called “adjoint” transport operators (e.g. Le Dimet and Talagrand, 1986; Talagrand and Courtier, 1987; Elbern et al., 1997; Menut et al., 2000). Indeed, any inversion can be implemented by iterations without explicit use of matrix inversion. For example, the solution equivalent to the one of Eq. (9) can be obtained by the steepest descent method iterations:

$$\hat{\mathbf{S}}^{\rho+1} = \hat{\mathbf{S}}^{\rho} - t_{\rho} \Delta \hat{\mathbf{S}}^{\rho}, \quad (39)$$

$$\Delta \hat{\mathbf{S}}^{\rho} = \nabla \Psi_m(\mathbf{S}^{\rho}) = \mathbf{T}^T \mathbf{C}_m^{-1} \Delta \mathbf{M}^{\rho}, \quad (40)$$

where $\Delta \mathbf{M}^{\rho} = \mathbf{M}(\mathbf{S}^{\rho}) - \mathbf{M}^*$, $\nabla \Psi_m(\mathbf{S})$ denotes a gradient of $\Psi_m(\mathbf{S})$ and t_{ρ} is non-negative coefficient. Equations (39–40) do not require challenging inversions of high dimension matrices (inversion of usually diagonal covariance matrix is trivial). The gradient $\nabla \Psi_m(\mathbf{S})$ can be simulated using numerical scheme employed for forward modeling. Namely, the elements of vector $\nabla \Psi_m(\mathbf{S})$ can be simulated in similar manner to Eqs. (2–4) and an equivalent of Eq. (39) can be written as follows (detailed derivations is given

in Appendix B):

$$\Delta \hat{S}^p(t, \mathbf{x}) = \int_t^{t_0} T^\#(t', \mathbf{x}) \left(\Delta \hat{S}^p(t', \mathbf{x}) + \sigma^{-2}(t', \mathbf{x}) \Delta m^p(t', \mathbf{x}) \right) (-dt'), \quad (41a)$$

where

$$\Delta m^p(t, \mathbf{x}) = m^*(t, \mathbf{x}) - \int_{t_0}^t T(t', \mathbf{x}) \left(m(t', \mathbf{x}) + s^p(t', \mathbf{x}) \right) dt', \quad (41b)$$

5 and $T^\#(t, \mathbf{x})$ is adjoint of transport operator $T(t, \mathbf{x})$ that is composed by adjoints $T_i^\#(t, \mathbf{x})$ of component processes $T_i(t, \mathbf{x})$:

$$T^\#(t, \mathbf{x}) = T_1^\# T_2^\# T_3^\# \dots T_{n-1}^\# T_n^\#. \quad (41c)$$

The vectors $\Delta \hat{S}^p(\mathbf{x}, t)$ and $\sigma^{-2}(t, \mathbf{x}) \Delta m^p(t, \mathbf{x})$ denote function equivalents of vectors $\Delta \hat{\mathbf{S}}^p$ and $\mathbf{C}_m^{-1} \Delta \mathbf{M}^p$ respectively. For example, if one intends to use continuous function $\Delta \hat{S}^p(t, \mathbf{x})$ in numerical calculations, it can be represented by vector $\Delta \hat{\mathbf{S}}^p$ with the following elements:

$$\left\{ \Delta \hat{\mathbf{S}}^p \right\}_l = \Delta \hat{S}^p(t_j; x_j; y_k; z_m), \quad (42a)$$

where index l can be determined same as given by Eq. (34b).

Similarly, if observation errors are uncorrelated, i.e. covariance matrix of measurements \mathbf{C}_m is diagonal with the elements on diagonal equal to $\sigma^2(t_j, x_j, y_k, z_m)$, the elements of vector $\mathbf{C}_m^{-1} \Delta \mathbf{M}^p$ relate to continuous function $\sigma^{-2}(t, \mathbf{x}) \Delta m^p(t, \mathbf{x})$ in straightforward way:

$$\left\{ \mathbf{C}_m^{-1} \Delta \mathbf{M}^p \right\}_l \rightarrow \sigma^{-2}(t_j, x_j, y_k, z_m) \Delta m^p(t_j, x_j, y_k, z_m). \quad (42b)$$

Retrieving global sources of aerosols from MODIS observations

O. Dubovik et al.

Title Page

Abstract

Introduction

Conclusions

References

Tables

Figures

⏪

⏩

◀

▶

Back

Close

Full Screen / Esc

Printer-friendly Version

Interactive Discussion

Retrieving global sources of aerosols from MODIS observations

O. Dubovik et al.

Title Page

Abstract

Introduction

Conclusions

References

Tables

Figures

◀

▶

◀

▶

Back

Close

Full Screen / Esc

Printer-friendly Version

Interactive Discussion

If observational errors do not have time correlations but have spatial correlations, then \mathbf{C}_m has array structure and can be included in the algorithm (see Eqs. B14 and B16 in Appendix B), provided one can formulate a weighting function $C^{-1}(t, \mathbf{x}, \mathbf{x}')$ from covariance function $C(t, \mathbf{x}, \mathbf{x}')$ performing analogous role to the one of matrix \mathbf{C}_m^{-1} in discrete representation. Inclusion of the spatial correlations during each time moment is feasible because the model is integrated by time steps and each time step can be treated rather independently. However, accounting for observational errors that are correlated in time is not feasible without changing structure of Eq. (41).

It is important to note that Eq. (41) is convenient for practical implementation of inversion. Indeed, Eq. (41) is allied to Eq. (4) with the difference that it uses $\Delta m^p(t, \mathbf{x})$ in place of $s(t, \mathbf{x})$ and $\Delta \hat{s}^p(t, \mathbf{x})$ in place of $m(t, \mathbf{x})$ and performs the backward time integration of adjoint operator $T^\#(t, \mathbf{x})$. If $T(t, \mathbf{x})$ is functionally equivalent to the matrix operator \mathbf{T} , then the adjoint operator $T^\#(t, \mathbf{x})$ is an equivalent to the transposed matrix \mathbf{T}^T . Therefore, the main idea of developing the adjoint operator $T^\#$ from T can be shown from considering matrix transposition. For example, since the integration of transport operator can be approximated on the basis of operator split approach (e.g. see Jacob, 1999) where matrices corresponding to different atmospheric processes are multiplied at each time step (e.g. see Eq. 3), the following matrix identity is helpful:

$$(\mathbf{T}_3 \mathbf{T}_2 \mathbf{T}_1)^T = (\mathbf{T}_1)^T (\mathbf{T}_2)^T (\mathbf{T}_3)^T. \quad (43)$$

This reversing of the order of operations by transposition results in overturned sequence of applying component processes within each time step Eq. (41c) and in reversing of the order of integration in Eq. (41a), i.e. in backward time integration Eq. (41a). Also, transposition of matrix \mathbf{T}_i changes rows and columns, therefore if \mathbf{T} is non-square, input of $(\mathbf{T}_i)^T$ should have dimension of \mathbf{T}_i output and output of $(\mathbf{T}_i)^T$ should have dimension of \mathbf{T}_i input. Thus, the adjoint model (executing Eq. 41) can be developed on the basis of the original model (executing Eq. 4) by reversing the order of operations and switching inputs and outputs of routines (e.g. Elbern et al., 1997; Menut et al., 2000).

Thus, using adjoint to transport model allows implementation LSM inversion (Eq. 9) without using explicit matrix inversion and therefore with moderate computational efforts. Each iteration in Eq. (41) requires one forward integration of transport model (Eq. 41b) followed by one backward integration of adjoint transport model (Eq. 41a).

5 Necessity to perform a number of iterations in Eq. (41) is a potential drawback of implementing inversions via adjoint modeling. Indeed, the steepest descent method iterations of Eqs. (39–40), in general, converge to the exact solution at a very large number of iterations. Even faster method of conjugated gradients may require up to N_S iterations (Press et al., 1992). Nevertheless, due to the local character of transport
10 processes, i.e. when an observation in any specific location can be influenced only by aerosol emitted within certain limited area surrounding this location, a rather limited number of simple iterations appear to be effective for global inverse modeling of high dimensionality. For instance, the iterations of Eq. (39–40) converge from an arbitrary initial guess to the solution, if the following sequence leads to zero matrix (Dubovik,
15 2004):

$$\prod_{p=1}^{\infty} (\mathbf{I} - t_p \mathbf{T}^T \mathbf{C}_m^{-1} \mathbf{T}) \Rightarrow 0, \quad (44)$$

where \mathbf{I} is unity matrix. It is clear, that fast convergence in Eqs. (39–40) can be achieved only if $\mathbf{T}^T \mathbf{T}$ is predominantly diagonal (\mathbf{C}_m is often diagonal and does not cause problems). Fortunately, in transport modeling, the diagonal elements of $\mathbf{T}^T \mathbf{T}$ dominate because local aerosol emission quickly influences only rather close locations (i.e. matrix
20 \mathbf{T} is rather sparse and has large number of zeros, see Eq. (B5) in Appendix B).

It should be noted, that Eqs. (41) expressing inversion via adjoint operators are generally analogous to techniques utilized in variational assimilation (e.g. Le Dimet and Talagrand, 1986; Talagrand and Courtier, 1987; Menut et al., 2000; Vukicevic et al.,
25 2001). Nevertheless, the statistical estimation approach employed in our studies allows establishing direct relationships of Eqs. (41) with conventional LSM minimization and therefore improves flexibility in implementing inversion. For example, direct using

Retrieving global sources of aerosols from MODIS observations

O. Dubovik et al.

[Title Page](#)[Abstract](#)[Introduction](#)[Conclusions](#)[References](#)[Tables](#)[Figures](#)[⏪](#)[⏩](#)[◀](#)[▶](#)[Back](#)[Close](#)[Full Screen / Esc](#)[Printer-friendly Version](#)[Interactive Discussion](#)

error covariances allows accounting for different levels of accuracy in inverted observations. Moreover, formulating inversion using statistical approach is convenient for including various a priori constraints into retrieval, for example, following multi-term LSM strategy discussed in Sect. 2.4.

5 2.6 Including a priori constraints into inversion via adjoint equations

Equations (41) can be easily adopted for implementing constraint inversion. For example, the inversion constraining solution $\hat{\mathbf{S}}$ by its a priori estimates \mathbf{S}^* shown via matrix inversion by Eq. (41) can be implemented iteratively, e.g. using steepest descent iterations:

$$10 \quad \hat{\mathbf{S}}^{\rho+1} = \hat{\mathbf{S}}^{\rho} - t_{\rho} \Delta \hat{\mathbf{S}}^{\rho}, \quad (45a)$$

$$\Delta \hat{\mathbf{S}}^{\rho} = \nabla \Psi_m(\mathbf{S}^{\rho}) + \nabla \Psi_S(\mathbf{S}^{\rho}) = \mathbf{T}^T \mathbf{W}_m^{-1} \Delta \mathbf{F}^{\rho} + \gamma_S \mathbf{W}_S^{-1} \Delta \mathbf{S}^{\rho}. \quad (45b)$$

Here we used weighting matrices $\mathbf{W}_{...}$ instead of covariance matrices $\mathbf{C}_{...}$ in order to align these equations with LSM multi-term formulations given by Eqs. (28–32). If we assume for simplicity that all measurements are statistically independent and have the same accuracy ε_m (i.e. $\mathbf{C}_m = \mathbf{I} \varepsilon_m^2 \rightarrow \mathbf{W}_m = \mathbf{I}$) and all a priori estimates are statistically independent and have the same accuracy ε_S ($\mathbf{C}_S = \mathbf{I} \varepsilon_S^2 \rightarrow \mathbf{W}_S = \mathbf{I}$) than we can write continuous analog to Eq. (45b) as follows:

$$15 \quad \Delta \hat{\mathbf{S}}^{\rho}(t, \mathbf{x}) = \int_t^{t_0} T^{\#}(t', \mathbf{x}) (\Delta \hat{\mathbf{S}}^{\rho}(t', \mathbf{x}) + \Delta m^{\rho}(t', \mathbf{x})) (-dt') + \gamma_S (\hat{\mathbf{S}}^{\rho}(t', \mathbf{x}) - \hat{\mathbf{S}}^*(t', \mathbf{x})). \quad (45c)$$

where $\gamma_S = \varepsilon_m^2 / \varepsilon_S^2$.

20 The iterative analog to Eq. (35) constraining the solution by limiting time and spatial derivatives of $\hat{\mathbf{S}}(t, \mathbf{x})$ can be written as follows:

$$\hat{\mathbf{S}}^{\rho+1} = \hat{\mathbf{S}}^{\rho} - t_{\rho} \Delta \hat{\mathbf{S}}^{\rho}, \quad (46a)$$

$$\Delta \hat{S}^p = \nabla \Psi_m(S^p) + \sum_{(q=t,x,y,z)} \gamma_q \nabla \Psi_q(S^p) = \mathbf{T}^T \mathbf{W}_m^{-1} \Delta F^p + \sum_{(q=t,x,y,z)} \gamma_q \Omega_q S^p. \quad (46b)$$

The function $\Delta \hat{S}^p(t, \mathbf{x})$ correspondent to vector $\Delta \hat{S}^p$ can be formulated as follows:

$$\begin{aligned} \Delta \hat{S}^p(t, \mathbf{x}) = & \int_t^{t_0} T^*(t, \mathbf{x}) (\Delta \hat{S}^p(t', \mathbf{x}) + \Delta m^p(t', \mathbf{x})) (-dt') \\ & + \sum_{(q=t,x,y,z)} \gamma_q \frac{\delta \Psi'_q(s^p(t, \mathbf{x}))}{\delta s(t, \mathbf{x}')} \end{aligned} \quad (47)$$

- 5 where $\mathbf{x}' = (x_j, y_k, z_m)$ and the functional derivative $\delta \Psi'_q(s^p)/\delta s$ relates to derivatives of correspondent quadratic form $\partial \Psi_q(S^p)/\partial S_l$. For example, for the norm of second derivatives of $s(t, \mathbf{x})$ over time ($\Psi'_t(s)$ shown in Eq. 37) the following relationship can be written:

$$\begin{aligned} \frac{\delta \Psi'_t(s^p(t, \mathbf{x}))}{\delta s(t_j, \mathbf{x}')} & \approx \frac{\partial \Psi_t(S^p)}{\partial S_l} = \\ 10 & = (\Delta t)^{-2} (S(t_{i+2}, \mathbf{x}') - 4S(t_{i+1}, \mathbf{x}') + 6S(t_j, \mathbf{x}') - 4S(t_{i-1}, \mathbf{x}') + S(t_{i-2}, \mathbf{x}')) \end{aligned} \quad (48)$$

where the index l can be calculated according Eq. (34) and $2 < i < N_t - 2$ (see Eq. 21). Analogous equations can be written for the terms corresponding to spatial coordinates x , y and z .

- 15 These formulations also can adopt the same a priori constraints, as those used in Kalman filter, i.e. when only continuity of sources is constrained a priori by assuming $S_t^* = S_{t-1} + \Delta S$ (see Eqs. 15 and 18). In this situation, one can use assumption that first derivative of $s(t, \mathbf{x})$ over time is close to zero, i.e. $\partial s(t, \mathbf{x})/\partial t \approx 0$. Correspondingly, Eq. (47) should be used with only one a priori term with the functional derivative $\delta \Psi'_t(s^p)/\delta s$, where $\Psi'_t(s^p)$ – the quadratic form for the norm of first derivatives

Retrieving global sources of aerosols from MODIS observations

O. Dubovik et al.

Title Page

Abstract

Introduction

Conclusions

References

Tables

Figures

⏪

⏩

◀

▶

Back

Close

Full Screen / Esc

Printer-friendly Version

Interactive Discussion

$\partial s(t, \mathbf{x})/\partial t$ (see Eq. 37), i.e.

$$\frac{\delta \Psi'_t (s^D(t, \mathbf{x}))}{\delta s(t_j, \mathbf{x}')} \approx \frac{\partial \Psi'_t (S^D)}{\partial S_l} = (\Delta t)^{-1} (S(t_{i+1}, \mathbf{x}') - 2S(t_i, \mathbf{x}') + S(t_{i-2}, \mathbf{x}')) \quad (49)$$

where the index l can be calculated according Eq. (34) and $1 < i < N_t - 1$ (see Eq. 21). If the deviations of $\partial s(t, \mathbf{x})/\partial t$ from zero are different in different locations and times then these differences can be accounted in formulating quadratic form $\Psi'_t(s^D)$ by including appropriate weighting. Thus, this way the Eq. (47) relies on the same a priori constraints as those used in Kalman filter Eq. (15). However, in Eq. (47) observations $m(t, \mathbf{x})$ during whole time period $t > t_j$ can contribute to the solution $S(t_j, \mathbf{x})$ while Eq. (15) relies only on observations $m(t_j, \mathbf{x})$ at time t_j .

Also, it should be noted that for clarity of presentation Eqs. (45c) and (47) were written for the case of the simplest covariance matrices of measurements and a priori data errors $\mathbf{C}_{\dots} = \varepsilon^2 \mathbf{I}_{\dots}$. However, the generalization of these equations to the cases when accuracies within each data set are different ($\{\mathbf{C}\}_{ii} \neq \{\mathbf{C}\}_{jj}, i \neq j$) or the covariance matrices are non-diagonal is rather straightforward (similar as shown by Eqs. 41–43).

2.7 Inversion of models with non-linearities

Previous sections described an approach to invert linear transport model (Eq. 5) provided the global measurements of aerosol mass \mathbf{M}^* are available. In practice, the transport model may be non-linear and the global data of aerosol fields are available only in form of satellite optical measurements:

$$f = F(m(t, \mathbf{x}), \lambda, \theta; \dots), \quad (50)$$

where $f(\dots)$ is generally a non-linear function depending on aerosol $m(t, \mathbf{x})$, instrument spectral specifications λ , observation geometry θ , etc. Therefore, the following non-linear equation should be solved instead of Eq. (4):

$$F^* = F(\mathbf{M}(S)) + \Delta F, \quad (51)$$

Retrieving global sources of aerosols from MODIS observations

O. Dubovik et al.

Title Page

Abstract

Introduction

Conclusions

References

Tables

Figures

⏪

⏩

◀

▶

Back

Close

Full Screen / Esc

Printer-friendly Version

Interactive Discussion

where F and ΔF are vectors of global optical data and their uncertainties. Since, the steepest descent method can be applied to both linear and non-linear problems, Eqs. (41, 45, 47) that use adjoint operators can be expanded for solving Eq. (51). For example, for a basic case when only optical measurements F^* are inverted with no a priori constraints, the steepest descent solution can be written as:

$$\hat{S}^{\rho+1} = \hat{S}^{\rho} - t_{\rho} \Delta \hat{S}^{\rho}, \quad (52a)$$

$$\Delta \hat{S}^{\rho} = \nabla \Psi_f(S^{\rho}) = \mathbf{K}_{\rho}^T \mathbf{C}_f^{-1} \Delta F^{\rho} = \mathbf{T}_{\rho}^T \mathbf{F}_{\rho}^T \mathbf{C}_f^{-1} \Delta F^{\rho}, \quad (52b)$$

where $\Delta F^{\rho} = F(S^{\rho}) - F^*$. Matrices \mathbf{K}_{ρ} , \mathbf{T}_{ρ} and \mathbf{F}_{ρ} denote Jacobi matrices of the first derivatives df/ds , dm/ds and df/dm calculated in the vicinity of the vector S^{ρ} :

$$\{\mathbf{K}_{\rho}\}_{jj} = \left. \frac{df_j(m(\mathbf{S}), \lambda, \theta, \dots)}{dS_j} \right|_{S=S^{\rho}}, \quad (53a)$$

and

$$\{\mathbf{T}_{\rho}\}_{j'i} = \left. \frac{dm_{j'}(\mathbf{S}, t, \mathbf{x})}{dS_i} \right|_{S=S^{\rho}}, \quad \{\mathbf{F}_{\rho}\}_{j'i'} = \left. \frac{df_j(\mathbf{M}, \lambda, \theta, \dots)}{\partial m_{i'}} \right|_{M^{\rho}=\mathbf{M}(S^{\rho})}, \quad (53b)$$

where indices j , j' , i and i' are the indices for the elements f_j , $m_{j'}$, $m_{i'}$, S_i of corresponding vectors $F^T = (f_1, f_2, \dots)$, $M^T = (m_1, m_2, \dots)$, and $S^T = (S_1, S_2, \dots)$. The following relationship between Jacobi matrices of df/ds , dm/ds and df/dm derivatives was used in Eq. (52):

$$\mathbf{K}_{\rho} = \mathbf{F}_{\rho} \mathbf{T}_{\rho}. \quad (53c)$$

The function $\Delta \hat{S}^{\rho}(t, \mathbf{x})$ correspondent to vector $\Delta \hat{S}^{\rho}$ can be formulated as follows:

$$\Delta \hat{S}^{\rho}(t, \mathbf{x}) = \int_t^{t_0} T_{\rho}^{\#}(t', \mathbf{x}) F_{\rho}^{\#}(t', \mathbf{x}) (\Delta \hat{S}^{\rho}(t', \mathbf{x}) + \Delta F^{\rho}(t', \mathbf{x})) (-dt'), \quad (54)$$

Retrieving global sources of aerosols from MODIS observations

O. Dubovik et al.

Title Page

Abstract

Introduction

Conclusions

References

Tables

Figures

◀

▶

◀

▶

Back

Close

Full Screen / Esc

Printer-friendly Version

Interactive Discussion

Retrieving global sources of aerosols from MODIS observations

O. Dubovik et al.

Title Page

Abstract

Introduction

Conclusions

References

Tables

Figures

◀

▶

◀

▶

Back

Close

Full Screen / Esc

Printer-friendly Version

Interactive Discussion

where $T_p^\#(t, \mathbf{x})$ and $F_p^\#(t, \mathbf{x})$ are adjoint operators for mass transport $T(s(t, \mathbf{x}))$ and the optical model $F(m(t, \mathbf{x}))$, index p indicates that these adjoint operators are equivalents of transposed Jacobi matrices \mathbf{T}_p^T and \mathbf{F}_p^T . The development of $F_p^\#(t, \mathbf{x})$ is quite transparent because optical properties $f(m(t, \mathbf{x}), \dots)$ usually are related only with local aerosol and therefore in practical implementations of Eq. (54) (that usually performed in discrete representation) $F_p^\#(t, \mathbf{x})$ can be explicitly replaced by the transposed Jacobi matrix \mathbf{F}_p^T .

Equation (54) can be easily expanded for implementing constraint inversion of $f = F(m(t, \mathbf{x}), \lambda, \theta, \dots)$. For example, in case when solution is constrained by a priori limiting time and spatial derivatives of $\hat{S}(t, \mathbf{x})$ (utilized in Eqs. 35 and 47) can be written as follows:

$$\begin{aligned} \Delta \hat{S}^p(t, \mathbf{x}) &= \int_t^{t_0} T_p^\#(t', \mathbf{x}) F_p^\#(t', \mathbf{x}) (\Delta \hat{S}^p(t', \mathbf{x}) + \Delta f^p(t', \mathbf{x})) (-dt') \\ &+ \sum_{(q=t,x,y,z)} \gamma_q \frac{\delta \Psi'_q(s^p(t, \mathbf{x}))}{\delta s(t, \mathbf{x}')} \end{aligned} \quad (55)$$

Using this $\Delta \hat{S}^p(t, \mathbf{x})$ the iterative retrieval would minimize the following quadratic form:

$$2 \Psi(\mathbf{S}) = 2 \Psi_f(\mathbf{S}) + 2 \sum_{(q=t,x,y,z)} \gamma_q \Psi_q(\mathbf{S}) = 2 (\Delta F)^T \Delta F + 2 \sum_{(q=t,x,y,z)} \gamma_q \mathbf{S}^T \Omega_q \mathbf{S}. \quad (56a)$$

This quadratic form can be generalized by the following functional:

$$\begin{aligned} 2 \Psi' &= 2 \iiint_{tx,y,z} \Delta f^\#(t, x, y, z) \Delta f(t, x, y, z) dx dy dz dt \\ &+ 2 \sum_{(q=t,x,y,z)} \gamma_q \int_{q_{\min}}^{q_{\max}} \left(\frac{\partial^n s(q, \dots)}{\partial q^n} \right)^2 dq, \end{aligned} \quad (56b)$$

where $\Delta f(t, x, y, z) = f^* - f(t, x, y, z)$ and $\Delta f^\#(t, x, y, z)$ denotes adjoint of $\Delta f(t, x, y, z)$.

Thus, the above derivations show rather high potential of using statistical estimation approach for implementing inverse modeling of aerosol transport. For example, it was demonstrated that following multi-term LSM strategy allows for flexible usage of various types of a priori constraints in inverse modeling. For example, Eqs. (47–49) show how the limitation on derivatives of aerosol (or other tracer) emission with respect to coordinates or time can be included into adjoint integration of tracer models that is widely used in variational assimilation for source identification of atmospheric tracers (e.g. Le Dimet and Talagrand, 1986; Talagrand and Courtier, 1987). Using such constraint in inverse modeling may have high potential because, in principle, a priori limitations on derivatives of emission variability is a weaker and more flexible way of constraining than using a priori values of emission. Equations (54–55) demonstrate the formulation of the approach for inverting satellite observations (e.g. radiances measured by passive satellite observations). This generalization may have the high potential, because using directly satellite observations in inverse modeling and satellite data assimilations has a number of advantages compare to relying on satellite retrieval products (Weaver et al., 2006). However, the utilization of steepest descent iteration in Eqs. (54–55) makes the use of Eqs. (55–56) less attractive for practical use because in general inverting radiative transfer equations by steepest method requires a large number of iterations (Dubovik and King, 2000). Therefore, it might be useful to explore a possibility of utilizing iterative strategy of conjugated gradients method (Appendix C), because method of conjugated gradients is known for superior convergence than steepest descent method.

3 Application of the inverse methodology for aerosol source retrieval from satellite observations

In this section, we attempt applying the inversion methodology (described in previous sections) for deriving information about global aerosol sources from satellite observa-

Retrieving global sources of aerosols from MODIS observations

O. Dubovik et al.

Title Page

Abstract

Introduction

Conclusions

References

Tables

Figures

⏪

⏩

◀

▶

Back

Close

Full Screen / Esc

Printer-friendly Version

Interactive Discussion

tions. First, we analyze a possibility to invert aerosol transport model, i.e. to derive “unknown input” (aerosol emissions) of the model from “known output” (aerosol mass distribution). Then we consider a possibility of applying such an inversion for deriving global aerosol sources from satellite observations. Our studies are based on GOCART aerosol transport model. We use satellite observations of aerosol by MODIS instrument.

3.1 GOCART based algorithm for inverting MODIS data

The GOCART – Goddard Chemistry Aerosol Radiation and Transport model is described in papers by Chin et al. (2000, 2002) and Ginoux et al. (2001). The model uses the assimilated meteorological data from the Goddard Earth Observing System Data Assimilation System (GEOS DAS) and provides four-dimensional distribution of aerosol mass at several atmospheric layers (20–30) with horizontal resolution of 2° latitude by 2.5° longitude. The model calculates aerosol composition and size distribution, optical thickness and radiative forcing. There are seven modules representing atmospheric processes: emission, chemistry, advection, cloud convection, diffusion (boundary layer turbulent mixing), dry deposition, and wet deposition. The model solves continuity Eq. (1) using an operator splitting technique (Eqs. 2–3). The model time step is 15 min for advection, convection and diffusion and 60 min for other processes.

Inverse algorithm described by Eqs. (41, 54) was implemented based on GOCART model. The adjoint transport operator $T^*_p(t, \mathbf{x})$ was developed by redesigning GOCART modules for each atmospheric process. Namely, the adjoint operation of advection was performed by original advection algorithm of GOCART (Lin and Rood, 1996) using signed-reverse wind fields (Vukicevic et al., 2001). The exact equivalence between such physically derived retro-transport and adjoint equations has been proven by rigorous derivations by Hourdin and Talagrand (2006). The adjoints of the local processes were developed by using analogies with correspondent transpose matrix operators. Specifically, cloud convection, diffusion, dry deposition, and wet deposition affect only vertical transport of aerosol motion. All these processes have local char-

Retrieving global sources of aerosols from MODIS observations

O. Dubovik et al.

Title Page

Abstract

Introduction

Conclusions

References

Tables

Figures

⏪

⏩

◀

▶

Back

Close

Full Screen / Esc

Printer-friendly Version

Interactive Discussion

acter in the sense that for a single time step in the model they work independently in each horizontally resolved vertical column. Therefore, such processes can be easily modeled via explicit use of matrices of rather small dimension and the corresponding adjoint operators can be obtained by direct transposition of those matrices. At first, we have arranged the cloud convection, diffusion, dry deposition, and wet deposition in matrix form and derived the transpose to those matrices. Then, for achieving faster calculation time we redesigned original programs so that their application to a vector provides an equivalent product to the application of correspondent transpose matrices. Chemical aging transformations of black and organic carbon aerosols change only proportion between different components and do not induce any vertical or horizontal aerosol motions. Therefore, adjoint of chemical processes can be constructed simply by changing the direction of chemical transformation.

In order to use satellite observations as the input for the inversion the conversion from modeled aerosol mass into optical parameters, should be included into adjoint developments. Correspondingly, operator F_p in Eq. (53) should be rearranged into adjoint $F_p^\#$ and used in the inversion according to Eq. (54). Since aerosol optical thickness operator F_p summing up the contribution from different layers and different aerosol types, its adjoint $F_p^\#$ redistribute the total sum to the individual layers and aerosol types.

The inversion algorithm (Eqs. 39–41) treats the strength of aerosol emission at each global location as an unknown. Therefore, in an ideal situation, when the observations provide enough information for retrieving all emission parameters, the emissions derived from satellite observation could potentially replace the original module of GOCART prescribing the aerosol emissions. Such an ideal situation can likely be expected if the observations are rather sensitive to all aerosol characteristics provided by output of GOCART model, i.e. if observations sensitive to all time and space (3×D) variations of all modeled aerosol components. Naturally, satellite observations (as well as observations of any other type) have some limitations and cannot provide the same amount of details as model simulation. Correspondingly, the inverse algorithm settings should address limitations of the used MODIS observations.

Retrieving global sources of aerosols from MODIS observations

O. Dubovik et al.

[Title Page](#)[Abstract](#)[Introduction](#)[Conclusions](#)[References](#)[Tables](#)[Figures](#)[⏪](#)[⏩](#)[◀](#)[▶](#)[Back](#)[Close](#)[Full Screen / Esc](#)[Printer-friendly Version](#)[Interactive Discussion](#)

The MODIS – MODerate resolution Imaging Spectroradiometer aboard both NASA's Terra and Aqua satellites provides near global daily observations of the Earth in a wide spectral range (0.41 to 15.0 μm). These measurements are used to derive spectral aerosol optical thickness and aerosol size parameters over both land and ocean (Kaufman et al., 1997; Tanré et al., 1997; Remer et al., 2005). The main available aerosol products include aerosol optical thickness (at three visible wavelengths over land and seven wavelengths over ocean), effective radius of the aerosol and fraction of optical thickness attributed to the fine mode. The present study uses the MODIS aerosol optical thickness product aggregated to 1° by 1° spatial resolution. The expected accuracy of MODIS optical thickness $\Delta\tau = \pm 0.03 \pm 0.05\tau$ over ocean (Tanré et al., 1997; Remer et al., 2005) and $\Delta\tau = \pm 0.05 \pm 0.15\tau$ over land (Kaufman et al., 1997; Remer et al., 2005).

Such passive remote sensor as MODIS has the following main limitations:

- no sensitivity to vertical variability of the aerosol;
- time and space limitation of observation coverage;
- limited capabilities of aerosol type identification.

Indeed, the top of the atmosphere radiances are mostly sensitive to the total aerosol content in the atmospheric column (that is optically characterized by aerosol optical thickness) and generally have no or very weak sensitivity to vertical variations of aerosol properties. Correspondingly, measurements of MODIS do not provide any information about aerosol vertical distribution (Kaufman et al., 1997; Tanré et al., 1997; Remer et al., 2005). Viewing specifications and aerosol retrieval limitations causes the limitations of MODIS observation coverage. Namely, MODIS provides aerosol retrievals with nearly complete global coverage every 2 days for cloud-free atmospheric conditions. The retrievals are not performed over pixels with very bright reflectance, such as over desert (Kaufman et al., 1997) or for the observations affected by glint reflection over ocean (Tanré et al., 1997). The possibility to identify aerosol type from MODIS data is also limited. GOCART differentiates emission and transport for each

Retrieving global sources of aerosols from MODIS observations

O. Dubovik et al.

Title Page

Abstract

Introduction

Conclusions

References

Tables

Figures

⏪

⏩

◀

▶

Back

Close

Full Screen / Esc

Printer-friendly Version

Interactive Discussion

of at least 11 types of aerosol particles: sulfate, hydrophilic and hydrophobic Organic Carbon (OC), hydrophilic and hydrophobic Black Carbon (BC), four size differentiated sea salt bins and seven (in some versions of GOCART up to seven) desert dust size differentiated bins (Chin et al., 2002, 2004; Ginoux et al., 2001). These aerosol components could be uniquely differentiated by such optical parameters as real part of the refractive index, absorption and particle size. However, as concluded from sensitivity studies (Tanré et al., 1996), the information content of MODIS data is insufficient for deriving such detailed information as aerosol absorption and refractive index, while it allows separating the contributions of fine and coarse aerosol particle into total optical thickness. On the other hand, separation between fine or coarse mode dominated aerosols allows some rather useful discrimination between aerosol groups. Specifically, desert dust and maritime aerosols are dominated by coarse mode particles, while biomass burning and urban pollution are dominated by fine mode particles (Dubovik et al., 2002).

Thus, MODIS data provide smaller amount of information compare to output of global model and therefore inversion of satellite observation is much less constrained than formal inversion of the model that derives unknown “input” from known model “output”. The problem of retrieving all aerosol emissions utilized by GOCART from MODIS observations is clearly ill-posed (from formal viewpoint the number of observations is significantly smaller than a number of retrieved parameters). One way to assure uniqueness of the retrieval is to use a priori constraints. For example, the original GOCART emissions can be used as a priori estimates of unknown emissions. This can be implemented on the basis of Eqs. (45). At the same time using such a priori estimates may limit in some cases the freedom of the algorithm in searching for the actual solution. The appropriate choice of correspondent Lagrange multipliers in Eq. (41) (or covariance matrices of a priori estimates in general case) is supposed to prevent appearance of significant biases in solution due to incorrect a priori information. However, the optimum choice of Lagrange multipliers is nontrivial because the level accuracy in the knowledge of aerosol emissions is rather uncertain. Therefore, it is appealing to

Retrieving global sources of aerosols from MODIS observations

O. Dubovik et al.

Title Page

Abstract

Introduction

Conclusions

References

Tables

Figures

⏪

⏩

◀

▶

Back

Close

Full Screen / Esc

Printer-friendly Version

Interactive Discussion

explore the potential of unsupervised retrieval that distributes the global aerosol emission based only on satellite observations and transport. In some way, this approach is an alternative to using a priori constraints and it can be implemented by reducing the number of variables in parameterization of aerosol emissions. Another possibility is to implement retrieval without addressing ill-posed character of the problem. Indeed, our algorithm is based on steepest descent iterations (see Eqs. 39–41) and therefore would not collapse even for ill-posed problem. However, the solution would strongly depend on initial guess (e.g. see Dubovik, 2004), i.e. in such scenario if the algorithm uses GOCART emissions as initial guess, it simply corrects GOCART emissions as needed to improve agreement between model and observations. However, the solution is not unique in the sense that if the initial guess is changed the retrieval results also change.

Thus, in order to understand the potential of aerosol sources retrieval from MODIS observations we will examine the effect of MODIS data limitations and test the performance of the retrievals by different scenarios: retrieval constrained by a priori data or/and constrained by reduced parameterization of aerosol emissions, unconstrained retrievals strongly dependent on the initial guess.

3.2 Inverse algorithm testing

A series of numerical tests was performed to verify and illustrate how the algorithm inverts the modeled data in “no error” environment when inverted aerosol fields fully consistent with the model and neither measurements nor model errors are present. First we verified how the algorithm inverts the model output, i.e. how it works in the ideal situation when observation measure all time and space variations of mass for each aerosol specie. The tests have shown that for such well-constrained situation the algorithm retrieves the emissions of all aerosols accurately. Then we tested a possibility to retrieve emissions from the remote sensing MODIS like data that do not have information on vertical variability of aerosol. The algorithm was applied to the global “measurements” of $\tau(0.55)$ – optical thickness at $0.55 \mu\text{m}$ of single aerosol type. Since

Retrieving global sources of aerosols from MODIS observations

O. Dubovik et al.

Title Page

Abstract

Introduction

Conclusions

References

Tables

Figures

⏪

⏩

◀

▶

Back

Close

Full Screen / Esc

Printer-friendly Version

Interactive Discussion

MODIS sees each global location not more than once each 24 h, we assumed in the numerical tests that $\tau(0.55)$ is available one time every 24 h for each global point. Correspondingly, in order to make emission retrieval appropriately constrained the variability of emission within 24 h was neglected. The tests were accommodated to the same time period as the one chosen for inverting actual observations, i.e. the meteorological fields correspondent to 2 last weeks of August 2000 were used to perform tests. For simplicity the aerosol was assumed as one component BC aerosol in the test and the “observations” were simulated as BC optical thickness $\tau_{BC}(0.55)$. Chemical transformations (used in GOCART model) of aerosol were neglected in this retrieval test. The “prescribed” emissions were assumed equal to the total of black and organic carbon emissions used in GOCART model for the same two weeks. The optical thickness was modeled from the GOCART mass of aerosol in total atmospheric column, by deriving the aerosol volume (using density 1 g/cm^3) and assuming that it has the same optical properties as fine mode of smoke during Zambian savanna burning (Dubovik et al., 2002). The appearance of aerosol sources was allowed at 10 lower aerosol layers (i.e. approximately below 2 km). Figures 2–3 illustrate the retrieval results for one specific day of 28 August. Figure 2 shows that the total emission in first 10 layers retrieved in the test agreed well with “assumed” emissions. The agreement looks encouraging taking especially into account the fact that the retrieval uses “zero emissions” (i.e. no sources) as initial guess for emission estimate. The same initiation of retrieval is used in all following tests unless specified differently. There are some minor differences between “prescribed” and retrieved emissions of Fig. 2, such as appearance of minor aerosol sources over ocean. Since the forward and backward aerosol mass and optical thickness simulated under the same assumptions without adding any modeled errors or other perturbations these differences can only be explained by limited number of retrieval iterations or by the effect of numerical errors and instabilities inherent for transport model simulations (Vukicevic et al., 2001).

The accuracy of optical thickness fitting during entire time period (considered in the

Retrieving global sources of aerosols from MODIS observations

O. Dubovik et al.

[Title Page](#)[Abstract](#)[Introduction](#)[Conclusions](#)[References](#)[Tables](#)[Figures](#)[⏪](#)[⏩](#)[◀](#)[▶](#)[Back](#)[Close](#)[Full Screen / Esc](#)[Printer-friendly Version](#)[Interactive Discussion](#)

test) was characterized by two residual values:

$$\sigma_{\text{abs}} = \frac{1}{N_i} \sqrt{\sum_i \left(\tau_i^* - \tau_i(\hat{\mathbf{S}}) \right)^2}, \quad (57a)$$

$$\sigma_{\text{rel}} = \frac{100}{N_k} \sqrt{\sum_i \left(\frac{\tau_k^* - \tau_k(\hat{\mathbf{S}})}{\tau_k^*} \right)^2}, \quad (\tau_k^* \geq 0.05), \quad (57b)$$

where absolute standard deviation σ_{abs} was simulated using all locations and times and relative standard deviation σ_{rel} simulated using only points where $\tau_{\text{BC}}(0.55)$ was not smaller than 0.05. The value σ_{abs} is directly related to the minimized quadratic form. Specifically, under assumption of measurement covariance matrix as $\mathbf{C}_{\dots} = \varepsilon^2 \mathbf{I}$, σ_{abs} corresponds to a first term in the quadratic form given by Eq. (56). The value σ_{rel} was introduced for characterizing accuracy of fitting observations of aerosol events with high loading. After 40 iterations the residual were $\sigma_{\text{abs}} \approx 0.005$ and $\sigma_{\text{rel}} \approx 9\%$, i.e. achieved accuracy of fitting is below the measurements accuracy expected for MODIS ($\Delta\tau = \pm 0.03 \pm 0.05\tau$ over ocean and $\Delta\tau = \pm 0.05 \pm 0.15\tau$ over land). It should be noted that Fig. 2 shows the total mass emitted onto the first 10 atmospheric layers. Unfortunately the exact vertical structure of emission was not reproduced well because the observations of $\tau_{\text{BC}}(0.55)$ do not provide any vertical information.

Figures 4–5 show the similar results for the test with coarse mode aerosol where desert dust emissions were retrieved from simulated “measurements” of the desert dust optical thickness $\tau_{\text{Dust}}(0.55)$. For the simplicity desert dust was considered as one component aerosol instead of eight size resolved components used in GOCART model. The test was conducted using meteorology and values of desert dust emissions the same as assumed in GOCART model for two weeks in August 2000. The values of fitting residual achieved after 40 iterations for this test were: $\sigma_{\text{abs}} \approx 0.01$ and $\sigma_{\text{rel}} \approx 15\%$. In a contrast to the BC and other fine mode aerosols that can be emitted not only at the model surface layer but also at layers above the surface (e.g. within the boundary

Retrieving global sources of aerosols from MODIS observations

O. Dubovik et al.

Title Page

Abstract

Introduction

Conclusions

References

Tables

Figures

⏪

⏩

◀

▶

Back

Close

Full Screen / Esc

Printer-friendly Version

Interactive Discussion

layer), desert dust and sea salt (another coarse mode aerosol) are emitted only at the surface level. This fact can be considered as an extra factor contributing in the constraining of the retrieval problem.

In the tests illustrated by Figs. 2–5 the “observations” were available in each global location, although as mentioned earlier this is not a case for actual MODIS data. The observations for each single day have the gaps, e.g. Fig. 6 shows $\tau_{\text{fine}}(0.55)$ provided by MODIS for 28 August, (compare with Fig. 3). To analyze the effects of the gaps in MODIS data on the global emission retrieval, another test was performed where “measured” $\tau(0.55)$ where sub-sampled by exactly the same way as the real MODIS data for same period of observations.

Figures 7 and 8 illustrate the results of such test for BC emissions retrieval. This test is analogous to the one shown on Figs. 2–3 with only difference that the observations $\tau_{\text{BC}}(0.55)$ had exactly the same coverage as actual MODIS observation collected during the same time period. The convergence of the retrieval process was slightly slower than in the test where $\tau_{\text{BC}}(0.55)$ had no gaps. After 40 iterations, fitting residuals were $\sigma_{\text{abs}} \approx 0.009$ and $\sigma_{\text{rel}} \approx 12\%$. These numbers are still lower than expected MODIS measurements accuracy and, as can be seen, from Fig. 8 fitted $\tau_{\text{BC}}(0.55)$ reproduces “observed” $\tau_{\text{BC}}(0.55)$ rather well. The retrieved emissions shown on Fig. 7 also in good agreement with the assumed emission, however the agreement slightly deteriorated if to compare with the emission retrieval from $\tau_{\text{BC}}(0.55)$ with no gaps illustrated by Fig. 2.

The retrieval of the desert dust emissions from $\tau_{\text{Dust}}(0.55)$ sub-sampled according to MODIS observations was less successful than retrieval BC emission. Figure 9 shows that the retrieval was not able adequately reproduce the “assumed” emissions. For example, some patterns of strong desert dust emissions in the Western Sahara do not appear correctly in the retrieved emission field. This difficulty in the retrieval can be explained by the fact the observations of $\tau_{\text{dust}}(0.55)$ do not sufficiently constrain the retrieval over the areas where the strongest desert dust sources are expected (Ginoux et al., 2001) because MODIS does not provide aerosol retrievals over bright desert surfaces (Kaufman et al., 1997; Remer et al., 2005; Hsu et al., 2004). As a

Retrieving global sources of aerosols from MODIS observations

O. Dubovik et al.

Title Page

Abstract

Introduction

Conclusions

References

Tables

Figures

⏪

⏩

◀

▶

Back

Close

Full Screen / Esc

Printer-friendly Version

Interactive Discussion

result, the “prescribed” emission and “retrieved” emission produces virtually identical $\tau_{\text{dust}}(0.55)$ (see Fig. 10), despite some false desert dust source locations from the retrieval (e.g. over the Atlantic ocean near the western Africa coast). The values of the fitting residuals are: $\sigma_{\text{abs}} \approx 0.006$ and $\sigma_{\text{rel}} \approx 12\%$.

5 The tests discussed above suggest that unsupervised retrieval of global BC or desert dust emissions is possible (although the retrieval of dust emission was less appealing) if MODIS like observations of $\tau_{\text{BC}}(0.55)$ or $\tau_{\text{Dust}}(0.55)$ are available. However, as explained earlier MODIS retrieval can only discriminate the contributions of fine and coarse modes of aerosol (i.e. $\tau_{\text{fine}}(0.55)$ and $\tau_{\text{coarse}}(0.55)$) into total aerosol optical thickness $\tau_{\text{total}}(0.55)$ and does not discriminate aerosol type. Correspondingly
10 distinction of aerosol in global emission retrieval can be done only between aerosols composed by fine and coarse particles. Several numerical tests were performed to evaluate consequences of such limitation on global emission retrieval from $\tau_{\text{fine}}(0.55)$ and $\tau_{\text{coarse}}(0.55)$ provided by MODIS. According to setting of GOCART model the sulfate, OC and BC aerosols are composed only by fine particles and minor fractions of fine particles also present in desert dust and sea salt. Figures 11–12 illustrate the results of the test where modeled $\tau_{\text{fine}}(0.55)$ was equal to the sum of the optical thicknesses of sulfate, black and organic carbon aerosols simulated using original GOCART model. Then the modeled $\tau_{\text{fine}}(0.55)$ were inverted using simplified model of single fine
20 mode aerosol. In this test the same conversion of aerosol mass to optical thickness was used as in inversion of $\tau_{\text{BC}}(0.55)$ (earlier test illustrated by Figs. 2–3). The retrieval used the same parameterization of removal processes as GOCART uses for BC. As can be seen on Figs. 11–12 the results of the retrieval using simplified single fine mode aerosol look encouraging. For example, the retrieved fine mode aerosol source shows (Fig. 11) all major features emission composed by assumed BC, OC and sulfate
25 sources. It should be noted that because sulfate is formed in the atmosphere via photochemical oxidations of its precursor gases, the source of sulfate is not limited over land. The differences in magnitudes and shapes of emission field that can be seen between assumed and retrieved emissions in Fig. 11 can be explained by the fact that

Retrieving global sources of aerosols from MODIS observations

O. Dubovik et al.

Title Page

Abstract

Introduction

Conclusions

References

Tables

Figures

⏪

⏩

◀

▶

Back

Close

Full Screen / Esc

Printer-friendly Version

Interactive Discussion

the algorithm used optical properties of single BC aerosol for reproducing observation of a combination of BC, OC and sulfates. Nonetheless, as Fig. 12 shows the simplified single fine mode aerosol effectively matches the observations. The fitting errors for this test were $\sigma_{\text{abs}} \approx 0.02$ (and $\sigma_{\text{rel}} \approx 25\%$). These values are higher than in previous tests but they are still below the expected accuracy of aerosol optical thickness provided by MODIS retrievals. This fact suggests that even simplified transport model with no discrimination by aerosol type can reproduce the global observations of $\tau_{\text{fine}}(0.55)$ at the accuracy level of MODIS observations.

As stated above an implementation of under-constrained retrieval could be the alternative approach to using the simplified single component aerosol model. In order to illustrate such methodology, we have implemented the version of the algorithm that utilizes all chemical processes used in GOCART and retrieves simultaneously emissions of several aerosol types. Specifically, the inversion algorithm was developed for simultaneous retrieval of hydrophilic and hydrophobic BC and OC global emissions. The numerical test shows that if “measured” $\tau_{\text{fine}}(0.55)$ was composed by BC and OC only the retrieval provides better fit than the retrieval based on single fine mode aerosol. The fitting errors were: $\sigma_{\text{abs}} \approx 0.005$ and $\sigma_{\text{rel}} \approx 15\%$, while the retrieval with single fine mode aerosol in better fitting errors $\sigma_{\text{abs}} \approx 0.01$ and $\sigma_{\text{rel}} \approx 20\%$. However, as expected, the partitioning between BC and OC emissions was not correct and strongly dependent on initial guess. Therefore, the retrieval cannot categorize retrieved emission by aerosol type from $\tau_{\text{fine}}(0.55)$ and if such discrimination is critical then substantial a priori constraints should be utilized.

In case of retrieving emissions of coarse aerosols the situation is simpler. Indeed, in GOCART model only two aerosol types have coarse particles: desert dust and sea salt. The locations of the emission sources are fundamentally different: dust is emitted over land while sea salt over water. This physical restriction can be used as a natural constraint in the emissions of desert dust and sea salt.

We have also performed a number of tests verifying the efficiency of using a priori constraints in the retrieval. As expected the tests showed that using a priori estimates

Retrieving global sources of aerosols from MODIS observations

O. Dubovik et al.

Title Page

Abstract

Introduction

Conclusions

References

Tables

Figures

⏪

⏩

◀

▶

Back

Close

Full Screen / Esc

Printer-friendly Version

Interactive Discussion

of unknown emissions helps to improve retrievals. However, the appropriate accuracy of a priori estimates is critical because significant differences between a priori estimates and actual “true” emissions may bias retrieval results. Tests showed that limitations on time and space variability of emissions can be useful for inverting data that have gaps in time and spatial coverage. Some illustrations will be shown in next section.

3.3 Inverting MODIS observations

The algorithm was applied to the actual measurements of $\tau_{\text{fine}}(0.55)$ and $\tau_{\text{coarse}}(0.55)$ obtained by MODIS. For global inversion of the optical thickness of fine mode aerosol $\tau_{\text{fine}}(0.55)$ we used the data obtained during the period of 18 to 30 August 2000. This is a period of known high biomass burning activity and performing global inversion was expected to illustrate a potential of the approach for improving knowledge about BC and OC emissions that are rather uncertain (Sato et al., 2003). For the test, the global retrieval product of $\tau_{\text{fine}}(0.55)$ delivered by MODIS at 1° by 1° was rescaled to GOCART horizontal resolution of 2° by 2.5° . If MODIS retrievals were available in more than 90% of 2° by 2.5° of GOCART grid then the average value of available $\tau_{\text{fine}}(0.55)$ was assigned to entire 2° by 2.5° grid. If MODIS data available in less than of 90% of 2° by 2.5° GOCART grid then data in such grid points were not used in the inversion. Figure 13 shows the results of the retrieval under the assumption of single fine mode aerosol. The retrieved emissions are averaged over the whole considered time period. Figure 14 compares average MODIS observations of $\tau_{\text{fine}}(0.55)$ with the values fitted by retrieval algorithm. The fitting accuracy of global instantaneous observations (rescaled to GOCART resolution) was $\sigma_{\text{abs}} \approx 0.04$ and $\sigma_{\text{rel}} \approx 48\%$ after 40 iterations. Thus, as follows from Fig. 14 and the values of σ_{abs} , and σ_{rel} , the $\tau_{\text{fine}}(0.55)$ simulated from retrieved sources reproduces most of spatial and temporal tendencies in MODIS observations. It is also important to note than even in the situation when retrieved emissions are not restricted to the land surface and also allowed over oceans the distribution of main aerosol sources does not significantly change (compare the

Retrieving global sources of aerosols from MODIS observations

O. Dubovik et al.

Title Page

Abstract

Introduction

Conclusions

References

Tables

Figures

⏪

⏩

◀

▶

Back

Close

Full Screen / Esc

Printer-friendly Version

Interactive Discussion

Retrieving global sources of aerosols from MODIS observationsO. Dubovik et al.

[Title Page](#)[Abstract](#)[Introduction](#)[Conclusions](#)[References](#)[Tables](#)[Figures](#)[⏪](#)[⏩](#)[◀](#)[▶](#)[Back](#)[Close](#)[Full Screen / Esc](#)[Printer-friendly Version](#)[Interactive Discussion](#)

panels a and b in Fig. 13). The retrieved emissions (Fig. 13) may be attributed largely to BC, OC and Sulfates. They also may include some emission of fine mode components of dust and possible sea salt, although the emissions of fine mode dust and sea salt are likely to be small in magnitudes and have rather predictable locations (e.g. sea salt emitted over the water and main dust sources are over the deserts). Indeed, the emissions retrieved over oceans have rather small magnitudes and can be interpreted as emissions of sea salt. In a contrast, separation of BC, OC and Sulfate sources is particularly difficult because the emissions of all these species are comparable in magnitudes and associated with the same sources, such as, biomass burning, fuel combustion and industrial activity (Chin et al., 2002). Therefore, for convenience of retrieval result interpretation, we displayed BC, OC and Sulfate sources assumed in GOCART for August of 2000 in Fig. 15. In addition, Fig. 16 shows total carbon emission from biomass burning obtained from a combination of satellite data and biogeochemical modes by van der Werf et al. (2004). It should be noted that the default biomass burning sources in GOCART model were also based on these data. The comparison of Fig. 13 with Figs. 15–16 suggests that the global placement of the major fine aerosol sources in the retrieved field of emission is in general agreement with known emission fields of carbon and sulfates. At the same time one can note some differences between retrieved emissions (Fig. 13) and emissions assumed in GOCART model (Fig. 15). Namely, the exact shapes and magnitudes of the main emission patterns in the retrieval generally differ from GOCART assumptions and carbon emissions provided by van der Werf et al. (2004). As discussed above, some of these differences can be attributed to the usage of the simplified assumption of single aerosol employed in the retrieval. However, it seems likely that the driving factor predetermined these differences is the mismatch between modeled global aerosol distribution and satellite observations. This mismatch can be caused by many factors including various limitations of both measurements and modeling. The main assumption of our approach is that the factor driving the disagreement between satellite observations and modeling is the uncertainty in emissions assumed by models, i.e. differences in the location

and magnitudes between modeled emissions and those observed by satellite. This assumption is recognized in modeling community (e.g. Kinne et al., 2003) and there are many efforts on utilizing observations for improving accuracy of emission modeling. For example, the emissions utilized by GOCART Fig. 15 as well as, carbon emissions showed in Fig. 16 are also determined with the aid of the aerosol information derived from satellite observation. However, the emission modeling utilized satellite information only about monthly variability of observation, while the emission retrieval approach considered here allows daily variability of the emissions. The fact is that the retrieved aerosol emissions allow better agreement between output of GOCART model than if standard emission fields of BC, OC and sulfates are used. For example, standard output of GOCART model results into much higher residuals ($\sigma_{\text{abs}} \approx 0.12$ and $\sigma_{\text{rel}} \approx 170\%$) than those achieved by retrieval ($\sigma_{\text{abs}} \approx 0.04$ and $\sigma_{\text{rel}} \approx 48\%$). At the same time, even the achieved lower residual values $\sigma_{\text{abs}} \approx 0.04$ and $\sigma_{\text{rel}} \approx 48\%$ are noticeably higher than the fitting errors that can be expected based on the results of numerical tests. Indeed the numerical test shown above provided generally better fits of “observations”. For example, the inversion of GOCART output using simplified single aerosol model resulted in the almost double smaller residuals ($\sigma_{\text{abs}} \approx 0.02$ and $\sigma_{\text{rel}} \approx 25\%$). Thus, these high residual of fitting MODIS observations indicate the retrieval limitations. Probably, the main factor limiting the level of observation fitting is the accuracy of τ_{fine} (0.55) provided by MODIS since the values $\sigma_{\text{abs}} \approx 0.04$ and $\sigma_{\text{rel}} \approx 48\%$ are close to accuracy of MODIS data ($\Delta\tau = \pm 0.03 \pm 0.05\tau$ over ocean and $\Delta\tau = \pm 0.05 \pm 0.15\tau$ over land). At the same, the observation accuracy is not the only factor limiting the retrieval approach. Other limitations and their possible effects on the retrieval will be discussed in next section.

Figures 17 and 18 show the results obtained from inversion of the optical thickness τ_{coarse} (0.55) provided by MODIS for coarse mode aerosol. The desert dust and sea salt emission distribution used by GOCART for the same time period of August 2000 is shown in Fig. 15. As follows from comparison of Figs. 17 and 15, the major desert dust emission sources, in principle, can be identified in the retrieved emission field. However the most intense desert dust sources (e.g. over Saharan Desert) seem to be

Retrieving global sources of aerosols from MODIS observations

O. Dubovik et al.

Title Page

Abstract

Introduction

Conclusions

References

Tables

Figures

⏪

⏩

◀

▶

Back

Close

Full Screen / Esc

Printer-friendly Version

Interactive Discussion

underestimated in magnitudes and have unrealistically spread locations. As discussed earlier the main cause of these uncertainties is the lack of MODIS observations over the desert dust sources (see Fig. 18). Therefore, even though the $\tau_{\text{coarse}}(0.55)$ are fitted rather accurately ($\sigma_{\text{abs}} \approx 0.04$ and $\sigma_{\text{rel}} \approx 48\%$ after 40 iterations), the desert dust retrieval is obviously less robust than in case of inversion of $\tau_{\text{fine}}(0.55)$. Also, some likely false sources can be seen over Atlantic Ocean near western coast of African continent. These sources correspond to rather high concentrations of $\tau_{\text{coarse}}(0.55)$ in the same region that cannot be explained by desert dust transport from desert dust sourced in Sahara. At the same time, high loading of biomass burning aerosol was transported from the African continent in the same period of time that is shown on Figs. 13–14. Correspondingly, one can speculate that $\tau_{\text{coarse}}(0.55)$ observed over that area could be attributed to the coarse mode of biomass burning aerosol. However the accurate derivation of biomass coarse mode fraction of smoke is probably challenging because smoke is dominated by small particles. Therefore some inconsistency of MODIS retrieval would be surprising in this situation. The agreement between retrieved sea salt emission (we attribute all coarse mode aerosol emissions over ocean) and assumed by GOCART model is rather dubious. That probably can be explained by the fact that typical loading of marine aerosol is rather low (Smirnov et al., 2003) and therefore it often is at the level of MODIS retrieval uncertainty. At the same time, both the retrieval and GOCART assumption (not shown) indicate the pronounced sea salt emissions over roaring forties region in the Southern Hemisphere.

In addition to the illustrations shown on Figs. 17–18 we have analyzed time and spatial changes in the retrieved emissions and we found several cases of unrealistically high variability in the retrieved emission patterns. Therefore, we have tried the usage of a priori constraints on the time and horizontal variability of the emission. The effects of applying such a priori constraints is illustrated by Fig. 19. There it can be seen that such constraints (especially those on spatial variability) help to eliminate some unrealistically strong emissions over oceans. However, the fitting residuals were higher ($\sigma_{\text{abs}} \approx 0.06$ and $\sigma_{\text{rel}} \approx 61\%$ after 40 iterations) once the a priori constraints were applied.

Retrieving global sources of aerosols from MODIS observations

O. Dubovik et al.

Title Page

Abstract

Introduction

Conclusions

References

Tables

Figures

⏪

⏩

◀

▶

Back

Close

Full Screen / Esc

Printer-friendly Version

Interactive Discussion

3.4 Issues and perspectives

Thus, the numerical tests and the applications to the real satellite data have shown that employed approach and the developed algorithm allow deriving useful information about global distribution of aerosol emissions without using excessive a priori information about locations and strength of aerosol sources. Correspondingly, one can expect that applying the algorithm to long time records of satellite observation should provide a climatology of global aerosol emissions that can be a very valuable asset in efforts aimed to improve understanding of aerosol forcing of global climate. Although all discussions above in this paper are focused on analysis only two week of observations the application of the developed algorithm to longer sets of observations is very feasible. For illustrating this capability of the algorithm we have processed 6 months of $\tau_{\text{fine}}(0.55)$ MODIS data in year 2001. Figure 20 shows the distribution of the fine mode aerosol global emissions for February, May and July of 2001. These retrievals can be potentially useful for studying dynamics of global aerosol emissions. For example, for Central and Southern Africa Fig. 20 shows higher emissions in February and July compare to emissions in May. Such dynamics can be explained by known seasonality of biomass burning. Also, the retrievals show high emission over Indian sub-continent in February that agrees with known high level of pollution in this region during winter. In future studies we expect to conduct comprehensive analysis of the long record of the retrievals and provide climatologically valuable emission fields. Such analysis can be rather extensive and likely will be combined with various improvements of the method. Therefore, the retrievals in Fig. 20 are shown here mainly for illustrating algorithm functionality and a comprehensive assessment of potential of this approach will be a subject of the continuation of these studies. Nonetheless, the analysis of both the limitations and possibilities of improvements in the developed method can already provide useful outlook on the potential of the presented developments.

Retrieving global sources of aerosols from MODIS observations

O. Dubovik et al.

Title Page

Abstract

Introduction

Conclusions

References

Tables

Figures

⏪

⏩

◀

▶

Back

Close

Full Screen / Esc

Printer-friendly Version

Interactive Discussion

3.4.1 Limitation of satellite observations

Obviously the quality of the global emission retrieval is driven by the content and quality of MODIS aerosol data. Specifically, as discussed earlier, MODIS data do not provide any information about vertical variability of aerosol properties and do not allow any distinction between aerosol types with different chemical composition (e.g. between BC, OC and sulfates). The lack of MODIS retrieval reliability over bright surfaces seriously limits the outcome of desert dust emission retrievals. The accuracy of MODIS retrieval also imposes considerable limitations on global emission retrievals. For example, the inversion of $\tau_{\text{fine}}(0.55)$ resulted to measurements fitting errors ($\sigma_{\text{abs}} \approx 0.04$ and $\sigma_{\text{rel}} \approx 48\%$) that are at same level as MODIS data accuracy ($\Delta\tau = \pm 0.03 \pm 0.05\tau$ over ocean and $\Delta\tau = \pm 0.05 \pm 0.15\tau$ over land). Our numerical tests suggest that such error level by itself would not allow us fully benefit from atmospheric modeling refinements. Indeed, in the numerical tests shown in Figs. 11–12, $\tau_{\text{fine}}(0.55)$ composed from BC, OC and sulfates (simulated using GOCART model) was fitted with noticeably higher accuracy ($\sigma_{\text{abs}} \approx 0.02$ and $\sigma_{\text{rel}} \approx 25\%$) under assumption of single fine mode aerosol that neglects the differences in chemical composition of these aerosols. It should be noted that values of errors in MODIS retrievals ($\Delta\tau = \pm 0.03 \pm 0.05\tau$ over ocean and $\Delta\tau = \pm 0.05 \pm 0.15\tau$ over land) are provided for MODIS total aerosol optical thickness $\tau_{\text{total}}(0.55)$, while the procedure separating $\tau_{\text{total}}(0.55)$ into $\tau_{\text{coarse}}(0.55)$ and $\tau_{\text{fine}}(0.55)$ that used in present studies is likely associated with some decline of accuracy of $\tau_{\text{coarse}}(0.55)$ and $\tau_{\text{fine}}(0.55)$ compare to accuracy of $\tau_{\text{total}}(0.55)$ (Remer et al., 2005; Anderson et al., 2005). Obviously, at least, some of the above-mentioned measurements limitations will be addressed in future studies. For example, a number of improvements in the operational MODIS aerosol algorithm are under developments (Remer et al., 2005). Also, there are some new retrieval algorithm developments (Hsu et al., 2004) that are expected to improve MODIS retrieval over bright surfaces.

In addition, the global emission retrieval can be applied not only to the MODIS data but also to the data provided by other aerosol satellite sensors, such as, MISR (Diner

Retrieving global sources of aerosols from MODIS observations

O. Dubovik et al.

Title Page

Abstract

Introduction

Conclusions

References

Tables

Figures

⏪

⏩

◀

▶

Back

Close

Full Screen / Esc

Printer-friendly Version

Interactive Discussion

et al., 1998; Kahn et al., 2005), POLDER (Deschamps et al., 1994; Deuze et al., 2001), APS (Mischenko et al., 2004), etc. For example MISR sensor has multi-angle measurement capability that generally allows retrieval of the larger number of aerosol parameters and results into more robust retrievals over strongly reflective surfaces (e.g. Kahn et al., 2005; Mischenko et al., 2004). Moreover, the satellite instruments with multi-angular polarimetric capabilities have sensitivity to detailed aerosol properties including such parameters as aerosol absorption and index of refraction. Correspondingly, the observation from satellite polarimeters may allow global retrieval to discriminate between emissions of aerosols of different chemical composition. In addition, using data from multiple satellite sensors as an input to the global inversion should be beneficial due to enhanced spatial and temporal data coverage that should be improved compare to the coverage of any single sensor.

3.4.2 Limitation of modeling accuracy

As discussed in the Sect. 2, the employed inversion approach optimizes the solution using known statistics of the measurement errors under assumption that the errors of the model are much smaller than those of measurements and the effect of the model errors can be neglected. Such assumption is employed in most inverse methodologies and it can be easily justified in many applications. For example atmospheric remote sensing relies on radiative transfer models that simulate atmospheric radiances with very high accuracy. Global modeling is not unified to the same level of certainty as radiative modeling and the effects of modeling uncertainties on the retrievals may not be negligible. Many factors may potentially contribute into the modeling uncertainty. For example, the meteorological fields, such as atmospheric temperature, pressure, distributions of winds, etc., used by models as inputs are known with limited accuracy. Significant uncertainty in four-dimensional distribution of clouds affects the aerosol modeling, e.g. via uncertainty in aerosol transport by cloud convection. The aerosol removal processes that are employed in the models are known only with a limited accuracy. Such atmospheric processes as those responsible for aerosol-cloud interactions are known only

Retrieving global sources of aerosols from MODIS observations

O. Dubovik et al.

Title Page

Abstract

Introduction

Conclusions

References

Tables

Figures

⏪

⏩

◀

▶

Back

Close

Full Screen / Esc

Printer-friendly Version

Interactive Discussion

qualitatively and do not have well-established quantitative formalism. The limitations of time and space resolution (e.g. GOCART model provides aerosol on the scale of $2^{\circ} \times 2.5^{\circ}$ in version used in this study) do not allow reproducing some local details of aerosol dynamics. In addition, all models suffer from numerical instabilities that result into modeling problems such as appearance of negative aerosol mass, failure to conserve aerosol mass in transport simulations, etc. All these uncertainties limit the accuracy of global aerosol modeling as demonstrated in recent model intercomparison studies via inter comparisons of different models outputs and also by comparison of modeling results with observations (e.g., Kinne et al., 2003, 2006; Textor et al., 2006).

At the same time, there are a number of efforts that will likely address in near future many of above mentioned uncertainty factors. For example, four-dimensional meteorological wind fields and cloud distributions are expected to be improved via assimilations of all available observations. The modeling resolution to be improved, e.g. new version of GOCART model with resolution of $1^{\circ} \times 1^{\circ}$ recently became available.

There are also some noticeable differences in modeling aerosol optical properties between approaches employed by the global models and by remote sensing. For example, GOCART, as most of models, is built on the assumption that all coarse aerosol particles belong either to dust or sea salt. The satellite retrieval algorithms (e.g. Kaufman et al., 1997; Tanré et al., 1997; Remer et al., 2005, etc.) rely on climatologies formed by aerosol retrievals obtained from remote sensing observations of ambient aerosol. In a contrast to global models, such climatologies (e.g. Remer et al., 1997; Dubovik, 2002) indicate the presence of coarse particles in practically all types of aerosol including biomass burning and urban pollution. Also, the aerosol composition is included differently in satellite retrieval algorithm compare to global models. The satellite retrievals usually utilize complex index of refraction derived from remote sensing observations for ambient aerosol, while the models tend to calculate radiative properties of aerosol based on chemical composition using index of refraction obtained from in situ or laboratory measurements for each chemical component. This difference also may be a source of inconsistency between remote sensing observations and mod-

Retrieving global sources of aerosols from MODIS observations

O. Dubovik et al.

Title Page

Abstract

Introduction

Conclusions

References

Tables

Figures

⏪

⏩

◀

▶

Back

Close

Full Screen / Esc

Printer-friendly Version

Interactive Discussion

els. For example, recent analysis of aerosol remote sensing retrievals (Kaufman et al., 2001; Dubovik et al., 2002) showed that mineral dust is less absorbing than it was previously considered (and assumed in most of global models). Correspondingly, the comparisons of aerosol global modeling showed systematic differences with remote sensing observations for the absorption of aerosol dominated by mineral dust (e.g. Takemura et al., 2002; Sato et al., 2003). One of possible ways of addressing this inconsistency is to include satellite retrieval as part of inverse modeling. In such approach the aerosol emissions will be retrieved directly from atmospheric radiances (e.g. using mathematical formalism described in Sect. 2.8). This technique also may be advantageous for retrieving global emission form the measurements by several satellite sensors since it should eliminate effects that could be caused by differences in the satellite retrieval algorithms.

3.4.3 Limitations of employed retrieval approach

The numerical inversion approach has some limitations by itself. Namely, as explained in Sect. 2.6, the inversion algorithm is based on steepest descent method. This is iterative method that usually has very slow convergence (e.g. Tarantolla, 1987). Nonetheless, the convergence is sufficiently fast in problems of global models inversion because the transport operator \mathbf{T} (written in matrix form) is rather sparse. In our applications, (see Sects. 3.2–3.3) after 40 iterations the retrieval algorithm was decreasing the fitting residual to the value much smaller than expected noise level in inverted satellite data. Since each iteration includes two runs of GOCART model (forward and backward), the inversion of some global data takes about 80 times more time than simulations of aerosol fields by GOCART model for the same time period. This is substantial increase in computation time compare to forward modeling. Nonetheless, taking into account global nature of the problem and quickly improving speed of modern computers these time expenses are probably acceptable. Even with the moderately powerful computers used for this study we did not feel necessity to put too much limitation due to the computational time. Nonetheless, we tried to identify possibilities to use smaller number of

Retrieving global sources of aerosols from MODIS observations

O. Dubovik et al.

Title Page

Abstract

Introduction

Conclusions

References

Tables

Figures

⏪

⏩

◀

▶

Back

Close

Full Screen / Esc

Printer-friendly Version

Interactive Discussion

iterations (e.g. Gill et al., 1982; Tarantolla, 1987). Theoretically, implementing method of conjugated gradients can accelerate the convergence. This method is known for superior convergence than steepest descent method and also uses only gradient vectors and, therefore, can be implemented using transport model adjoint operators (see details in Appendix C). However, in practice rounding errors often cause the computed directions to rapidly loose conjugacy, and the method behaves more like an iterative method and it makes converge much slower than theoretically predicted (Gill et al., 1982). In order to check this possibility of accelerating inversion convergence we have implemented method of conjugated gradients as described in Appendix C. The tests showed improvements in convergence: after only 20 iterations method of conjugated gradients was reaching the same level of residual as steepest descent method after 40 iterations. However, as can be seen from derivations in Appenidx C, our implementation of the one iteration of the method of conjugated gradients required running GOCART model 4 times, instead of two runs as it was used in the steepest descent method. Therefore, 20 iterations by method of conjugated gradients were equal in computing time to 40 iterations by steepest descent method and using the method of conjugated gradients practically did not allow us to accelerate inversion. At the same time, implementing the method of conjugated gradients required more efforts because the formal logistic of the method of conjugated gradients is noticeably more complex than that of the steepest descent method. Thus our efforts did not reveal a practical advantage of using the method of conjugated gradients. Nonetheless, there might be a need of some more studies on possibilities to accelerate convergence of the inversion, in particular taking into account prospective future developments. For example, inevitable increase in resolution of aerosol global models will result in less sparse equations and, therefore, in possible slowing in convergence of the steepest decent method iterations. Similarly, steepest decent method may converge slower if satellite retrieval (discussed in Sect. 2.8) will be included as a part of inverse modeling, because of rather complex mathematical structure of radiative transfer equations.

Using diverse a priori constrains is another direction requiring further exploration. In

Retrieving global sources of aerosols from MODIS observations

O. Dubovik et al.

Title Page

Abstract

Introduction

Conclusions

References

Tables

Figures

⏪

⏩

◀

▶

Back

Close

Full Screen / Esc

Printer-friendly Version

Interactive Discussion

Retrieving global sources of aerosols from MODIS observationsO. Dubovik et al.

[Title Page](#)[Abstract](#)[Introduction](#)[Conclusions](#)[References](#)[Tables](#)[Figures](#)[⏪](#)[⏩](#)[◀](#)[▶](#)[Back](#)[Close](#)[Full Screen / Esc](#)[Printer-friendly Version](#)[Interactive Discussion](#)

Sect. 2.7 we have described the mathematical techniques for using a priori estimates of emissions or a priori limitations on derivatives of time and space variability of emissions. Using these a priori constraints can substantially extend the field of the retrieved parameters. For example, using a priori estimate of emissions MODIS data can be used in emission retrieval discriminating aerosol type in spite of the lack of information in MODIS data about aerosol type. However, in such situation the retrieval may be too dependent on used a priori assumptions. Correspondingly, it is necessary to make sure that used a priori information is really available in amount used in the retrieval. Otherwise, if the constraints are used to make solution unique but they are not supported by actual knowledge, the retrieval can be unique and stable but, at the same time, misleading and therefore useless. Therefore, in this study we have developed and tested retrieval using a priori estimates of emissions but we placed the focus of our applications on the retrieval that did not use such a priori constraints. We have also shown (Fig. 19) that using a priori limitations on time and space derivatives of emission variability one can retain physically realistic time and space continuity (with no sharp oscillations) of the emission fields, even if inverted measurements do not provide sufficient constraints. However, generally we found that due to rather coarse time (24 h) and space ($2.0^\circ \times 2.5^\circ$) resolution used in this study these constraints do not seem to be critical in our retrievals. Nonetheless, in future studies attempting retrieval with much higher resolutions the importance of continuity constraints will likely increase.

4 Conclusion

This paper describes development of an algorithm using inverse modeling for retrieving global sources of aerosol from satellite observations.

The numerical inversion in the algorithm was structured as multi-term least-squares-type fitting. This scheme of statistical optimization allows for high flexibility in constraining the retrieval. For example, it allows using multiple constraints in single retrieval. Also the possibility of constraining time and space variability of the retrieved

global aerosol emissions by applying a priori limitations on the partial derivatives of retrieved characteristics was discussed and demonstrated. Such a way of constraining is not common in inverse modeling while it is widely used in atmospheric remote sensing. The similarities and differences of the developed inversion scheme with standard Kalman filter inverse modeling approach and Phillips-Tikhonov-Twomey constrained remote sensing inversion are discussed. In order to apply the numerical inversion for simultaneous retrieval of global aerosol fields for extended period of time at space and time resolution of model the fitting was expressed using an adjoint operators in the form convenient for practical implementation of the inversion. Applying various a priori constraints in the retrieval utilizing adjoint operation to the global model is discussed.

The algorithm was practically implemented on the basis of GOCART aerosol transport model for retrieving global aerosol emissions with $2^\circ \times 2.5^\circ$ horizontal resolution from global distribution of aerosol optical thickness. The conducted numerical tests showed that the algorithm accurately derives aerosol emissions by inverting detailed aerosol mass global distribution produced from forward run of GOCART model. At the same time the test revealed that once MODIS data used as an input for the inversion some extra constraints are needed for making retrieval unique due to limitation in coverage and information content of MODIS observations. Specifically, the emission variability within 24 h was neglected. Also aerosol types were discriminated only by particle size but not by their chemical composition. The emissions of fine and coarse mode aerosols were retrieved from the MODIS fine and coarse mode aerosol optical thickness data respectively. Both numerical test and the results of actual MODIS data inversion showed that the developed method allows appropriate retrieval of the location and the strength of the fine mode global emissions. Namely, the global placement of the fine mode aerosol sources retrieved from MODIS observations during two weeks in August 2000 was coherent with available independent knowledge. That was particularly encouraging since the developed inverse method did not use any a priori information about sources and it was initialized under “no aerosol emission” assumption. The retrieval reproduced two weeks of instantaneous global observations of MODIS

Retrieving global sources of aerosols from MODIS observations

O. Dubovik et al.

[Title Page](#)[Abstract](#)[Introduction](#)[Conclusions](#)[References](#)[Tables](#)[Figures](#)[⏪](#)[⏩](#)[◀](#)[▶](#)[Back](#)[Close](#)[Full Screen / Esc](#)[Printer-friendly Version](#)[Interactive Discussion](#)

Retrieving global sources of aerosols from MODIS observationsO. Dubovik et al.

[Title Page](#)[Abstract](#)[Introduction](#)[Conclusions](#)[References](#)[Tables](#)[Figures](#)[⏪](#)[⏩](#)[◀](#)[▶](#)[Back](#)[Close](#)[Full Screen / Esc](#)[Printer-friendly Version](#)[Interactive Discussion](#)

with the standard deviation in fitting of aerosol optical thickness of ~ 0.04 . The optical thickness during high aerosol loading events of loading was reproduced with the standard deviation of $\sim 48\%$. Such agreement between global modeling and observation seems to be quite encouraging given that the coherency between models and observations may be limited by a number of factors. For example, the MODIS observations have limited accuracy. The variability of aerosol can be much higher than the model resolution, there are uncertainties in meteorological data (wind fields, 3-dimensional cloud distribution, etc.), formalization of atmospheric processes has limited accuracy due to employed physical assumptions, numerical instabilities, etc. As a result, the model prediction can significantly differ from observations even for monthly and yearly averaged regional aerosol properties (Kinne et al., 2003; Sato et al., 2003).

The applications of the algorithm for the retrieval of coarse mode retrieval was less successful, mainly because of lack of MODIS data over desert dust sources due to the fact that MODIS retrievals are not performed over surface with very bright reflectance such as desert dust. This situation will be much improved since the most recent version of MODIS (collection 5) should include the retrieval over desert provided by algorithm of Hsu et al. (2004).

The efficiency of using a priori constraints on values of the emissions or on their variability was also evaluated. The use of such a priori constraints is a clear alternative to a straightforward reduction of the number of retrieved parameters characterizing the aerosol emission. For example, in spite of limitations in MODIS data, if the algorithm uses GOCART emission fields as a priori estimates it can be set for retrieval of aerosol emissions in the same format as they used in GOCART model (i.e. fully discriminated by chemical composition and sizes). Such strategy is usually employed in assimilation approach. However in that retrieval scenario tends to tie up the retrieved emissions to a priori estimates of emissions that may devalue the usage of satellite observations. Therefore, further efforts are desirable for minimizing the possible effect of overconstraining the solution and in present paper we did not utilize a priori estimates for inverting MODIS observations. Instead we applied constraints that limit general time and

spatial variability of emissions and demonstrated that such general constraints were useful for eliminating some unrealistic features in underdetermined retrievals such as retrieval of coarse mode aerosol emissions from MODIS observations.

To illustrate performance of the algorithm for processing long records of satellite observations we have inverted optical thickness of fine mode aerosol provided by MODIS for first six months of year 2001. The derived emissions demonstrate realistic distribution of global aerosol emission patterns and their seasonal dynamics.

Thus, the developed method can be a useful tool for improving global aerosol sources in chemical models. Nevertheless, this paper described only the first phase of the efforts and further analysis is necessary for understanding full potential of the method. Specifically, we plan using MODIS data for generating climatological records of remote sensing driven aerosol emission fields that are expected to provide a useful input for improving global aerosol sources in chemical models. The usage a priori constraints and the method convergence are planned to be refined and optimized. Also, at least some of the satellite measurements limitations are expected to be addressed in future studies. For example, a number of MODIS aerosol algorithm improvements are under developments that are expected to improve MODIS retrieval over bright surfaces. Moreover, the global emission retrieval can be a combination of the products provided by other aerosol satellite sensors, such as MODIS, CALIPSO, MISR, PARASOL, APS etc. Using data from multiple satellite sensors as an input should improve spatial and temporal constraints for the global emission retrieval compare to the usage of the data from any single sensor. In addition, using data from multi-angle radiometers (MISR), polarimeters (PARASOL, APS) and lidar data (CALIPSO) may allow global retrieval to discriminate between emissions of aerosols of different chemical composition.

Retrieving global sources of aerosols from MODIS observations

O. Dubovik et al.

Title Page

Abstract

Introduction

Conclusions

References

Tables

Figures

⏪

⏩

◀

▶

Back

Close

Full Screen / Esc

Printer-friendly Version

Interactive Discussion

Appendix A

Adjoint operator

According to its formal definition (e.g. Tarantola. 1987), the adjoint of \mathbf{G} , $\mathbf{G}^\#$, is a linear operator defined by equality of scalar products:

$$\langle \mathbf{G}^\# \mathbf{x}, \mathbf{y} \rangle = \langle \mathbf{x}, \mathbf{G} \mathbf{y} \rangle. \quad (\text{A1})$$

If scalar product is defined as follows:

$$\langle \mathbf{a}, \mathbf{b} \rangle = \mathbf{a}^T \mathbf{b}, \quad (\text{A2})$$

Then, the right side of Eq. (A1) is:

$$\langle \mathbf{x}, \mathbf{G} \mathbf{y} \rangle = \mathbf{x}^T \mathbf{G} \mathbf{y}. \quad (\text{A3})$$

The left side of Eq. (A1) is:

$$\langle \mathbf{G}^\# \mathbf{x}, \mathbf{y} \rangle = (\mathbf{G}^\# \mathbf{x})^T \mathbf{y} = \mathbf{x}^T (\mathbf{G}^\#)^T \mathbf{y}. \quad (\text{A4})$$

Thus, in order to achieve the equality between Eqs. (A3) and (A4) we can write for $\mathbf{G}^\#$:

$$\mathbf{G}^\# = \mathbf{G}^T. \quad (\text{A5})$$

It should be noted that Tarantola (1987) gives more general definition of adjoint operator that is not used here.

Appendix B

Derivation of Eq. (41)

Equation (2) can be written for one time step in matrix form as follows:

$$\mathbf{M}_n = \mathbf{T}_{n-1}(\mathbf{M}_{n-1} + \mathbf{S}_{n-1}), \quad (\text{B1})$$

where subscripts “ $n-1$ ” and “ n ” are associated with times steps t_{n-1} and $t_n=t_{n-1}+\Delta t$, i.e. matrix \mathbf{T}_{n-1} and vectors \mathbf{S}_{n-1} , \mathbf{M}_{n-1} and \mathbf{M}_n represent $T(t_{n-1}, \mathbf{x})$, $s(t_{n-1}, \mathbf{x})$, $m(t_{n-1}, \mathbf{x})$ and $m(t_{n-1}+\Delta t, \mathbf{x})$ correspondingly. For time steps t_{n-2} , t_{n-1} and t_n one can write:

$$\begin{aligned} \mathbf{M}_n &= \mathbf{T}_{n-1}(\mathbf{M}_{n-1} + \mathbf{S}_{n-1}) = \mathbf{T}_{n-1}(\mathbf{T}_{n-2}(\mathbf{M}_{n-2} + \mathbf{S}_{n-2}) + \mathbf{S}_{n-1}) = \\ &= \mathbf{T}_{n-1}\mathbf{T}_{n-2}\mathbf{M}_{n-2} + \mathbf{T}_{n-1}\mathbf{T}_{n-2}\mathbf{S}_{n-2} + \mathbf{T}_{n-1}\mathbf{S}_{n-1}. \end{aligned} \quad (\text{B2})$$

Correspondingly, the mass transport for t_0, t_1, \dots, t_n can be expressed as:

$$\mathbf{M}_n = \left(\prod_{i=0}^{i=n-1} \mathbf{T}_i \right) \mathbf{M}_0 + \sum_{k=0}^{k=n-1} \left(\prod_{i=k}^{i=n-1} \mathbf{T}_i \right) \mathbf{S}_k, \quad (\text{B3})$$

where

$$\prod_{i=0}^{i=n-1} \mathbf{T}_i = \mathbf{T}_{n-1}\mathbf{T}_{n-2}\dots\mathbf{T}_2\mathbf{T}_1\mathbf{T}_0. \quad (\text{B4})$$

Based on Eq. (B3) the entire matrix Eq. (5) for mass distribution during time period from t_0 to t_n can be written as follows:

$$\begin{pmatrix} \mathbf{M}_n^* \\ \dots \\ \mathbf{M}_3^* \\ \mathbf{M}_2^* \\ \mathbf{M}_1^* \end{pmatrix} = \begin{pmatrix} \mathbf{T}_{n-1} & \prod_{i=n-2}^{i=n-1} \mathbf{T}_i & \dots & \prod_{i=2}^{i=n-1} \mathbf{T}_i & \prod_{i=1}^{i=n-1} \mathbf{T}_i & \prod_{i=0}^{i=n-1} \mathbf{T}_i \\ \dots & \dots & \dots & \dots & \dots & \dots \\ 0 & 0 & \dots & \mathbf{T}_2 & \prod_{i=1}^{i=2} \mathbf{T}_i & \prod_{i=0}^{i=2} \mathbf{T}_i \\ 0 & 0 & \dots & 0 & \mathbf{T}_1 & \prod_{i=0}^{i=1} \mathbf{T}_i \\ 0 & 0 & \dots & 0 & 0 & \mathbf{T}_0 \end{pmatrix} \begin{pmatrix} \mathbf{S}_{n-1} \\ \dots \\ \mathbf{S}_2 \\ \mathbf{S}_1 \\ \mathbf{S}_0 \end{pmatrix}, \quad (\text{B5})$$

Retrieving global sources of aerosols from MODIS observations

O. Dubovik et al.

Title Page

Abstract

Introduction

Conclusions

References

Tables

Figures

◀

▶

◀

▶

Back

Close

Full Screen / Esc

Printer-friendly Version

Interactive Discussion

where \mathbf{M}_n^* denotes mass distribution of aerosol emitted during time period from t_0 to t_n : i.e.

$$\mathbf{M}_n^* = \mathbf{M}_n - \left(\prod_{i=0}^{n-1} \mathbf{T}_i \right) \mathbf{M}_0. \quad (\text{B6})$$

Thus, Eq. (B5) is equivalent to generalized matrix expression:

$$5 \quad \mathbf{M}^* = \mathbf{M} - \mathbf{T}\mathbf{M}_0 = \mathbf{T}\mathbf{S}, \quad (\text{B7})$$

This is slightly modified form of Eq. (5). Correspondingly, for the correction term $\Delta\hat{\mathbf{S}}^p$ of the steepest descent iterative solution given by Eq. (40) can be written as:

$$\Delta\hat{\mathbf{S}}^p = \mathbf{T}^T \mathbf{C}_m^{-1} \Delta\mathbf{M}^p = \mathbf{T}^T \Delta^p = \begin{pmatrix} \mathbf{T}_{n-1}^T & \dots & 0 & 0 & 0 \\ \prod_{i=n-2} \mathbf{T}_i^T & \dots & 0 & 0 & 0 \\ \dots & \dots & \dots & \dots & \dots \\ \prod_{i=n-1} \mathbf{T}_i^T & \dots & \mathbf{T}_2^T & 0 & 0 \\ \dots & \dots & \dots & \dots & \dots \\ \prod_{i=n-1} \mathbf{T}_i^T & \dots & \prod_{i=1} \mathbf{T}_i^T & \mathbf{T}_1^T & 0 \\ \dots & \dots & \dots & \dots & \dots \\ \prod_{i=n-1} \mathbf{T}_i^T & \dots & \prod_{i=2} \mathbf{T}_i^T & \prod_{i=1} \mathbf{T}_i^T & \mathbf{T}_0^T \\ \dots & \dots & \dots & \dots & \dots \\ \prod_{i=n-1} \mathbf{T}_i^T & \dots & \prod_{i=2} \mathbf{T}_i^T & \prod_{i=1} \mathbf{T}_i^T & \mathbf{T}_0^T \end{pmatrix} \begin{pmatrix} \Delta_n^p \\ \Delta_{n-1}^p \\ \dots \\ \Delta_3^p \\ \Delta_2^p \\ \Delta_1^p \end{pmatrix}, \quad (\text{B8})$$

where $\Delta^p = \mathbf{C}_m^{-1} \Delta\mathbf{M}^p$, Δ_i^p denotes the component of vector Δ^p corresponding to time step t_i and the following identity for a transposed of the matrix multiplication product is used:

$$\left(\prod_{i=0}^{i=n} \mathbf{T}_i \right)^T = (\mathbf{T}_n \mathbf{T}_{n-1} \dots \mathbf{T}_2 \mathbf{T}_1 \mathbf{T}_0)^T = \mathbf{T}_0^T \mathbf{T}_1^T \mathbf{T}_2^T \dots \mathbf{T}_{n-1}^T \mathbf{T}_n^T = \prod_{i=n} \mathbf{T}_i^T. \quad (\text{B9})$$

Retrieving global sources of aerosols from MODIS observations

O. Dubovik et al.

Title Page

Abstract

Introduction

Conclusions

References

Tables

Figures

⏪

⏩

◀

▶

Back

Close

Full Screen / Esc

Printer-friendly Version

Interactive Discussion

From Eq. (B8), ΔS^p can be obtained as:

$$\Delta S^p = \begin{pmatrix} \Delta S_n^p \\ \Delta S_{n-1}^p \\ \dots \\ \Delta S_2^p \\ \Delta S_1^p \\ \Delta S_0^p \end{pmatrix} = \begin{pmatrix} \mathbf{T}_{n-2}^T \Delta_{n-1}^p + \mathbf{T}_{n-2}^T \mathbf{T}_{n-1}^T \Delta_n^p \\ \dots \\ \sum_{k=3}^{k=n-1} \left(\prod_{i=n-1}^{i=k} \mathbf{T}_i^T \Delta_k^p \right) \\ \sum_{k=2}^{k=n-1} \left(\prod_{i=n-1}^{i=k} \mathbf{T}_i^T \Delta_k^p \right) \\ \sum_{k=1}^{k=n-1} \left(\prod_{i=n-1}^{i=k} \mathbf{T}_i^T \Delta_k^p \right) \end{pmatrix} = \begin{pmatrix} \mathbf{T}_{n-2}^T \left(\Delta_{n-1}^p + \mathbf{S}_{n-1}^p \right) \\ \dots \\ \mathbf{T}_2^T \left(\Delta_3^p + \Delta S_3^p \right) \\ \mathbf{T}_1^T \left(\Delta_2^p + \Delta S_2^p \right) \\ \mathbf{T}_0^T \left(\Delta_1^p + \Delta S_1^p \right) \end{pmatrix}. \quad (\text{B10})$$

From this equation it can be seen that ΔS_i^p can be calculated via the following sequence starting from $i=n$ as follows:

$$\Delta S_{i-1}^p = \mathbf{T}_{i-1}^T \left(\Delta_i^p + \Delta S_i^p \right). \quad (\text{B11})$$

The component Δ_i^p of vector Δ^p corresponding to time step t_i can be easily formulated if observational errors $\Delta \mathbf{M}^*$ do not have time correlations but may have spatial correlations. In this case then \mathbf{C}_m has array structure:

$$\mathbf{C}_m = \begin{pmatrix} \mathbf{C}_{m_n} & & & & \\ \dots & \dots & \dots & \dots & \\ \dots & \dots & \mathbf{C}_{m_2} & 0 & \\ \dots & \dots & 0 & \mathbf{C}_{m_1} & \end{pmatrix}, \quad (\text{B12})$$

Retrieving global sources of aerosols from MODIS observations

O. Dubovik et al.

Title Page

Abstract

Introduction

Conclusions

References

Tables

Figures

◀

▶

◀

▶

Back

Close

Full Screen / Esc

Printer-friendly Version

Interactive Discussion

and Δ^p can be decomposed:

$$\Delta^p = \begin{pmatrix} \Delta_n^p \\ \dots \\ \Delta_2^p \\ \Delta_1^p \end{pmatrix} = \begin{pmatrix} \mathbf{C}_{m_n}^{-1} \left(\mathbf{M}_n \left(\hat{\mathbf{S}}^p \right) - \mathbf{M}_n^* \right) \\ \dots \\ \mathbf{C}_{m_2}^{-1} \left(\mathbf{M}_2 \left(\hat{\mathbf{S}}^p \right) - \mathbf{M}_2^* \right) \\ \mathbf{C}_{m_1}^{-1} \left(\mathbf{M}_1 \left(\hat{\mathbf{S}}^p \right) - \mathbf{M}_1^* \right) \end{pmatrix}. \quad (\text{B13})$$

Thus, Eq. (B11) gives relationship between $\Delta \mathbf{S}_{i-1}^p$ corresponding to time step t_{i-1} and $\Delta \mathbf{S}_i^p$ corresponding to time step $t_i = t_{i-1} + \Delta t$. Once time step is very small, i.e. $\Delta t \rightarrow 0$ then Eq. (B11) can be rewritten via integral equivalent:

$$\Delta \hat{\mathbf{S}}^p(t, \mathbf{x}) = \int_t^{t_0} T^\#(t', \mathbf{x}) \left(\Delta \hat{\mathbf{S}}^p(t', \mathbf{x}) + \Delta^p(t', \mathbf{x}) \right) (-dt'), \quad (\text{B14})$$

where function $\Delta^p(t, \mathbf{x})$ is continuous analog to vector Δ^p that can be formulated via weighting function $C^{-1}(t, \mathbf{x}, \mathbf{x}')$ (from covariance function $C_t(t, \mathbf{x}, \mathbf{x}')$) performing analogous role to the one of matrix $\mathbf{C}_{m_i}^{-1}$ in discrete representation, i.e.:

$$\left\{ \Delta_i^p \right\} = \left\{ \mathbf{C}_{m_i}^{-1} \Delta \mathbf{M}^p \right\}_i \rightarrow \iiint_{x', y', z'} C_t^{-1}(t_i, x_j, y_k, z_m, x', y', z') \Delta m^p(t_j, x', y', z') dx' dy' dz'. \quad (\text{B15})$$

The $T^\#(t, \mathbf{x})$ is adjoint of transport operator $T(t, \mathbf{x})$ that is composed by adjoints $T_i^\#(t, \mathbf{x})$ of component processes $T_i(t, \mathbf{x})$:

$$T^\#(t, \mathbf{x}) = T_1^\# T_2^\# T_3^\# \dots T_{n-1}^\# T_n^\#. \quad (\text{B16})$$

If errors of observation are uncorrelated, i.e. covariance matrix of measurements \mathbf{C}_m is diagonal with the elements on diagonal equal to $\sigma^2(t_i, x_j, y_k, z_m)$, the elements of

vector $\mathbf{C}_m^{-1} \Delta \mathbf{M}^p$ relate to continues function $\sigma^{-2}(t, \mathbf{x}) \Delta m^p(t, \mathbf{x})$ in straightforward way (see Eq. 42 in body text) then Eq. (B14) can be written as:

$$\Delta \hat{s}^p(t, \mathbf{x}) = \int_t^{t_0} T^\#(t', \mathbf{x}) \left(\Delta \hat{s}^p(t', \mathbf{x}) + \sigma^{-2}(t', \mathbf{x}) \Delta m^p(t', \mathbf{x}) \right) (-dt'). \quad (\text{B17})$$

where

$$\Delta m^p(t, \mathbf{x}) = m^*(t, \mathbf{x}) - \int_{t_0}^t T(t', \mathbf{x}) \left(m(t', \mathbf{x}) + s^p(t', \mathbf{x}) \right) dt', \quad (\text{B18})$$

The symbols $\Delta \hat{s}^p(\mathbf{x}, t)$ and $\sigma^{-2}(t, \mathbf{x}) \Delta m^p(t, \mathbf{x})$ denote function equivalents to the vectors $\Delta \hat{\mathbf{S}}^p$ and $\mathbf{C}_m^{-1} \Delta \mathbf{M}^p$ respectively.

Thus, the steepest descent iterative solution written via matrix expression in Eq. (40) can be replaced by the integral equivalents (Eqs. B17–B18). Further discussion is given in Sect. 2.5.

Appendix C

Application of conjugated gradient method to inversion based on adjoint transformation of the transport forward model

C1 Basic formulations of the conjugated gradient method

Let us formally write linear system as follows:

$$\mathbf{A}\mathbf{x} = \mathbf{y}^*. \quad (\text{C1})$$

Then, the solution of this system by the conjugated gradient method is the following iterative process:

$$\mathbf{x}^{k+1} = \mathbf{x}^k - \alpha_k \mathbf{p}_k, \quad (C2)$$

where

$$\alpha_k = \frac{\mathbf{p}_k^T \nabla_k}{\mathbf{p}_k^T \mathbf{A} \mathbf{p}_k} = \frac{\nabla_k^T \nabla_k}{\mathbf{p}_k^T \mathbf{A} \mathbf{p}_k}, \quad (C3)$$

and the gradient ∇_k is:

$$\nabla_x(\mathbf{x}^k) = \mathbf{A} \mathbf{x}_k = \mathbf{A} \mathbf{x}^k - \mathbf{y}^*. \quad (C4)$$

The vector \mathbf{p}_k is determined as the following:

$$\mathbf{p}_k = \nabla_k + \beta \mathbf{p}_{k-1}, \quad (C5)$$

where

$$\beta = \frac{\nabla_k^T \nabla_k}{\nabla_{k-1}^T \nabla_{k-1}}. \quad (C6)$$

The initial condition for the iterative process is the following:

$$\mathbf{p}_0 = \nabla_0. \quad (C7)$$

C2 Application to inversion of the transport forward model using adjoint operators

For inverting aerosol mass transport model $\mathbf{M} = \mathbf{T}(\mathbf{S} + \mathbf{M}_0)$ by the basic LSM the following equation should be solved:

$$(\mathbf{T}^T \mathbf{C}^{-1} \mathbf{T}) \mathbf{S} = \mathbf{T}^T \mathbf{C}^{-1} \mathbf{M}^*, \quad (C8)$$

where $\mathbf{M}^* = \mathbf{M}^{\text{meas}} - \mathbf{T} \mathbf{M}_0$.

Retrieving global sources of aerosols from MODIS observations

O. Dubovik et al.

Title Page

Abstract

Introduction

Conclusions

References

Tables

Figures

⏪

⏩

◀

▶

Back

Close

Full Screen / Esc

Printer-friendly Version

Interactive Discussion

Correspondingly, for applying the method of conjugated gradients we can determine the matrix \mathbf{A} and vector \mathbf{y}^* as:

$$\mathbf{A} = \mathbf{T}^T \mathbf{C}^{-1} \mathbf{T}, \quad (\text{C9})$$

$$\mathbf{y}^* = \mathbf{T}^T \mathbf{C}^{-1} \mathbf{M}^*, \quad (\text{C10})$$

$$5 \quad \nabla_k = \mathbf{A} \mathbf{S}^k - \mathbf{y}^* = (\mathbf{T}^T \mathbf{C}^{-1} \mathbf{T}) \mathbf{S}_k - \mathbf{T}^T \mathbf{C}^{-1} \mathbf{M}^* = \mathbf{T}^T \mathbf{C}^{-1} (\mathbf{T} \mathbf{S}_k - \mathbf{M}^*) = \mathbf{T}^T \mathbf{C}^{-1} \Delta \mathbf{M}_k, \quad (\text{C11})$$

$$\rho_k^T \mathbf{A} \rho_k = (\mathbf{T} \rho_k)^T \mathbf{C}^{-1} (\mathbf{T} \rho_k) = \rho_k^T \mathbf{T}^T \mathbf{C}^{-1} \mathbf{T} \rho_k \quad (\text{C12})$$

Finally, we have the following procedure:

$$\rho_k = \nabla_k + \beta_{k-1} \rho_{k-1}, \quad (\text{C13})$$

$$\rho_{-1} = \mathbf{0} \text{ and } \beta_{-1} = \mathbf{0} \quad (\text{C14})$$

$$10 \quad \nabla_k = \mathbf{T}^T \mathbf{C}^{-1} \Delta \mathbf{M}_k, \quad (\text{C15})$$

where $\Delta \mathbf{M}_k = \mathbf{T} \mathbf{S}_k - \mathbf{M}^*$. This equation can be used only for the first iteration (Then ∇_k can be calculated using Eq. C20).

$$\beta_{k-1} = \frac{\nabla_k^T \nabla_k}{\nabla_{k-1}^T \nabla_{k-1}}. \quad (\text{C16})$$

$$\mathbf{S}^{k+1} = \mathbf{S}^k - \alpha_k \rho_k, \quad (\text{C17})$$

15 where

$$\alpha_k = \frac{\nabla_k^T \nabla_k}{\rho_k^T \mathbf{T}^T \mathbf{C}^{-1} \mathbf{T} \rho_k}, \quad (\text{C18})$$

Retrieving global sources of aerosols from MODIS observations

O. Dubovik et al.

Title Page

Abstract

Introduction

Conclusions

References

Tables

Figures

⏪

⏩

◀

▶

Back

Close

Full Screen / Esc

Printer-friendly Version

Interactive Discussion

The vector $\mathbf{b}_k = \mathbf{T}^T \mathbf{C}^{-1} \mathbf{T} \mathbf{p}_k$ can be calculated using adjoint transformations:

$$b_k(t, \mathbf{x}) = \int_t^{t_0} \mathcal{T}^\#(t', \mathbf{x}) \left(b_k(t', \mathbf{x}) + \sigma^{-2}(t', \mathbf{x}) \Delta g_k(t', \mathbf{x}) \right) (-dt') \quad (\text{C19})$$

where $b_k(t, \mathbf{x})$ are the components of the vector $\mathbf{T}^T \mathbf{C}^{-1} \mathbf{T} \mathbf{p}_k$, and $\Delta g_k(t, \mathbf{x})$ are the components of the vector $\mathbf{T} \mathbf{p}_k$.

5 In addition, we can use the following equation:

$$\mathbf{V}_{k+1} = \mathbf{A} \mathbf{S}^{k+1} - \mathbf{y}^* = \mathbf{A}(\mathbf{S}^k - \alpha_k \mathbf{p}_k) - \mathbf{y}^* = \mathbf{A}(\mathbf{S}^k - \mathbf{y}^*) - \alpha_k \mathbf{A} \mathbf{p}_k = \mathbf{V}_k - \alpha_k \mathbf{A} \mathbf{p}_k. \quad (\text{C20})$$

Thus, for implementing the method we need to run transport model 2 times for calculating $\mathbf{T}^T \mathbf{C}^{-1} \mathbf{T} \mathbf{p}_k$: one forward for $\mathbf{T} \mathbf{p}_k$ and one backward $\mathbf{T}^T \mathbf{C}^{-1} \mathbf{T} \mathbf{p}_k$ (where $\mathbf{S} = \mathbf{T} \mathbf{p}_k$). The problem may appear if transport operator does not allow use of

10 negative sources, then we should always carry two terms $\mathbf{S}_k = \mathbf{T} \mathbf{p}_k = \mathbf{S}_k^{(+)} + \mathbf{S}_k^{(-)}$, then $\mathbf{T} \mathbf{S} = \mathbf{T}(\mathbf{S}_k^{(+)} + \mathbf{S}_k^{(-)}) = \mathbf{T} \mathbf{S}_k^{(+)} - \mathbf{T}(-\mathbf{S}_k^{(-)})$.

Acknowledgements. We thank the EOS Project Science Office for the support. We acknowledge support from NASA Radiation Science Program managed by H. Maring. We thank R. Levy for the help with MODIS data analysis and G. van der Werf and J. Collatz for assistance with
15 obtaining global carbon emission map. We also thank L. Bounoua, and J. Collatz for reading the paper and providing useful comments.

References

- Anderson, T. L., Wu, Y., Chu, D. A., Schmid, B., Redemann, J., and Dubovik, O.: Testing the MODIS satellite retrieval of aerosol fine-mode fraction, *J. Geophys. Res.*, 110(D18), D18204, doi:10.1029/2005JD005978, 2005.
- 20 Balkanski, Y. J., Jacob, D. J., Gardener, G. M., Graustein, W. C., and Turekian, K. K.: Transport and residence times of tropospheric aerosols inferred from a global 3-dimensional simulations of PB-210, *J. Geophys. Res.*, 98, 20 573–20 586, 1993.

- Brasseur, G. P., Orlando, J. J., and Tyndall, G. S.: Atmospheric Chemistry and Global Change, Oxford University Press; 1st edition, 654p, 1999.
- Cacuci, D. G.: Sensitivity theory for non-linear systems. I: Nonlinear functional analysis approach, *J. Math. Phys.*, 22, 2794–2802, 1981.
- 5 Chin, M., Rood, R. B., Lin, S. J., Muller, J. F., and Thompson, A. M.: Atmospheric sulfur cycle simulated in the global model GOCART: Model description and global properties, *J. Geophys. Res.*, 105(D20), 24 671–24 687, 2000.
- Chin, M., Ginoux, P., Kinne, S., Torres, O., Holben, B. N., Duncan, B. N., Martin, R. V., Logan, J. A., Higurashi, A., and Nakajima, T.: Tropospheric aerosol optical thickness from the GO-
 10 CART model and comparisons with satellite and Sun photometer measurements, *J. Atmos. Sci.*, 59(3), 461–483 2002.
- Chin, M., Chu, D. A., Levy, R., Remer, L. A., Kaufman, Y. J., Holben, B. N., Eck, T., and Ginoux, P.: Aerosol distribution in the northern hemisphere during ACE-Asia: Results from global model, satellite observations, and sunphotometer measurements, *J. Geophys. Res.*, 109, D23S90, doi:10.1029/2004JD004829, 2004.
- 15 Collins, W. D., Rasch, P. J., Eaton, B. E., Khattatov, B. V., Lamarque, J. F., and Zender, C. S.: Simulating aerosols using a chemical transport model with assimilation of satellite aerosol retrievals: Methodology for INDOEX, *J. Geophys. Res.*, 106(D7), 7313–7336, 2001.
- Collins, W. D., Rasch, P. J., Eaton, B. E., Fillmore, D. W., Kiehl, J. T., Beck, C. T., and Zender, C. S.: Simulation of aerosol distributions and radiative forcing for INDOEX: Regional climate
 20 impacts, *J. Geophys. Res.*, 107(D19), 8028, doi:10.1029/2000JD000032, 2002.
- Courtier, P. and Talagrand, O.: Variational assimilation of meteorological observations with the adjoint of the vorticity equations: Part II. Numerical results, *Quart. J. Roy. Meteorol. Soc.*, 113, 1311–1328, 1987.
- 25 Dee, D. P. and Da Silva, A. M.: Data assimilation in the presence of forecast bias, *Quart. J. Roy. Meteorol. Soc.*, 124(545), 269–295, Part A, 1998.
- Deschamps, P. Y., Breon, F. M., Leroy, M., Podaire, A., Bricaud, A., Buries, J. C., and Seze, G.: The POLDER mission: Instrument characteristics and scientific objectives, *IEEE Trans. Geosci. Remote Sens.*, 32, 598–615, 1994.
- 30 Deuzé, J. M., Breon, F. M., Devaux, C., Goloub, P., Herman, M., Lafrance, B., Maignan, F., Marchand, A., Nadal, F., Perry, G., and Tanré, D.: Remote sensing of aerosols over land surfaces from POLDER-ADEOS-1 polarized measurements, *J. Geophys. Res.*, 106, 4913–4926, 2001.

Retrieving global sources of aerosols from MODIS observations

O. Dubovik et al.

Title Page

Abstract

Introduction

Conclusions

References

Tables

Figures

◀

▶

◀

▶

Back

Close

Full Screen / Esc

Printer-friendly Version

Interactive Discussion

Diner, D. J., Beckert, J. C., Reilly, T. H., Bruegge, C. J., Conel, J. E., Kahn, R. A., Martonchik, J. V., Ackerman, T. P., Davies, R., Gerstl, S. A. W., Gordon, H. R., Muller, J. P., Myneni, R. B., Sellers, P. J., Pinty, B., and Verstraete, M.: Multi-angle Imaging SpectroRadiometer (MISR) instrument description and experiment overview, *IEEE Trans. Geosci. Remote Sens.*, 36, 1072–1087, 1998.

Dubovik, O. and King, M. D.: A flexible inversion algorithm for retrieval of aerosol optical properties from sun and sky radiance measurements, *J. Geophys. Res.*, 105(D16), 20 673–20 696, 2000.

Dubovik, O., Holben, B. N., Eck, T. F., Smirnov, A., Kaufman, Y. J., King, M. D., Tarré, D., and Slutsker, I.: Variability of absorption and optical properties of key aerosol types observed in worldwide locations, *J. Atmos. Sci.*, 59, 590–608, 2002.

Dubovik, O.: Optimization of Numerical Inversion in Photopolarimetric Remote Sensing, in: *Photopolarimetry in Remote Sensing*, edited by: Videen, G., Yatskiv, Y., and Mishchenko, M., Kluwer Academic Publishers, Dordrecht, Netherlands, 65–106, 2004a.

Edie, W. T., Dryard, D., James, F. E., Roos, M., and Sadoulet, B.: *Statistical Methods in Experimental Physics*, North-Holland Publishing Company, Amsterdam, 155 pp., 1971.

Elbern, H., Schmidt, H., and Ebel, A.: Variational data assimilation for tropospheric chemistry modeling, *J. Geophys. Res.*, 102, 15 967–15 985, 1997.

Elbern, H., Schmidt, H., Talagrand, O., and Ebel, A.: 4D-variational data assimilation with an adjoint air quality model for emission analysis, *Environ. Modell. Software*, 15, 539–548, 2000.

Elbern, H. and Schmidt, H.: Ozone episode analysis by four-dimensional variational chemistry data assimilation, *J. Geophys. Res.*, 106, 3569–3590, 2001.

Enting, I. G., Trudinger, C. M., and Francey, R. J.: A synthesis inversion of the concentration and $\delta^{13}\text{C}$ of atmospheric CO_2 , *Tellus, Ser. B*, 47(1–2), 35–52, 1995.

Gill, P. E., Murray, W., and Wright, M. E.: *Practical optimization*, Academic Press, London, p. 401, 1982.

Ginoux, P., Chin, M., Tegen, I., Prospero, J., Holben, B. N., Dubovik, O., and Lin, S. J.: Sources and distributions of dust aerosols simulated with the GOCART model, *J. Geophys. Res.*, 106, 20 255–20 274, 2001.

Ghan, S., Easter, R., Chapman, E., Abdul-Razzak, H., Zhang, Y., Leung, L., Laulainen, N., Saylor, R., and Zaveri, R.: A physically based estimate of radiative forcing by anthropogenic sulfate aerosol, *J. Geophys. Res.*, 106, 5279–5293, 2001a.

Retrieving global sources of aerosols from MODIS observations

O. Dubovik et al.

[Title Page](#)[Abstract](#)[Introduction](#)[Conclusions](#)[References](#)[Tables](#)[Figures](#)[⏪](#)[⏩](#)[◀](#)[▶](#)[Back](#)[Close](#)[Full Screen / Esc](#)[Printer-friendly Version](#)[Interactive Discussion](#)

- Ghan, S., Laulainen, N., Easter, R., Wagener, R., Nemesure, S., Chapman, E., Zhang, Y., and Leung, R.: Evaluation of aerosol direct forcing in MIRAGE, *J. Geophys. Res.*, 106, 5295–5316, 2001b.
- Hakami, A., Henze, D. K., Seinfeld, J. H., Chai, T., Tang, Y., Carmichael, G. R., and Sandu, A.: Adjoint inverse modeling of black carbon during the Asian Pacific Regional Aerosol Characterization Experiment, *J. Geophys. Res.*, 110, D14301, doi:10.1029/2004JD005671, 2005.
- Hartley, D. and Prinn, R.: Feasibility of determining surface emissions of trace gases using an inverse method in a 3-dimensional chemical-transport model, *J. Geophys. Res.*, 98(D3), 5183–5197, 1993.
- Hsu, N. C., Tsay, S. C., King, M. D., and Herman, J. R.: Aerosol properties over bright-reflecting source regions, *IEEE Trans. Geosci. Remote Sens.*, 42, 557–569, 2004.
- Hourdin, F. and Talagrand, O.: Eulerian backtracking of atmospheric traces: I Adjoint derivation and parametrisation of subgrid-scale transport, *Quart. J. Am. Meteorol. Soc.*, 132, 567–583, 2006.
- Jacob, D. J.: Introduction to Atmospheric Chemistry, 266 pp., Princeton University Press, 1999.
- Kahn, R. A., Gaitley, B. J., Martonchik, J. V., Diner, D. J., and Crean, K. A.: Multiangle Imaging Spectroradiometer (MISR) global aerosol optical depth validation based on 2 years of coincident Aerosol Robotic Network (AERONET) observations, *J. Geophys. Res.*, 110, doi:10.1029/2004JD004706, 2005.
- Kaminski, T., Heimann, M., and Giering, R.: A coarse grid three dimensional global inverse model of the atmospheric transport, 1, Adjoint model and Jacobian matrix, *J. Geophys. Res.*, 104, 18 535–18 553, 1999a.
- Kaminski, T., Heimann, M., and Giering, R.: A coarse grid threedimensional global inverse model of the atmospheric transport, 2, Inversion of the transport of CO₂ in the 1980s, *J. Geophys. Res.*, 104, 18 555–18 581, 1999b.
- Kasibhatla, P. S., Heimann, M., Rayner, P., Mahowald, N., Prinn, R. G., Hartley, D. E.: Inverse Methods in Global Biogeochemical Cycles, American Geophysical Union, 324 pp, 2000.
- Kalman, R. E.: A New approach to linear filtering and prediction problems, *J. Basic. Eng.*, 82, 35–40, 1960.
- Kaufman, Y. J., Tanré, D., Remer, L. A., et al.: Operational remote sensing of tropospheric aerosol over land from EOS moderate resolution imaging spectroradiometer, *J. Geophys. Res.*, 102, 17 051–17 067, 1997.
- Kaufman, Y. J., Tanré, D., and Boucher, O.: A satellite view of aerosols in the climate system,

Retrieving global sources of aerosols from MODIS observations

O. Dubovik et al.

Title Page

Abstract

Introduction

Conclusions

References

Tables

Figures

◀

▶

◀

▶

Back

Close

Full Screen / Esc

Printer-friendly Version

Interactive Discussion

- Nature, 419(6903), 215–223, 2002.
- King, M. D., Byrne, D. M., Herman, B. M., and Reagan, J. A.: Aerosol size distributions obtained by inversion of spectral optical depth measurements, *J. Atmos. Sci.*, 21, 2153–2167, 1978.
- 5 King, M. D., Kaufman, Y. J., Tanré, D., and Nakajima, T.: Remote sensing of tropospheric aerosols from space: Past, present, and future, *Bull. Amer. Meteorol. Soc.*, 80, 2229–2259, 1999.
- Kinne, S., Lohmann, U., Feichter, J., Schulz, M., Timmreck, C., Ghan, S., Easter, R., Chin, M., Ginoux, P., Takemura, T., Tegen, I., Koch, D., Herzog, M., Penner, J., Pitari, G., Holben, B., Eck, T., Smirnov, A., Dubovik, O., Slutsker, I., Tanré, D., Torres, O., Mishchenko, M., Geogdzhayev, I., Chu, D. A., and Kaufman, Y.: Monthly averages of aerosol properties: A global comparison among models, satellite data and AERONET ground data, *J. Geophys. Res.*, 108, 4634, doi:10.1029/2001JD001253, 2003.
- 10 Kinne, S., Schulz, M., Textor, C., et al.: An AeroCom initial assessment – optical properties in aerosol component modules of global models, *Atmos. Chem. Phys.*, 6, 1815–1834, 2006, <http://www.atmos-chem-phys.net/6/1815/2006/>.
- Khattatov, B., Lamarque, J.-F., Lyjak, L. V., Menard, R., Levelt, P., Tie, X., Brasseur, G. P., and Gille, J. C.: Assimilation of satellite observations of long-lived chemical species in global chemistry-transport models, *J. Geophys. Res.*, 105, 29 135–29 144, 2000.
- 20 Koch, D.: The transport and direct radiative forcing of carbonaceous and sulfate aerosol in the GISS GCM, *J. Geophys. Res.*, 106, 20 311–20 332, 2001.
- Koch, D., Jacob, D., Tegen, I., Rind, D., and Chin, M.: Tropospheric sulfur simulation and sulfate direct forcing in the Goddard Institute for Space Studies (GISS) general circulation model, *J. Geophys. Res.*, 104, 23 799–23 822, 1999.
- 25 Le Dimet, F. and Talagrand, O.: Variational algorithms for analysis and assimilation of meteorological observations: Theoretical aspects, *Tellus, Ser. A*, 38, 97–110, 1986.
- Lin, S.-J. and Rood, R. B.: Multidimensional flux-form semi-Lagrangian transport schemes, *Mon. Wea. Rev.*, 124, 2046–2070, 1996.
- Marchuk, G. I.: *Method of numerical mathematics* (in Russian), Nauka, Moscow, 1977.
- 30 Marchuk, G.: *Mathematical Models in Environmental Problems*, Elsevier, New York, 1986.
- Menut, L., Vautard, R., Beekmann, M., and Honoré, C.: Sensitivity of photochemical pollution using the adjoint of a simplified chemistry-transport model, *J. Geophys. Res.*, 105(D12), 15 379–15 402, 2000.

Retrieving global sources of aerosols from MODIS observations

O. Dubovik et al.

Title Page

Abstract

Introduction

Conclusions

References

Tables

Figures

◀

▶

◀

▶

Back

Close

Full Screen / Esc

Printer-friendly Version

Interactive Discussion

- Menut, L.: Adjoint modeling for atmospheric pollution process sensitivity at regional scale, *J. Geophys. Res.*, 108(D17), 8562, doi:10.1029/2002JD002549, 2003.
- Mishchenko, M. I., Cairns, B., Hansen, J. E., Travis, L. D., Burg, R., Kaufman, Y. J., Martins, J. V., and Shettle, E. P.: Monitoring of aerosol forcing of climate from space: analysis of measurement requirements, *J. Quant. Spectrosc. Radiat. Transfer*, 88, 149–161, 2004.
- 5 Nakajima, T., Tonna, G., Rao, R., Boi, P., Kaufman, Y., and Holben, B.: Use of sky brightness measurements from ground for remote sensing of particulate polydispersions, *Appl. Opt.*, 35, 2672–2686, 1996.
- Navon, I. M.: Practical and theoretical aspects for adjoint parameter estimation and identifiability in meteorology and oceanography, *Dyn. Atmos. Oceans*, 27, 55–79, 1997.
- 10 Patra, P. K., Maksyutov, S., Sasano, Y., Nakajima, H., Inoue, G., and Nakazawa, T.: An evaluation of CO₂ observations with Solar Occultation FTS for Inclined-Orbit Satellite sensor for surface source inversion, *J. Geophys. Res.*, 108(D24), 4759, doi:10.1029/2003JD003661, 2003.
- 15 Phillips, B. L.: A technique for numerical solution of certain integral equation of first kind, *J. Assoc. Comp. Mach.*, 9, 84–97, 1962.
- Press, W. H., Teukolsky, S. A., Vetterling, W. T., and Flannery, B. P.: *Numerical Recipes in FORTRAN. The art of Scientific Computing*, Cambridge University Press, 965 pp., 1992.
- Rao, C. R.: *Linear Statistical Inference and Its Applications*, Wiley, New York, 500 pp., 1965.
- 20 Reddy, M. S. and Boucher, O.: A study of the global cycle of carbonaceous aerosols in the LMDZT general circulation model, *J. Geophys. Res.*, 109(D14), D14202, doi:10.1029/2003JD004048, 2004
- Remer, L. A., Kaufman, Y. J., Tanré, D., Mattoo, S., Chu, D. A., Martins, J. V., Li, R.-R., Ichoku, C., Levy, R. C., Kleidman, R. G., Eck, T. F., Vermote, E., and Holben, B. N.: The MODIS Aerosol Algorithm, Products and Validation, *J. Atmos. Sci.*, 62, 947–973, 2005.
- 25 Rodgers, C. D.: Retrieval of atmospheric temperature and composition from remote measurements of thermal radiation, *Rev. Geophys. Space Phys.*, 14, 609–624, 1976.
- Roeckner, E., Arpe, K., Bengtsson, L., Christoph, M., Claussen, M., Duemenil, L., Esch, M., Giorgetta, M., Schlese, U., and Schulzweida, U.: The atmospheric general circulation model ECHAM-4: Model description and simulation of present-day climate, Tech. Rep. 218, Max-Planck-Inst. für Meteorol., Hamburg, Germany, 1996.
- 30 Sato, M., Hansen, J., Koch, D., Lacis, A., Ruedy, R., Dubovik, O., Holben, B., Chin, M., and Novakov, T.: Global atmospheric black carbon inferred from AERONET, *Proc. Nat. Acad.*

Retrieving global sources of aerosols from MODIS observationsO. Dubovik et al.

[Title Page](#)[Abstract](#)[Introduction](#)[Conclusions](#)[References](#)[Tables](#)[Figures](#)[⏪](#)[⏩](#)[◀](#)[▶](#)[Back](#)[Close](#)[Full Screen / Esc](#)[Printer-friendly Version](#)[Interactive Discussion](#)

- Sci., 100(11), 6319–6324, 2003.
- Schmidt, H. and Martin, D.: Adjoint sensitivity of episodic ozone in Paris area to emissions on the continental scale, *J. Geophys. Res.*, 108(D17), 8561, doi:10.1029/2001JD001583, 2003.
- Smirnov A., Holben, B. N., Dubovik, O., Frouin, R., Eck, T. F., and Slutsker, I.: Maritime component in aerosol optical models derived from Aerosol Robotic Network data, *J. Geophys. Res.*, 108(D1), 4033, doi:10.1029/2002JD002701, 2003.
- Strand, O. N. and Westwater, E. R.: Statistical estimation of the numerical solution of a Fredholm internal equation of the first kind, *J. Assoc. Comput. Mach.*, 15, 104–114, 1968.
- Takemura, T., Okamoto, H., Maruyama, Y., Numaguti, A., Hiragushi, A., and Nakajima, T.: Global three dimensional simulation of aerosol optical thickness distribution of various origins, *J. Geophys. Res.*, 105, 17 853–17 873, 2000.
- Takemura, T., Nakajima, T., Dubovik, O., Holben, B., and Kinne, S.: Single scattering albedo and radiative forcing of various aerosol species with a global three-dimensional model, *J. Clim.*, 4, 333–352, 2002.
- Talagrand, O.: A study of the dynamics of four dimensional data assimilation, *Tellus*, 33, 43–60, 1981a.
- Talagrand, O.: On the mathematics of data assimilation, *Tellus*, 33, 321–339, 1981b.
- Talagrand, O. and Courtier, P.: Variational assimilation of meteorological observations with the adjoint of the vorticity equations: Part I., *Theory, Quart. J. Roy. Meteorol. Soc.*, 113, 1311–1328, 1987.
- Tarantola, A.: *Inverse Problem Theory: Methods for Data Fitting and Model Parameter Estimation*, Elsevier, Amsterdam, 614 pp., 1987.
- Tanré, D., Herman, M., and Kaufman, Y. J.: Information on aerosol size distribution contained in solar reflected spectral radiances, *J. Geophys. Res.*, 101, 19 043–19 060, 1996.
- Tanré, D., Kaufman, Y. J., Herman, M., and Mattoo, S.: Remote sensing of aerosol properties over oceans using the MODIS/EOS spectral radiances, *J. Geophys. Res.*, 102, 16 971–16 988, 1997.
- Tegen, I., Hollrig, P., Chin, M., Fung, I., Jacob, D., and Penner, J.: Contribution of different aerosol species to the global aerosol extinction optical thickness: Estimates from model results, *J. Geophys. Res.*, 102, 23 895–23 915, 1997.
- Tegen, I., Koch, D., Lacis, A., and Sato, M.: Trends in tropospheric aerosol loads and corresponding impact on direct radiative forcing between 1950 and 1990: A model study, *J. Geophys. Res.*, 105, 26 971–26 989, 2000.

Retrieving global sources of aerosols from MODIS observations

O. Dubovik et al.

Title Page

Abstract

Introduction

Conclusions

References

Tables

Figures

◀

▶

◀

▶

Back

Close

Full Screen / Esc

Printer-friendly Version

Interactive Discussion

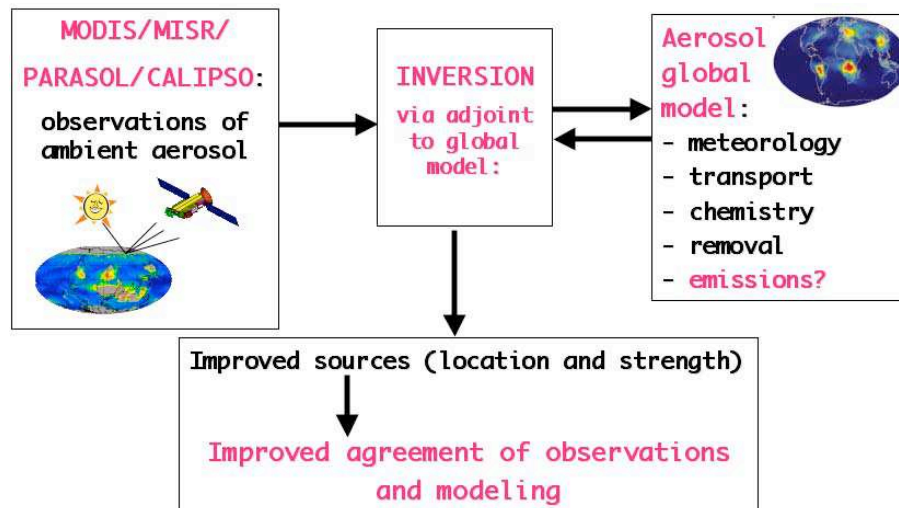
- Textor, C., Schulz, M., Guibert, S., et al.: Analysis and quantification of the diversities of aerosol life cycles within AeroCom, *Atmos. Chem. Phys.*, 6, 1777–1813, 2006, <http://www.atmos-chem-phys.net/6/1777/2006/>.
- 5 Tikhonov, A. N.: On the solution of incorrectly stated problems and a method of regularization, *Dokl. Akad. Nauk SSSR*, 151, 501–504, 1963.
- Twomey, S.: On the numerical solution of Fredholm integral equations of the first kind by the inversion of the linear system produced by quadrature, *J. Assoc. Comp. Mach.*, 10, 97–101, 1963.
- 10 Van der Werf, G. R., Randerson, J. T., Collatz, G. J., Giglio, L., Kasibhatla, P. S., Arellano, A. F., Olsen, S. C., and Kasischke, E. S.: Continental-scale partitioning of fire emissions during the 1997 to 2001 El Niño/La Niña period, *Science*, 303(5654), 73–76, 2004.
- Vautard, R., Beekmann, M., and Menut, L.: Applications of adjoint modelling in atmospheric chemistry: Sensitivity and inverse modeling, *Environ. Model. Software*, 15, 703–709, 2000.
- 15 Vukicevic, T. and Hess, P.: Analysis of tropospheric transport in the Pacific Basin using the adjoint technique, *J. Geophys. Res.*, 105, 7213–7230, 2000.
- Vukicevic, T., Steyskal, M., and Hecht, M.: Properties of advection algorithms in the context of variational data assimilation, *Mon. Wea. Rev.*, 129(5), 1221–1231, 2001.
- 20 Weaver, C., da Silva, A., Chin, M., Ginoux, P., Dubovik, O., Flittner, D., Zia, A., Remer, L., Holben, B. N., and Gregg, W.: Direct Insertion of MODIS Radiances in a Global Aerosol Transport Model, *J. Atmos. Sci.*, 64(3), 808–827, 2007.

Retrieving global sources of aerosols from MODIS observationsO. Dubovik et al.

[Title Page](#)[Abstract](#)[Introduction](#)[Conclusions](#)[References](#)[Tables](#)[Figures](#)[⏪](#)[⏩](#)[◀](#)[▶](#)[Back](#)[Close](#)[Full Screen / Esc](#)[Printer-friendly Version](#)[Interactive Discussion](#)

Retrieving global sources of aerosols from MODIS observations

O. Dubovik et al.

**Fig. 1.** The scheme of the retrieval concept.[Title Page](#)[Abstract](#)[Introduction](#)[Conclusions](#)[References](#)[Tables](#)[Figures](#)[◀](#)[▶](#)[◀](#)[▶](#)[Back](#)[Close](#)[Full Screen / Esc](#)[Printer-friendly Version](#)[Interactive Discussion](#)

Retrieving global sources of aerosols from MODIS observations

O. Dubovik et al.

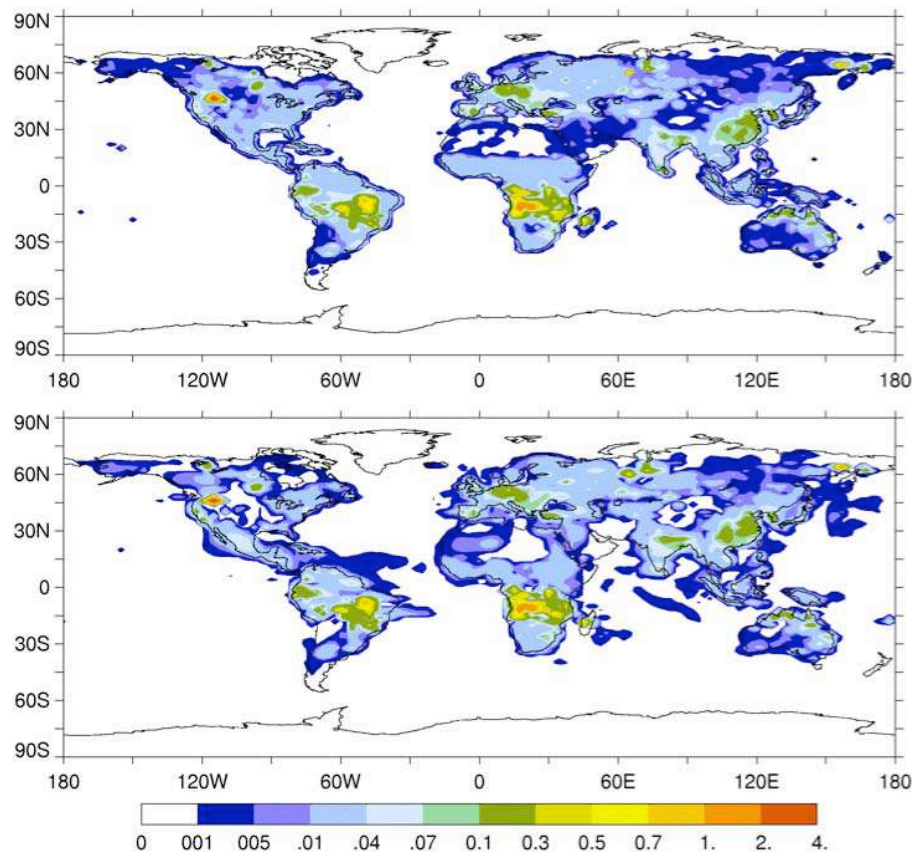


Fig. 2. Illustration of inversion tests: upper panel – BC sources (10^7 kg of mass/day) “prescribed” for 28 August 2000; lower panel shows BC aerosol emission retrieved for the same day (in total 9 days the data were inverted).

[Title Page](#)[Abstract](#)[Introduction](#)[Conclusions](#)[References](#)[Tables](#)[Figures](#)[◀](#)[▶](#)[◀](#)[▶](#)[Back](#)[Close](#)[Full Screen / Esc](#)[Printer-friendly Version](#)[Interactive Discussion](#)

Retrieving global sources of aerosols from MODIS observations

O. Dubovik et al.

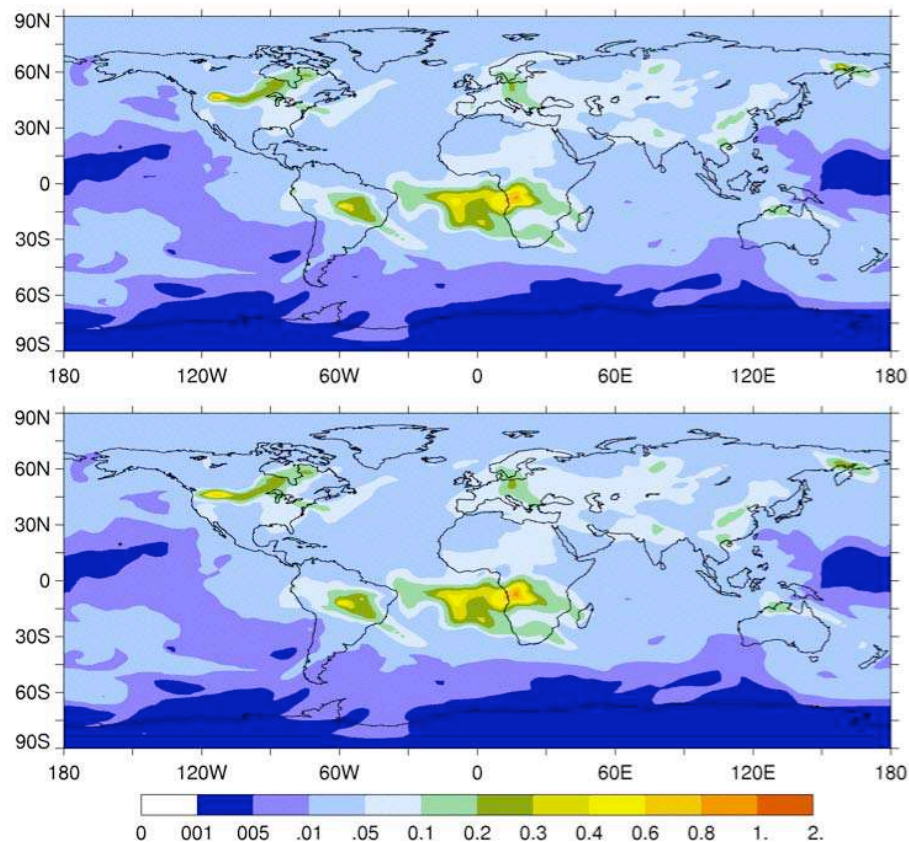


Fig. 3. Illustration of inversion tests: upper panel – 28 August 2000 “measurements” of $\tau_{BC}(0.55)$ simulated using “prescribed” BC aerosol emission; lower panel – $\tau_{BC}(0.55)$ simulated using retrieved BC emission.

[Title Page](#)[Abstract](#)[Introduction](#)[Conclusions](#)[References](#)[Tables](#)[Figures](#)[◀](#)[▶](#)[◀](#)[▶](#)[Back](#)[Close](#)[Full Screen / Esc](#)[Printer-friendly Version](#)[Interactive Discussion](#)

Retrieving global sources of aerosols from MODIS observations

O. Dubovik et al.

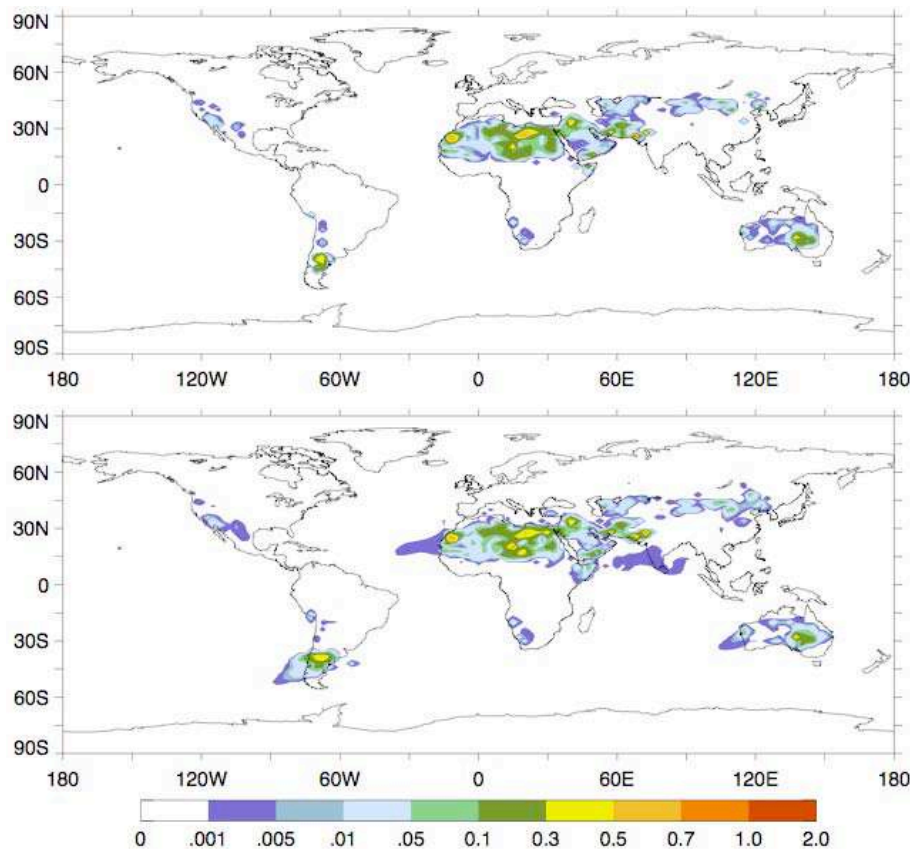


Fig. 4. Illustration of inversion tests: upper panel – Dust sources (10^8 kg of mass/day) “pre-scribed” for 28 August 2000; lower panel shows Dust aerosol emission retrieved for the same day (in total 9 days the data were inverted).

[Title Page](#)[Abstract](#)[Introduction](#)[Conclusions](#)[References](#)[Tables](#)[Figures](#)[◀](#)[▶](#)[◀](#)[▶](#)[Back](#)[Close](#)[Full Screen / Esc](#)[Printer-friendly Version](#)[Interactive Discussion](#)

Retrieving global sources of aerosols from MODIS observations

O. Dubovik et al.

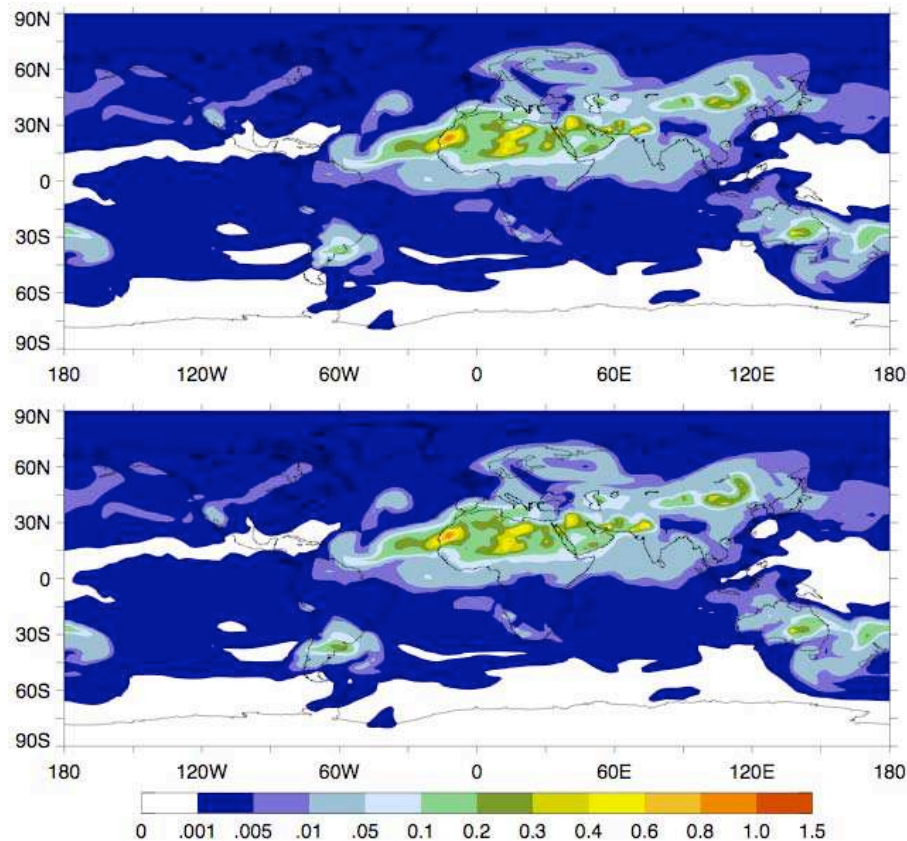


Fig. 5. Illustration of inversion tests: upper panel – “28 August 2000 measurements” of $\tau_{\text{Dust}}(0.55)$ simulated using “prescribed” Dust aerosol emission; lower panel – $\tau_{\text{Dust}}(0.55)$ simulated using retrieved Dust emission.

[Title Page](#)[Abstract](#)[Introduction](#)[Conclusions](#)[References](#)[Tables](#)[Figures](#)[◀](#)[▶](#)[◀](#)[▶](#)[Back](#)[Close](#)[Full Screen / Esc](#)[Printer-friendly Version](#)[Interactive Discussion](#)

Retrieving global sources of aerosols from MODIS observations

O. Dubovik et al.

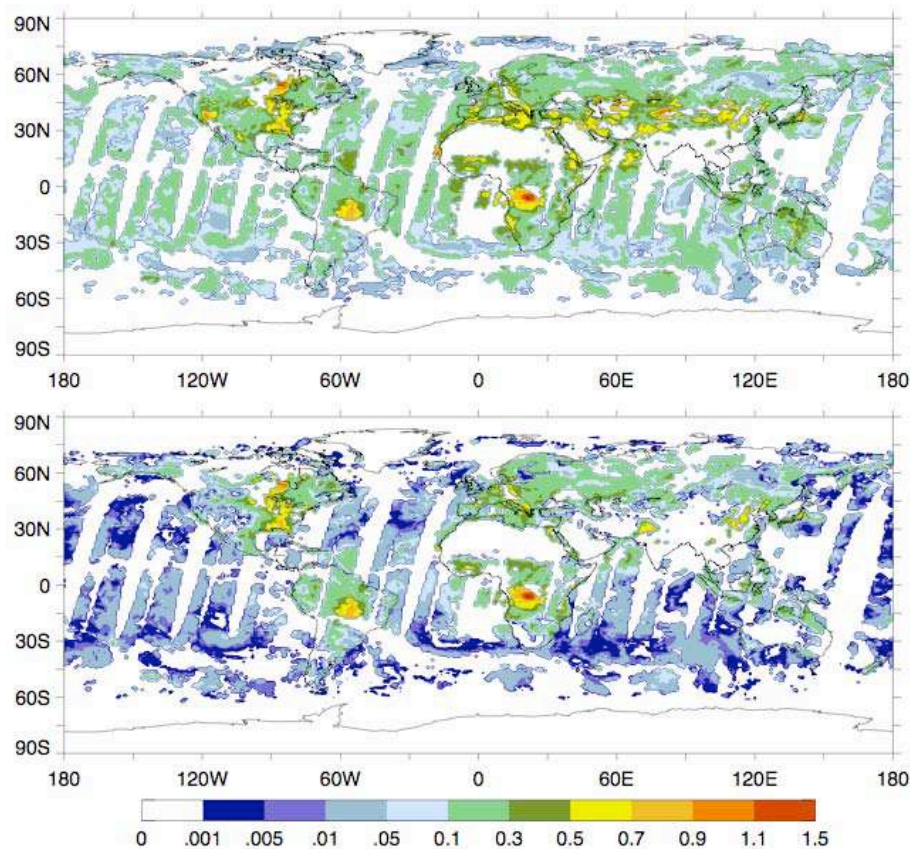


Fig. 6. Illustration of availability of MODIS aerosol retrieval products for one day (28 August 2000 measurements): upper panel – $\tau_{\text{total}}(0.55)$; lower panel – $\tau_{\text{fine}}(0.55)$.

[Title Page](#)[Abstract](#)[Introduction](#)[Conclusions](#)[References](#)[Tables](#)[Figures](#)[◀](#)[▶](#)[◀](#)[▶](#)[Back](#)[Close](#)[Full Screen / Esc](#)[Printer-friendly Version](#)[Interactive Discussion](#)

Retrieving global sources of aerosols from MODIS observations

O. Dubovik et al.

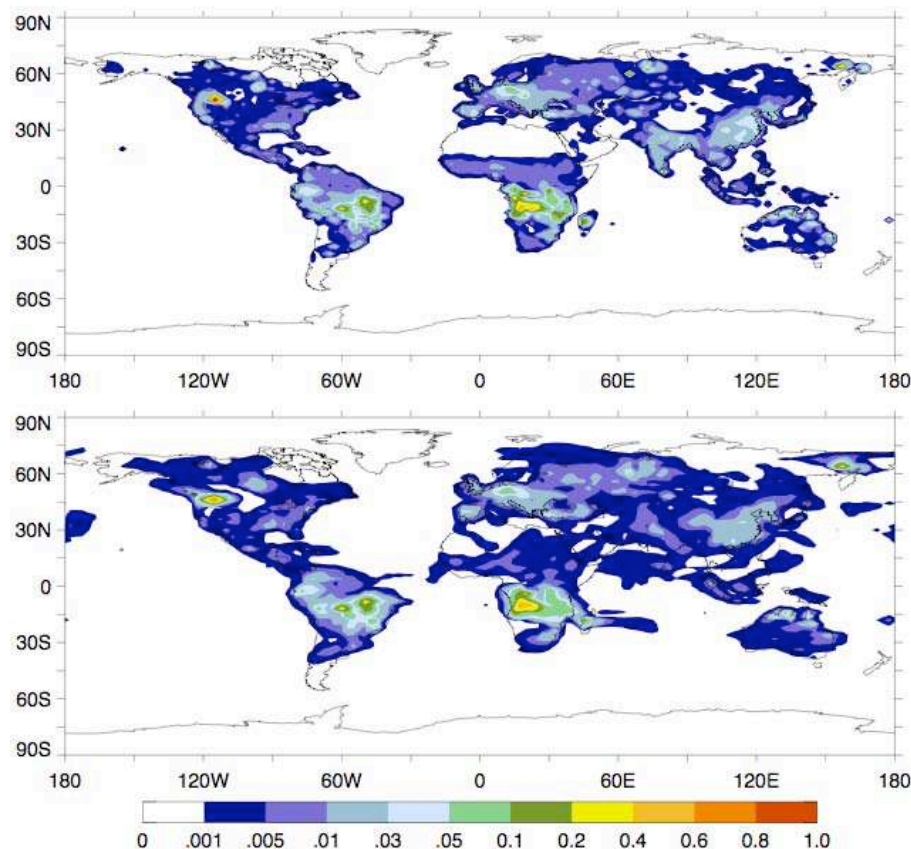


Fig. 7. Illustration of inversion test results of retrieving BC aerosol emission from $\tau_{BC}(0.55)$ simulated by the model and sub-sampled according to the actual coverage of MODIS observation collected during the same time period: upper panel – “prescribed” averaged BC emission for 20–28 August 2000 (10^7 kg of mass/day); lower panel shows averaged BC aerosol emission retrieved for the same period.

[Title Page](#)[Abstract](#)[Introduction](#)[Conclusions](#)[References](#)[Tables](#)[Figures](#)[◀](#)[▶](#)[◀](#)[▶](#)[Back](#)[Close](#)[Full Screen / Esc](#)[Printer-friendly Version](#)[Interactive Discussion](#)

Retrieving global sources of aerosols from MODIS observations

O. Dubovik et al.

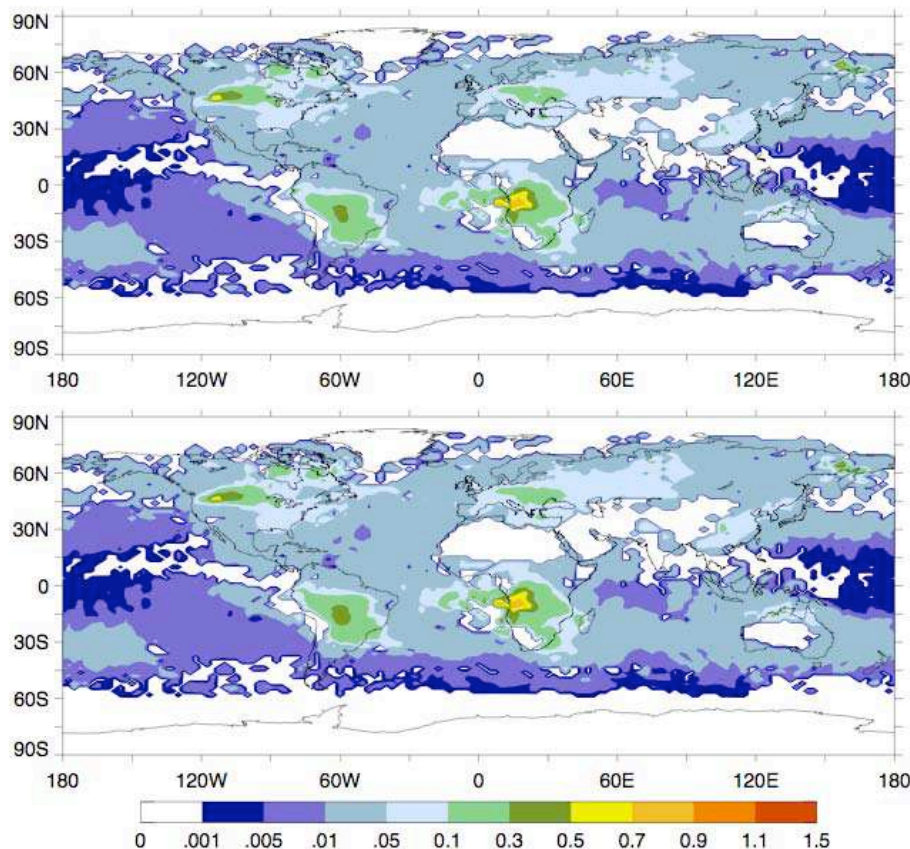


Fig. 8. Illustration of inversion test results of retrieving BC aerosol emission from $\tau_{BC}(0.55)$ simulated by the model and sub-sampled according to the actual coverage of MODIS observation collected during the same time period: upper panel – averaged (20–28 August 2000) measurements of $\tau_{BC}(0.55)$ simulated using “prescribed” BC aerosol emission; lower panel – averaged (20–28 August 2000) “measurements” of $\tau_{BC}(0.55)$ simulated using retrieved BC emission.

[Title Page](#)[Abstract](#)[Introduction](#)[Conclusions](#)[References](#)[Tables](#)[Figures](#)[◀](#)[▶](#)[◀](#)[▶](#)[Back](#)[Close](#)[Full Screen / Esc](#)[Printer-friendly Version](#)[Interactive Discussion](#)

Retrieving global sources of aerosols from MODIS observations

O. Dubovik et al.

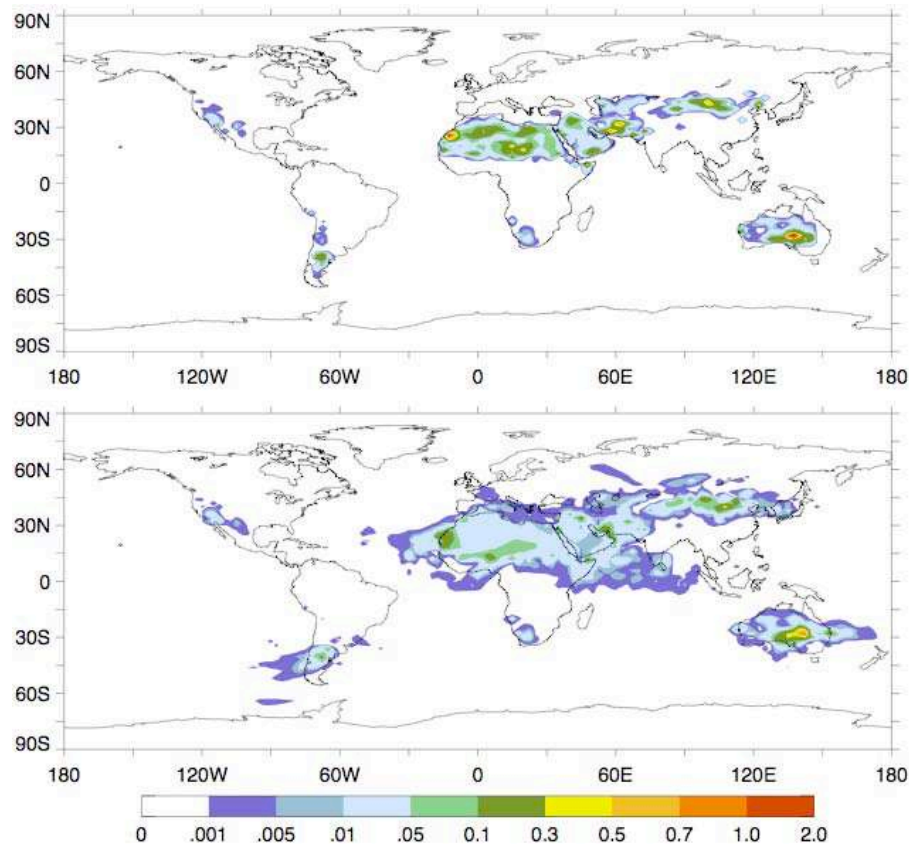


Fig. 9. Illustration of inversion test results of retrieving Dust aerosol emission from $\tau_{\text{Dust}}(0.55)$ simulated by the model and sub-sampled according to the actual coverage of MODIS observation collected during the same time period: upper panel – “prescribed” averaged Dust emission for 20–28 August 2000 (10^8 kg of mass/day); lower panel shows averaged Dust aerosol emission retrieved for the same period.

[Title Page](#)[Abstract](#)[Introduction](#)[Conclusions](#)[References](#)[Tables](#)[Figures](#)[◀](#)[▶](#)[◀](#)[▶](#)[Back](#)[Close](#)[Full Screen / Esc](#)[Printer-friendly Version](#)[Interactive Discussion](#)

Retrieving global sources of aerosols from MODIS observations

O. Dubovik et al.

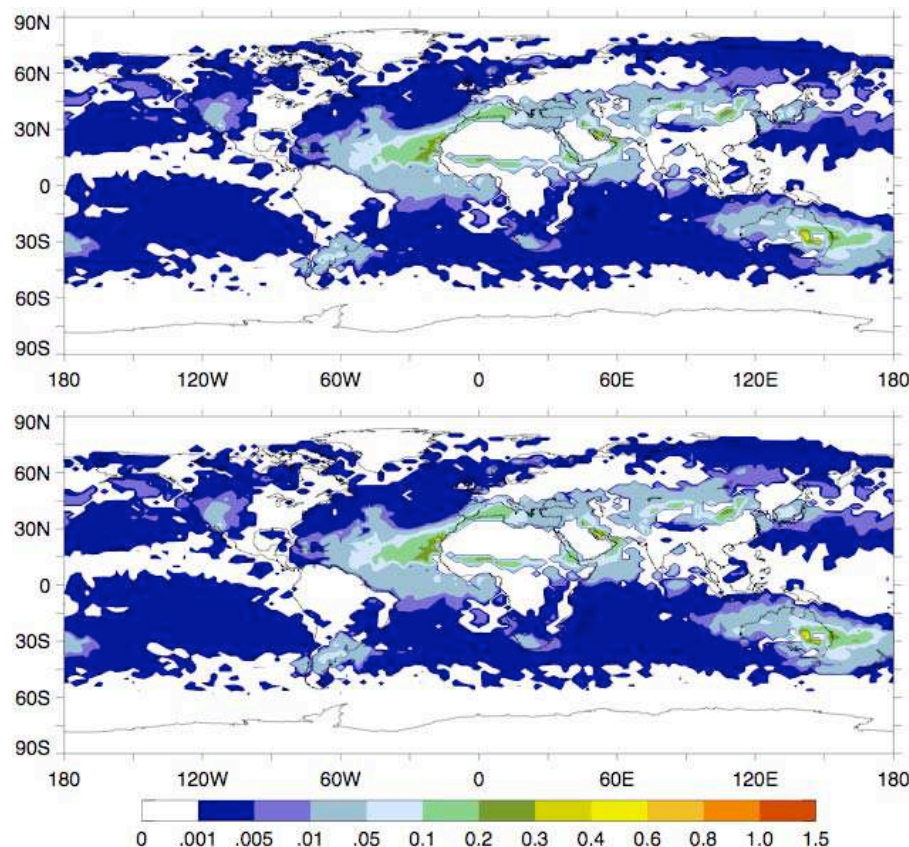


Fig. 10. Illustration of inversion test results of retrieving Dust aerosol emission from $\tau_{\text{Dust}}(0.55)$ simulated by the model and sub-sampled according to the actual coverage of MODIS observation collected during the same time period: upper panel – averaged (20–28 August 2000) “measurements” of $\tau_{\text{Dust}}(0.55)$ simulated using “prescribed” Dust aerosol emission; lower panel – averaged (20–28 August 2000) “measurements” of $\tau_{\text{Dust}}(0.55)$ simulated using retrieved Dust emission.

[Title Page](#)[Abstract](#)[Introduction](#)[Conclusions](#)[References](#)[Tables](#)[Figures](#)[◀](#)[▶](#)[◀](#)[▶](#)[Back](#)[Close](#)[Full Screen / Esc](#)[Printer-friendly Version](#)[Interactive Discussion](#)

Retrieving global sources of aerosols from MODIS observations

O. Dubovik et al.

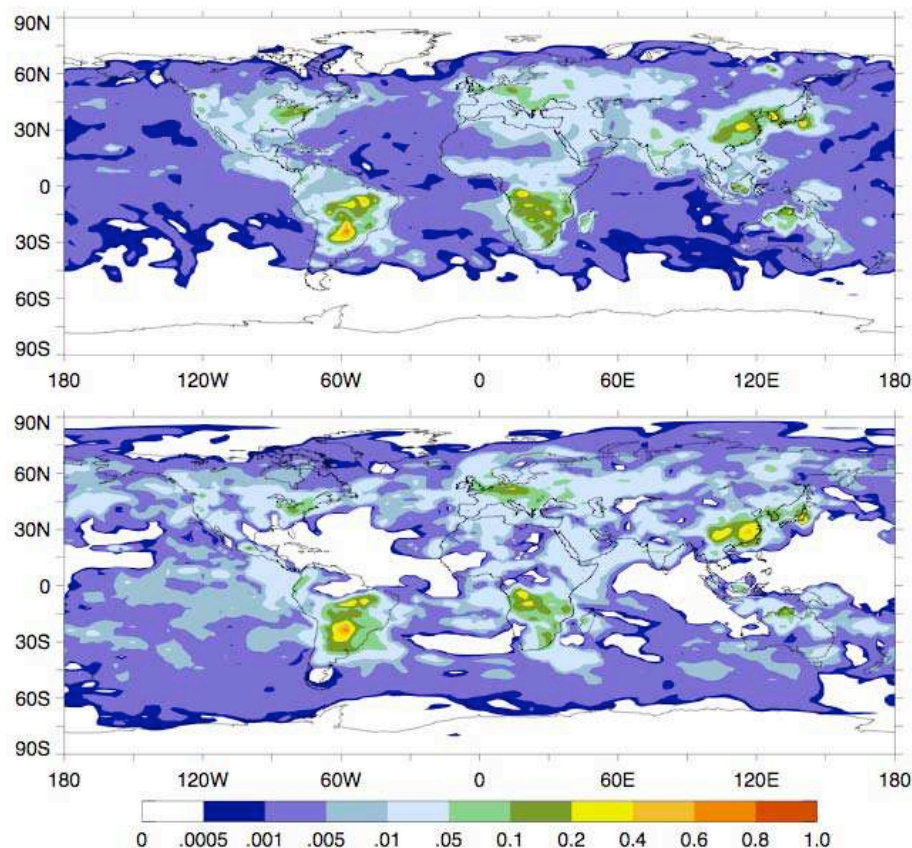


Fig. 11. Illustration of inversion test results of retrieving aerosol emission from $\tau(0.55) = \tau_{\text{BC}}(0.55) + \tau_{\text{OC}}(0.55) + \tau_{\text{sulfates}}(0.55)$ simulated according BC, OC and sulfates emission assumed in GOCART model for 20–28 August 2000: upper panel – “prescribed” averaged total BC, OC and sulfates emission for 20–28 August 2000 (10^7 kg of mass/day); lower panel shows averaged aerosol emission retrieved for the same period under assumption of single aerosol type (BC).

[Title Page](#)[Abstract](#)[Introduction](#)[Conclusions](#)[References](#)[Tables](#)[Figures](#)[◀](#)[▶](#)[◀](#)[▶](#)[Back](#)[Close](#)[Full Screen / Esc](#)[Printer-friendly Version](#)[Interactive Discussion](#)

Retrieving global sources of aerosols from MODIS observations

O. Dubovik et al.

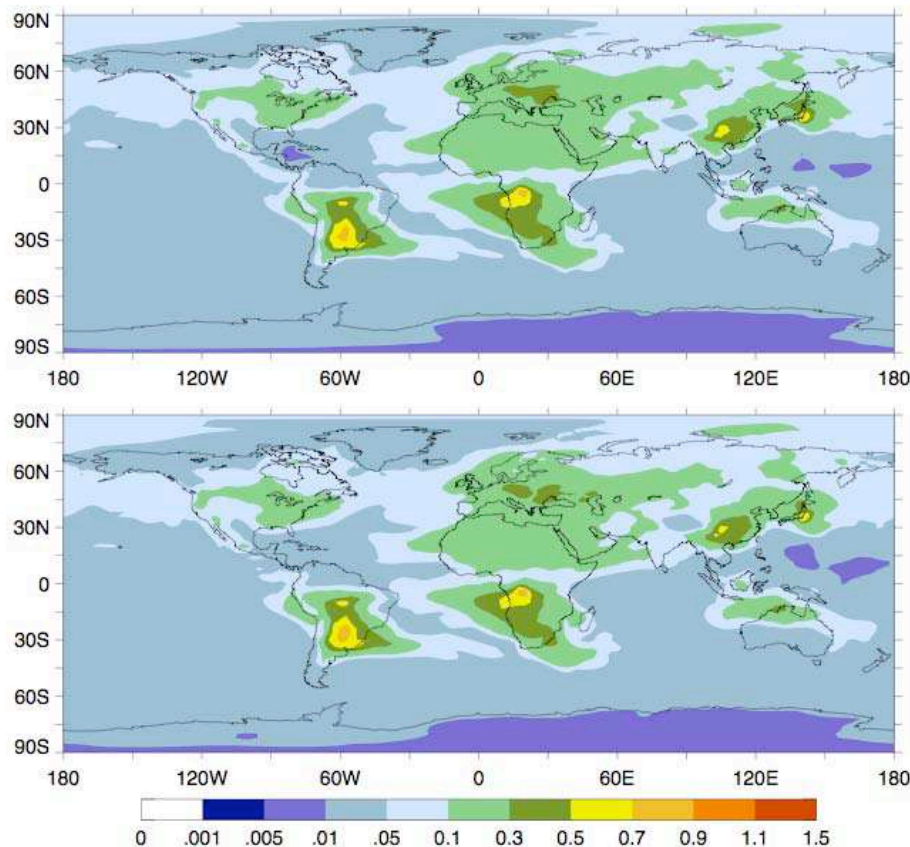


Fig. 12. Illustration of inversion tests results of retrieving aerosol emission from $\tau(0.55) = \tau_{\text{BC}}(0.55) + \tau_{\text{OC}}(0.55) + \tau_{\text{sulfates}}(0.55)$ simulated according BC and OC assumed in GOCART model for 20–28 August 2000: upper panel – $\tau(0.55) = \tau_{\text{BC}}(0.55) + \tau_{\text{OC}}(0.55) + \tau_{\text{sulfates}}(0.55)$ on 20–28 August 2000 simulated using BC, OC and sulfates assumed in GOCART model; lower panel shows $\tau_{\text{BC}}(0.55)$ simulated using retrieved BC emission.

[Title Page](#)[Abstract](#)[Introduction](#)[Conclusions](#)[References](#)[Tables](#)[Figures](#)[◀](#)[▶](#)[◀](#)[▶](#)[Back](#)[Close](#)[Full Screen / Esc](#)[Printer-friendly Version](#)[Interactive Discussion](#)

Retrieving global sources of aerosols from MODIS observations

O. Dubovik et al.

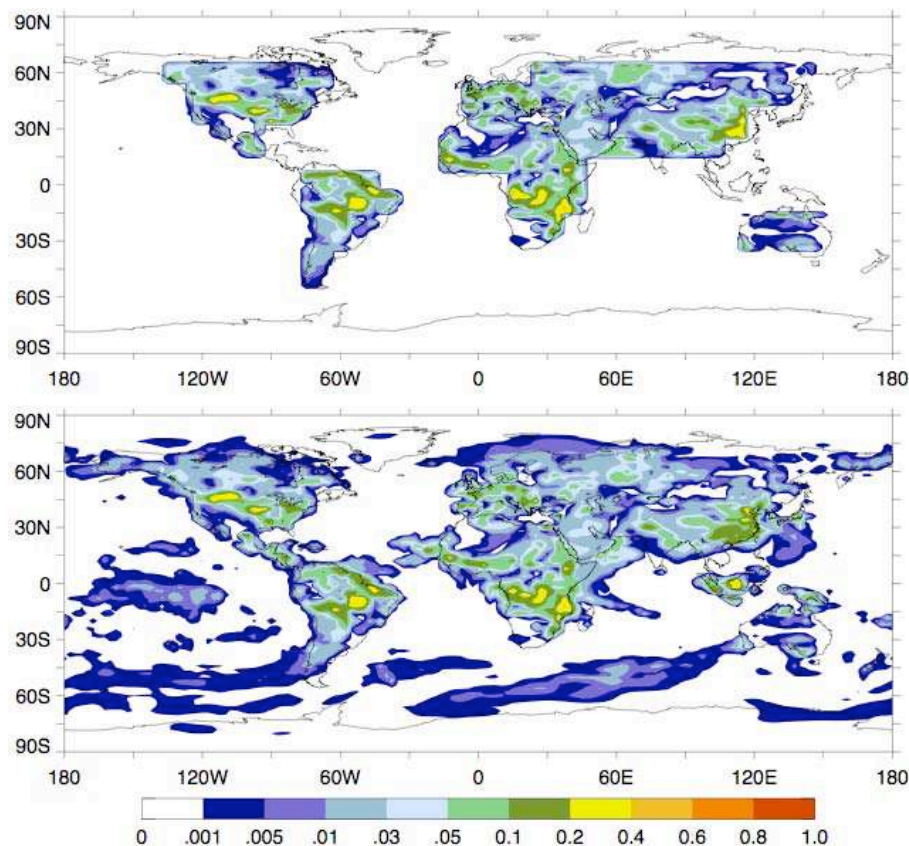


Fig. 13. Averaged (20–28 August 2000) fine aerosol sources (10^7 kg mass/day) retrieved from $\tau_{\text{fine}}(0.55)$ MODIS data: upper panel – retrieval with emission constrained to land only; lower panel – retrieval with emission not constrained to land.

[Title Page](#)[Abstract](#)[Introduction](#)[Conclusions](#)[References](#)[Tables](#)[Figures](#)[◀](#)[▶](#)[◀](#)[▶](#)[Back](#)[Close](#)[Full Screen / Esc](#)[Printer-friendly Version](#)[Interactive Discussion](#)

Retrieving global sources of aerosols from MODIS observations

O. Dubovik et al.

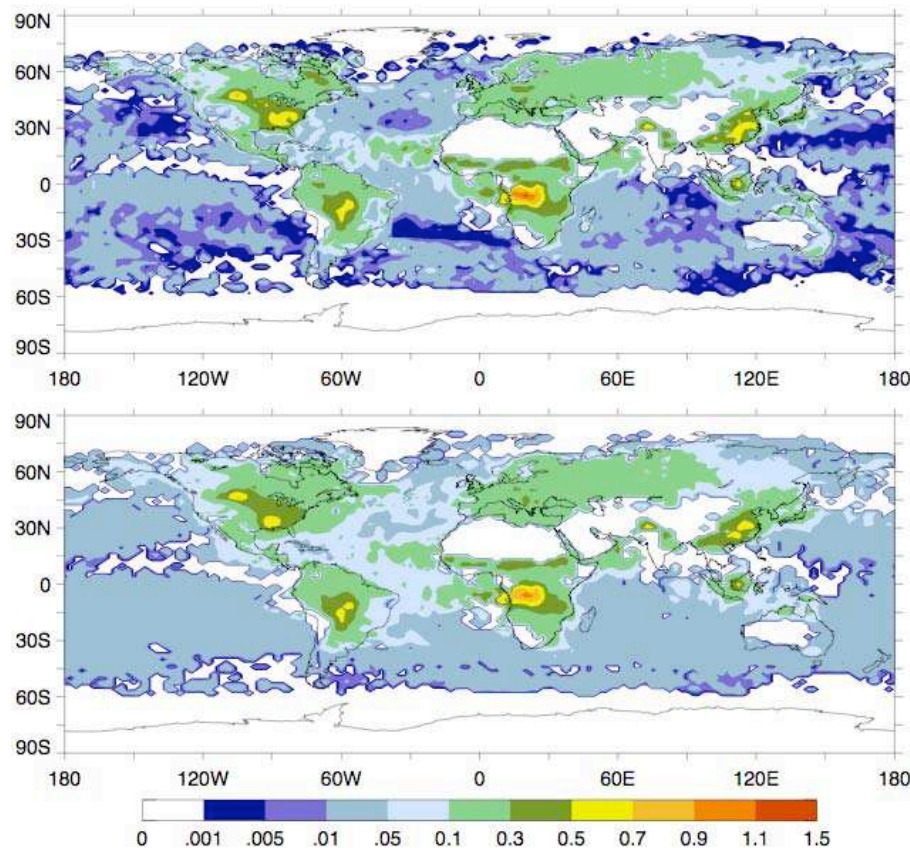


Fig. 14. Illustration of fitting MODIS data in the inversion: upper panel – averaged (19–30 August 2000) measurements of $\tau_{\text{fine}}(0.55)$, lower panel – averaged over the same time period measurements of $\tau_{\text{fine}}(0.55)$ measurements using retrieved emission.

[Title Page](#)[Abstract](#)[Introduction](#)[Conclusions](#)[References](#)[Tables](#)[Figures](#)[◀](#)[▶](#)[◀](#)[▶](#)[Back](#)[Close](#)[Full Screen / Esc](#)[Printer-friendly Version](#)[Interactive Discussion](#)

Retrieving global sources of aerosols from MODIS observations

O. Dubovik et al.

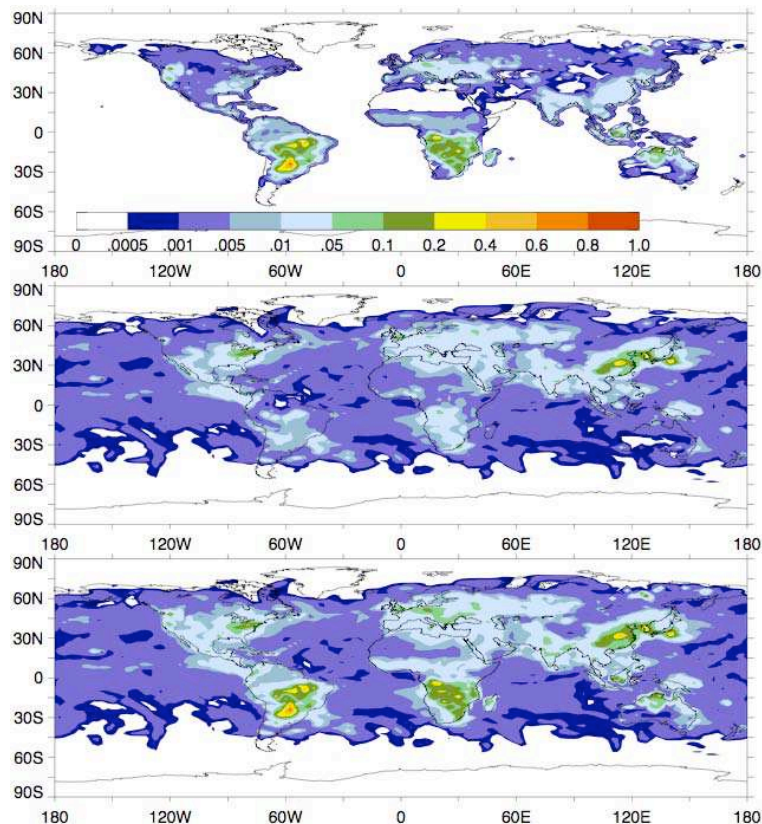


Fig. 15. Averaged (20–28 August 2000) aerosol sources of sulfates, black and organic carbon (unit 10^7 kg mass /day) assumed in GOCART model: upper panel – BC+OC emissions; middle panel – sulfate source (emission + atmospheric production; lower panel – total BC + OC + sulfate sources.

[Title Page](#)[Abstract](#)[Introduction](#)[Conclusions](#)[References](#)[Tables](#)[Figures](#)[◀](#)[▶](#)[◀](#)[▶](#)[Back](#)[Close](#)[Full Screen / Esc](#)[Printer-friendly Version](#)[Interactive Discussion](#)

Retrieving global sources of aerosols from MODIS observations

O. Dubovik et al.

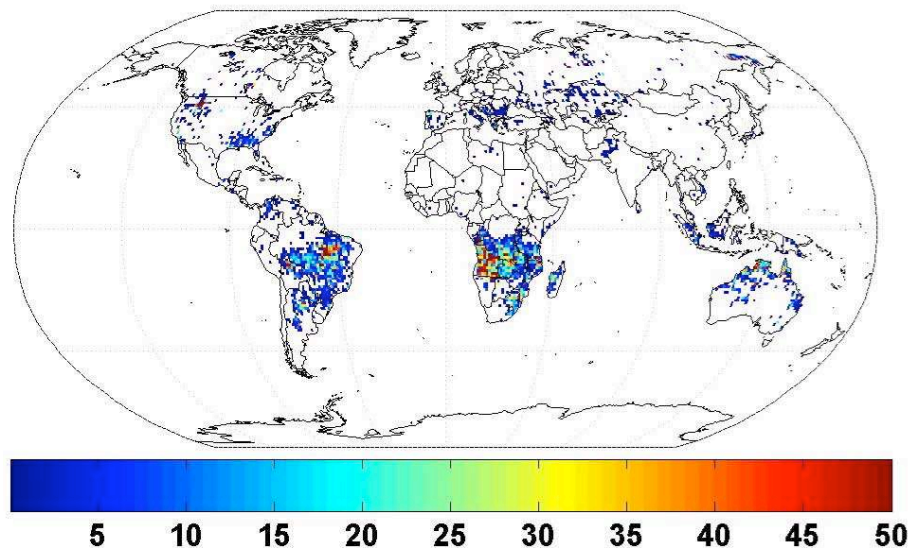


Fig. 16. Monthly (August 2000) carbon emission (g/m^2) obtained from combining satellite hotspots and burned area with a biogeochemical model (Van der Werf et al., 2003).

[Title Page](#)[Abstract](#)[Introduction](#)[Conclusions](#)[References](#)[Tables](#)[Figures](#)[⏪](#)[⏩](#)[◀](#)[▶](#)[Back](#)[Close](#)[Full Screen / Esc](#)[Printer-friendly Version](#)[Interactive Discussion](#)

Retrieving global sources of aerosols from MODIS observations

O. Dubovik et al.

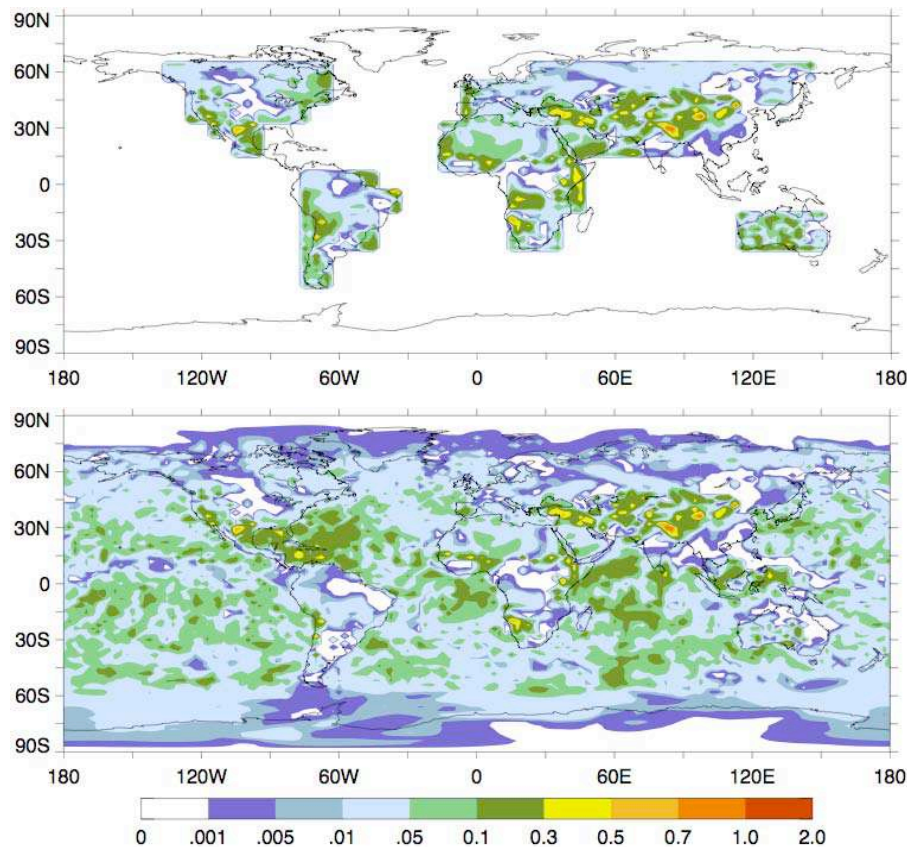


Fig. 17. Averaged (20–28 August 2000) coarse aerosol sources (10^8 kg mass/day) retrieved from $\tau_{\text{coarse}}(0.55)$ MODIS data; upper panel – retrieval with emission constrained to land only; lower panel – retrieval with emission not constrained to land.

[Title Page](#)[Abstract](#)[Introduction](#)[Conclusions](#)[References](#)[Tables](#)[Figures](#)[◀](#)[▶](#)[◀](#)[▶](#)[Back](#)[Close](#)[Full Screen / Esc](#)[Printer-friendly Version](#)[Interactive Discussion](#)

Retrieving global sources of aerosols from MODIS observations

O. Dubovik et al.

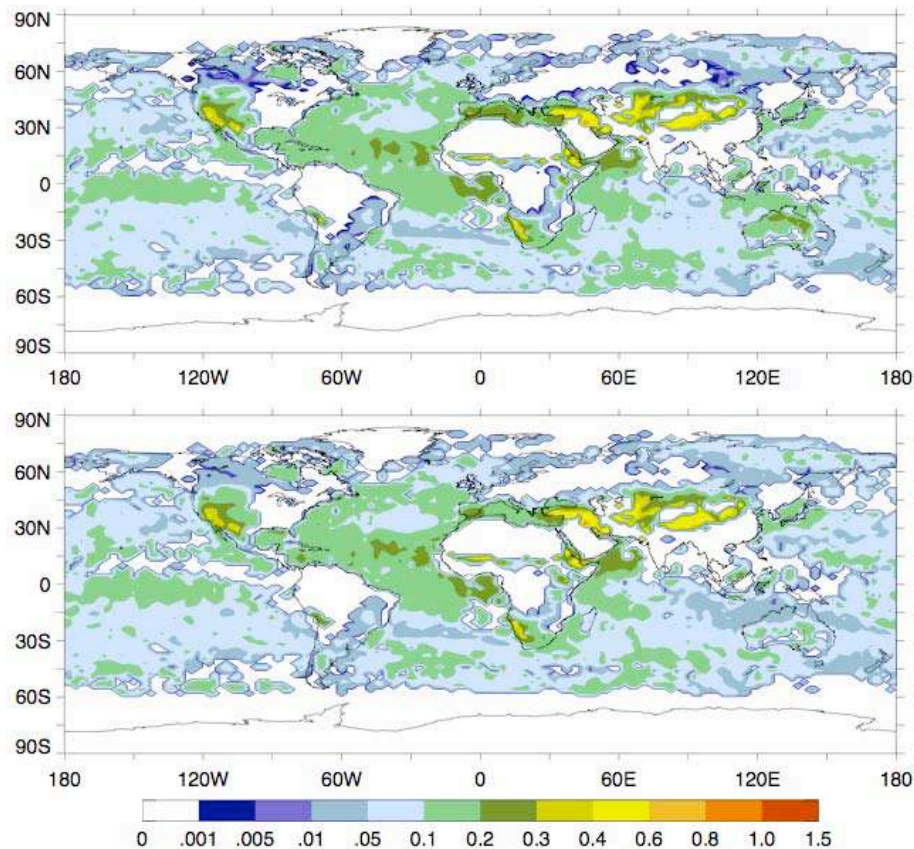


Fig. 18. Illustration of fitting MODIS data in the inversion: upper panel – averaged (19–30 August 2000) MODIS measurements of $\tau_{\text{coarse}}(0.55)$, lower panel – averaged over the same time period $\tau_{\text{coarse}}(0.55)$ measurements simulated using retrieved emission.

[Title Page](#)[Abstract](#)[Introduction](#)[Conclusions](#)[References](#)[Tables](#)[Figures](#)[◀](#)[▶](#)[◀](#)[▶](#)[Back](#)[Close](#)[Full Screen / Esc](#)[Printer-friendly Version](#)[Interactive Discussion](#)

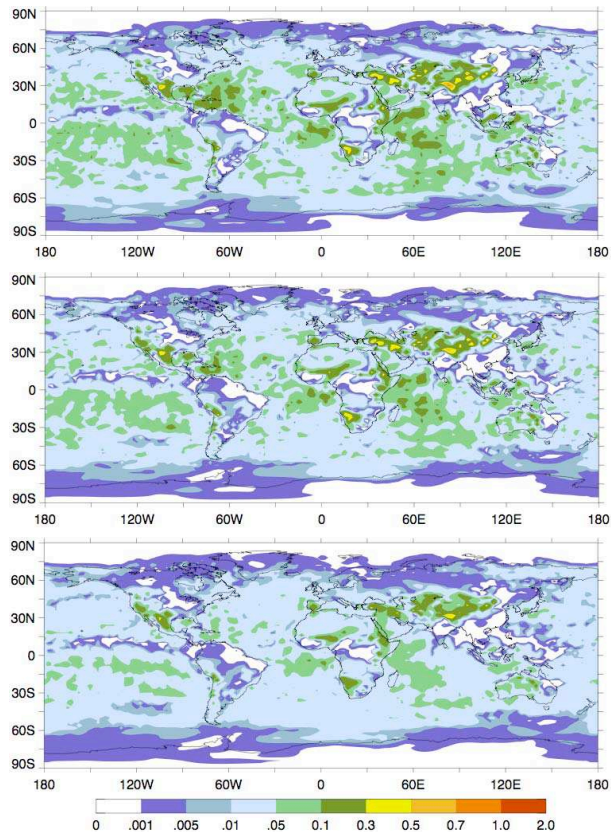


Fig. 19. Illustration of the smoothness constraint (on time and horizontal continuity) effect on the retrieval of global coarse mode sources (unit 10^8 kg mass/day): upper panel – only time continuity smoothness constraints were applied; middle panel – the smoothness constraints were applied only to limit horizontal (xy) variability of aerosol emissions; lower panel – the smoothness constraints were applied to limit both time and horizontal (xy) variability of aerosol emissions.

Retrieving global sources of aerosols from MODIS observations

O. Dubovik et al.

Title Page

Abstract

Introduction

Conclusions

References

Tables

Figures



Back

Close

Full Screen / Esc

Printer-friendly Version

Interactive Discussion

Retrieving global sources of aerosols from MODIS observations

O. Dubovik et al.

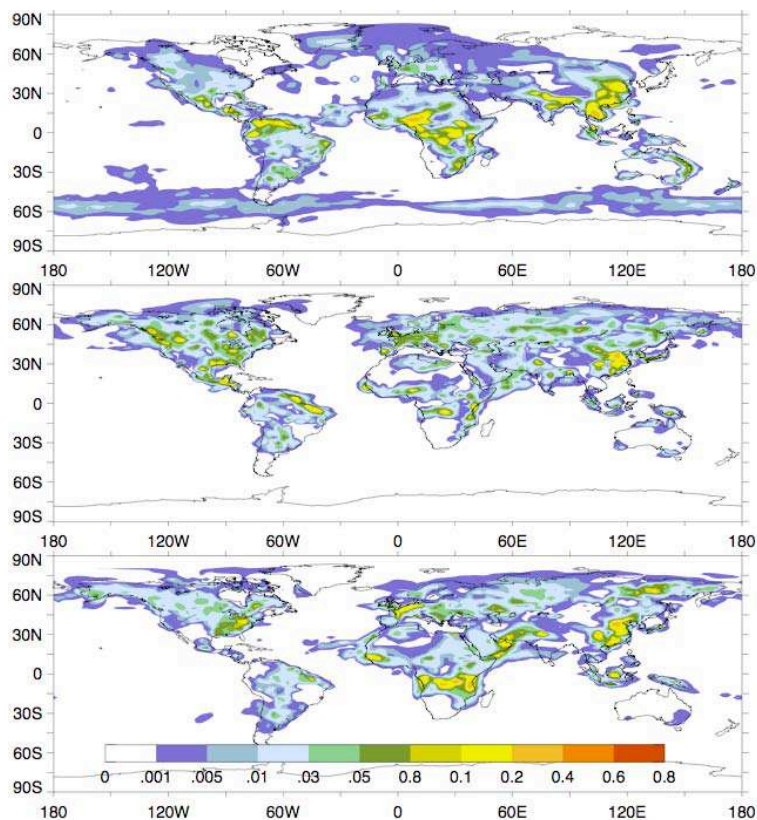


Fig. 20. Illustration of fine mode aerosol source (unit 10^7 kg mass/day) retrieval for extended time periods: upper panel – February 2001; middle panel – May 2001; lower panel – July 2001.

[Title Page](#)[Abstract](#)[Introduction](#)[Conclusions](#)[References](#)[Tables](#)[Figures](#)[◀](#)[▶](#)[◀](#)[▶](#)[Back](#)[Close](#)[Full Screen / Esc](#)[Printer-friendly Version](#)[Interactive Discussion](#)